STATISTICAL INTERPRETATION OF THE RELATION BETWEEN ICP-OES/MS GEOCHEMICAL AND MINERALOGICAL DATA OBTAINED FROM LAKE AND FLOODPLAIN SEDIMENTS (AMUQ VALLEY / SE TURKEY)

A THESIS SUBMITTED TO
THE GRADUATE SCHOOL OF NATURAL AND APPLIED SCIENCES
OF
MIDDLE EAST TECHNICAL UNIVERSITY

BY

DEVİN AYKASIM

IN PARTIAL FULFILLMENT OF THE REQUIREMENTS
FOR
THE DEGREE OF MASTER OF SCIENCE
IN
GEOLOGICAL ENGINEERING

FEBRUARY 2022

Approval of the thesis:

STATISTICAL INTERPRETATION OF THE RELATION BETWEEN ICP-OES/MS GEOCHEMICAL AND MINERALOGICAL DATA OBTAINED FROM LAKE AND FLOODPLAIN SEDIMENTS (AMUQ VALLEY / SE TURKEY)

submitted by **DEVİN AYKASIM** in partial fulfillment of the requirements for the degree of **Master of Science in Geological Engineering, Middle East Technical University** by,

Prof. Dr. Halil Kalıpçılar

Dean, Graduate School of **Natural and Applied Sciences** _____

Prof. Dr. Erdin Bozkurt

Head of the Department, **Geological Engineering** _____

Assoc. Prof. Dr. Fatma Toksoy Köksal

Supervisor, **Geological Engineering, METU** _____

Assoc. Prof. Dr. Ulaş Avşar

Co-Supervisor, **Geological Engineering, METU** _____

Examining Committee Members:

Assoc. Prof. Dr. Zehra Semra Karakaş

Geological Engineering, Ankara University _____

Assoc. Prof. Dr. Fatma Toksoy Köksal

Geological Engineering, METU _____

Assoc. Prof. Dr. Hüseyin Evren Çubukçu

Geological Engineering, Hacettepe University _____

Assist. Prof. Dr. Ali İmer

Geological Engineering, METU _____

Assoc. Prof. Dr. Kaan Sayit

Geological Engineering, METU _____

Date: 03.02.2022

I hereby declare that all information in this document has been obtained and presented in accordance with academic rules and ethical conduct. I also declare that, as required by these rules and conduct, I have fully cited and referenced all material and results that are not original to this work.

Name, Last name : Devin Aykasım

Signature :

ABSTRACT

STATISTICAL INTERPRETATION OF THE RELATION BETWEEN ICP-OES/MS GEOCHEMICAL AND MINERALOGICAL DATA OBTAINED FROM LAKE AND FLOODPLAIN SEDIMENTS (AMUQ VALLEY / SE TURKEY)

Aykasım, Devin
Master of Science, Geological Engineering
Supervisor: Assoc. Prof. Dr. Fatma Toksoy Köksal
Co-Supervisor: Assoc. Prof. Dr. Ulaş Avşar

February 2022, 145 pages

In the Amuq Valley region, mineralogical and elemental geochemical investigations were carried out along the undisturbed core samples that were taken from the Amuq Lake and from the vicinity of the mounds within this region. Mineralogical content of the sediments along these cores were examined by X-Ray Diffraction (XRD) and Scanning Electron Microscope – Energy Dispersive X-Ray Spectroscopy (SEM-EDS). Inductively Coupled Plasma – Optical Emission Spectrometry / Mass Spectrometry (ICP-OES/MS) analyses were conducted on the samples to detect quantitative concentrations of major, minor and trace elements. A method was developed by MapInfo software to convert intensities of bulk powder and oriented air-dried clay fraction X-ray diffractogram peaks to numerical values. Numerical values obtained from XRD and ICP-OES/MS analyses were correlated by Correlation Matrix and Principal Component Analysis (PCA). Hence, advantages and disadvantages of this method was determined, and mineral-element relationships were statistically identified. Statistical evaluation of the data revealed that quartz,

serpentine, feldspars and clay minerals have higher correlation coefficients in the floodplain samples while calcite and aragonite have higher correlation coefficients in the lake samples. A significant effect of environmental difference was determined on aragonite correlations. It was also examined that the clay mineral peaks before 20° 2θ on bulk powder X-ray diffractograms exhibit different mineralogical and elemental relationship in contrast to the other clay mineral peaks. Moreover, element vs. mineral correlations revealed possible presence of impurities like rutile in quartz while other minerals generally correlate with their chemical constituents except clay minerals which also correlate with rare earth elements.

Keywords: Amuq Valley, Lake and Floodplain Sediments, Mineralogical and Geochemical Data, Statistical Evaluation

ÖZ

GÖL İLE TAŞKIN YATAĞI SEDİMANLARINDAN ELDE EDİLEN MİNERALOJİK VE ICP-MS/OES JEOKİMYASAL VERİLER ARASINDAKİ İLİŞKİNİN İSTATİSTİKSEL YORUMLANMASI (AMİK OVASI / GD TÜRKİYE)

Aykasım, Devin
Yüksek Lisans, Jeoloji Mühendisliği
Tez Yöneticisi: Doç. Dr. Fatma Toksoy Köksal
Ortak Tez Yöneticisi: Doç. Dr. Ulaş Avşar

Şubat 2022, 145 sayfa

Amik Ovası bölgesinde Amik Gölü'nden ve bu bölgedeki höyüklerin çevresinden alınan bozulmamış karot örnekleri boyunca mineralojik ve elementel jeokimyasal araştırmalar yapılmıştır. Bu karotlar boyunca sedimanların mineralojik içerikleri, hem tüm kayaç hem de yönlendirilmiş kil fraksiyonlarından alınan X-Işını Kırınımı (XRD) ölçümleri ve Taramalı Elektron Mikroskobu – Enerji Dağılım Spektroskopisi (SEM-EDS) analizleri ile incelenmiştir. İhtiva edilen element miktarları hakkında nicel bir bilgi elde etmek için numuneler üzerinde İndüktif Eşleşmiş Plazma Optik Emisyon Spektroskopisi / Kütle Spektroskopisi (ICP-OES/MS) analizleri yapılmıştır. XRD difraktogramlarındaki piklerin yoğunluklarını sayısal değerlere dönüştürmek için MapInfo yazılımı tabanlı bir yöntem kullanılarak XRD ve ICP-OES/MS analizlerinin sonuçları Korelasyon Matrisi ve Temel Bileşen Analizi (PCA) ile ilişkilendirildi. Böylece bu yöntemin avantaj ve dezavantajları belirlenmiş ve mineral-element ilişkileri istatistiksel olarak ortaya konulmuştur. Elde edilen veriler üzerinde yapılan istatistiksel değerlendirmeler, taşkın yatağı örneklerinde kuvars, serpantin, feldspat ve kil minerallerinin, göl örneklerinde ise kalsit ve aragonitin

daha yüksek korelasyon katsayılarına sahip olduğunu ortaya koymuştur. Aragonit korelasyonları üzerinde çevresel farklılığın önemli bir etkisi tespit edilmiştir. Tüm kayaç XRD difraktogramlarında 20° 2θ öncesi kil mineral piklerinin diğer kil mineral piklerinin aksine farklı mineralojik ve elementel korelasyonlar gösterdiği de dikkat çekmiştir. Ayrıca, element-mineral korelasyonları, kuvars içinde olası bir rutil muhteviyatını ortaya çıkarırken, nadir toprak elementleri ile ilişkili olan kil mineralleri hariç diğer minerallerin genellikle kimyasal bileşenleriyle korelasyonlar gösterdikleri tespit edilmiştir.

Anahtar Kelimeler: Amik Ovası, Göl ve Taşkın Yatağı Sedimanları, Mineralojik ve Jeokimyasal Veri, İstatistiksel Yorumlama

To my family, ones who have always been there for me…

ACKNOWLEDGMENTS

First and foremost, I would like to express my profound thanks to my supervisor Assoc. Prof. Dr. Fatma Toksoy Köksal for her guidance, encouragements and intense support during my whole education life. I would also like to thank my co-supervisor Assoc. Prof. Dr. Ulaş Avşar for his guidance, criticism, suggestions and wisdom throughout the research.

I am really grateful to Assoc. Prof. Dr. Murat Akar for his support and patience during the field trip in Hatay. Besides, I would like to thank all the examining committee members for their suggestions and criticism. I would like to express my special thanks of gratitude to Assoc. Prof. Dr. Hüseyin Evren Çubukçu for his support for SEM-EDS measurements.

The assistance of Zeynep Bektaş, Ayşegül Doğan, Özlem Karadaş, Serap Şen, Alım Elibol, Ali Can Soyuslu, Onur Hasan Kırman, Gökhan Tektaş and Seren Burgaç in this research project are also gratefully acknowledged.

This study is funded by The Scientific and Technological Research Council of Turkey (TÜBİTAK) within the scope of "Geological and Archaeological Traces of Climatic Changes in Amuq Valley during Holocene" project under grant number 119Y222, and hosted by Department of Geological Engineering, Middle East Technical University.

TABLE OF CONTENTS

LIST OF TABLES

TABLES

LIST OF FIGURES

FIGURES

CHAPTER 1

INTRODUCTION

Hatay, the southernmost city of Turkey, has been an important settlement area for mankind since BC 100000. Amuq Valley (also called as Plane of Antioch and Amik Ovası) has been one of the most fertile lands in this region and considering its geopolitical location, many civilizations had preferred to settle there after Bronze Age. In consequence, Amuq Valley and its surroundings have always been a focus of interest for geologists and archaeologists as they provide a unique data collection that preserves both geological and archaeological records of environmental and social turbulences experienced during the Holocene epoch.

A geoarcheological study entitled "Geological and Archaeological Traces of Climatic Changes in Amuq Valley during Holocene" that is funded by TÜBİTAK (Project no: 119Y222) has been ongoing in Amuq Valley region, especially Amuq Lake, ancient mounds of Tell Atchana, Tell Kurdu, and Tell Tayinat. Huge data set on mineral and chemical contents of sediments from undisturbed core samples would have been obtained at end of the project to get the purpose of the project. How huge data set will be evaluated in healthy and easy way is a question. This thesis, as a part of the project, therefore, was carried out to have a practical approach to deal with huge data set. For this purpose, undisturbed core samples from lacustrine and alluvial sediments of Holocene in Amuq Valley region were mineralogically and geochemically interpreted. Then, the mineral and chemical data were statistically correlated and evaluated, and an statistical approach was obtained. The obtained statistical approach and results by evalution of the data can make easier data evaluation to be obtained in rest of the project and could be used to enlight significant geological properties of the study area.

In this thesis study, 50 samples of lacustrine sediments from the middle of Amuq Lake, and a total of 99 samples of alluvial deposits from Tell Atchana, Tell Kurdu, and Tell Tayinat, ancient mounds located in Amuq Valley region (Table 1.1), were used.

Table 1.1. UTM coordinates, locations and analysed core lengths of the cores used in this study

Core Name	**Core Location**	**Coordinates**		**Analysed Core Length (m)**
		E	**N**	
AL-5	Amuq Lake	256713.00	4025144.00	9.73
KR-1	Tell Kurdu	271095.43	4024123.21	10.09
AT-1	Tell Atchana	265195.32	4013765.39	8.29
TA-2	Tell Tayinat	264618.97	4014423.19	7.57

The TÜBİTAK project including this thesis study, have been carried out by taking the regional geology and the geological history into consideration. Amuq Lake is located in the graben area of Amuq Valley that is surrounded by NE-SW trending Amanus Mountain on the west, Kurt Mountains on the east, and Kuseyr Plateau on the south (Korkmaz & Gürbüz, 2008) (Figure 1.1). There are two significant igneous formations in the vicinity of the study area which are Kızıldağ (Hatay) ophiolites on the west and Quaternary basalts (Rojay et al., 2001) of Karasu rift on the northeast. As Amuq Lake was drained in late 20th century in order fight against malaria, to avoid floodings and to provide new agricultural fields (Varnacı, 2008), lacustrine unconsolidated Quaternary samples were retrieved from the dry lake by using enhanced piston coring technique in scope of the TÜBİTAK project by which samples were provided for this thesis. Obtained cores were synchronously split into two during 36 days of fieldwork in Hatay for high-resolution photographing, and sub-sampled in Middle East Technical University (Ankara) for further laboratory analyses.

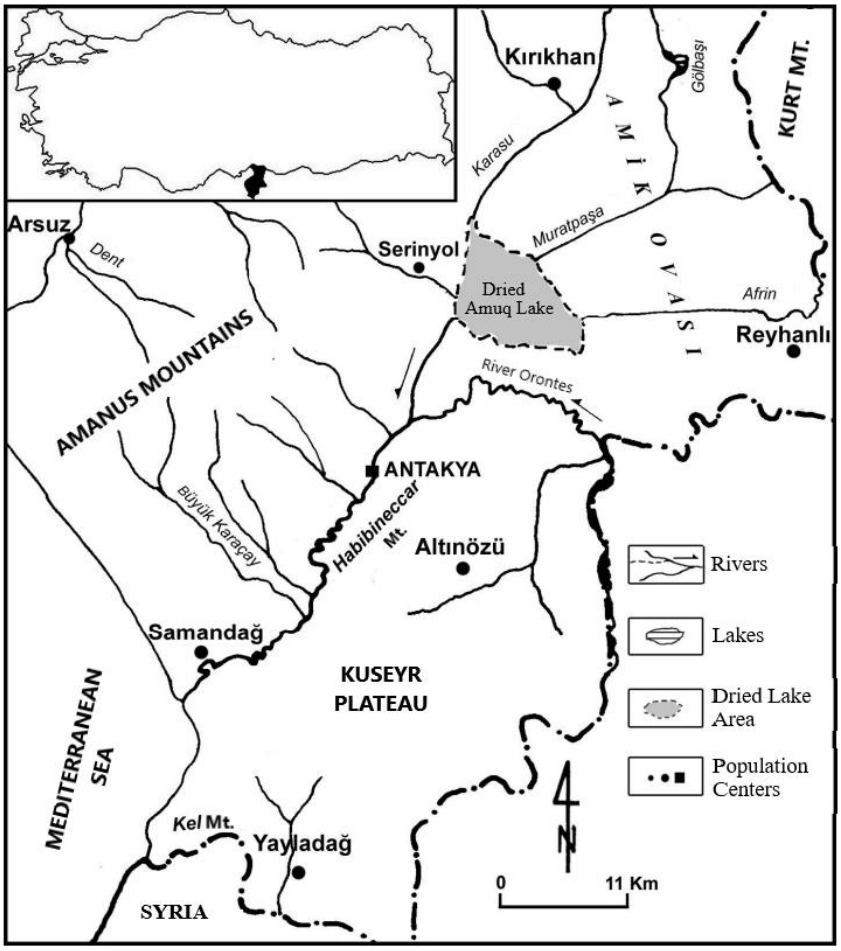

Figure 1.1. Location map of dried Amuq Lake (Korkmaz & Gürbüz, 2008)

Mineralogical content of the sediments along cores obtained from these locations were examined by X-Ray Diffraction (XRD) analyses at Department of Geological Engineering in Middle East Technical University. Both non-clay and clay minerals contents were determined. The occurences, moreover, were examined by Scanning Electron Microscopy – Energy Dispersive X-Ray Spectroscopy (SEM-EDS) to have well-done mineralogical characterization. Geochemical data were obtained by Inductively Coupled Plasma – Optical Emission Spectrometry / Mass Spectrometry (ICP-OES/MS) analyses in Central Laboratory (MERLAB), Middle East Technical University. Quantitative concentrations of major, minor and trace elements were detected through these geochemical analyses, and sufficient data were obtained for geochemical characterization.

Mineral intensity data obtained from XRD diffractograms of both bulk powder samples and air-dried oriented clay fractions were converted to numerical values by using MapInfo software in order to avoid any possible mistakes that might be caused by automatic evaluation of the XRD diffractogram interpretation software. As these mineralogical results were interpreted among themselves by forming scatter charts and using statistical techniques such as Principal Component Analysis (PCA), a multivariate statistical analysis technique commonly preferred to ease statistical evaluations by categorizing the correlating variables, and correlation matrices which were used for better visualization of the correlations. As some elements are comparable with some certain types of minerals, correlations between the results of XRD and ICP-OES/MS analyses were also checked by these methods. Elemental correlations were also discussed by using Principal Component Analysis.

Eventually, after characterization of the mineralogy and geochemistry of the samples from the study area, the relation between geochemical and mineralogical data was revealed and interpreted by stating the statistical evidences. In addition, these statistical analyses were used to clarify mineral-mineral, element-element, and mineral-element relationships of lake and floodplain sediments in Amuq Valley.

1.1 Aim of the Study

The main purpose of this study is to reveal statistical correlations between geochemical and mineralogical data obtained and characterized from the lake and floodplain sediments of Amuq Valley for both strengthening mineralogical and geochemical knowledge about this region and also uncovering the relationship between geochemistry and mineralogy of the lake and floodplain samples by visualizing some statistical evidences. Furthermore, the study area has great importance for geological and archaeological studies as it hosted various civilizations and was exposed to different environmental conditions and many people studied there for various purposes. Characterization of geological features

from this large data set obtained from this study area would also be very useful for future geological and archaeological studies.

In addition, it is also aimed to evaluate the efficiency of quantifying the intensity data obtained from both bulk powder samples and air-dried oriented clay fractions by using MapInfo software manually. As XRD diffractogram interpretation softwares usually determine erroneous backgrounds for intensity measurements, automatic evaluation would have affected the statistical interpretations critically. As clay mineralogy is interpreted by taking four different clay fraction diffractograms (air-dried, ethylene glycolized, 300 °C heated, and 550 °C heated) into consideration together, intensity data were retrieved from the air-dried diffractograms as they are the least modified ones. By using the intensity data of air-dried oriented clay fraction diffractograms, it was aimed to reveal whether these diffractograms reflect geochemical variations as much as the bulk powder sample diffractograms.

This study aims to conduct a statistical evaluation with a spatial-free and temporal-free approach by considering only the mineralogical and geochemical characteristics as much as possible. As this study was carried out within the scope of "Geological and Archaeological Traces of Climatic Changes in Amuq Valley during Holocene" project funded by The Scientific and Technological Research Council of Turkey (TÜBİTAK), the results obtained from this study are also going to be useful for further paleoclimatic investigations conducted within this project.

1.2 Study Area

Amuq Valley is located within Hatay, the southermost province of Turkey, a buffer zone that Anatolian, Mediterranean and Near Eastern cultures intersect. Amanus (Nur) Mountains and Taurus (Toros) Mountains restrict the valley on the west and north, and limestone hills along Turkey-Syria border enclose the valley on the east and south (Durusu Tanrıöven, 2010). Orontes (Asi) River flows into the valley from the south and Afrin and Karasu streams enter from north and east (Gerritsen et al.,

2008). In this research, lacustrine and alluvial floodplain cores were obtained from Amuq Lake, Tell Atchana, Tell Kurdu, and Tell Tayinat (Figure 1.2).

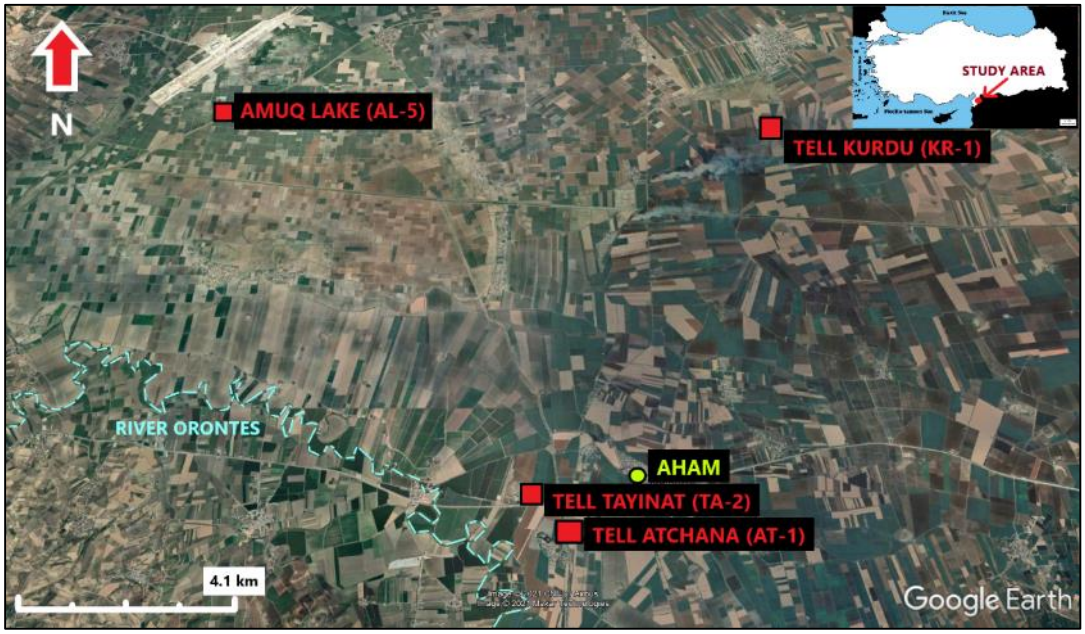

Figure 1.2. Sediment coring locations of Amuq Lake, Tell Kurdu, Tell Atchana and Tell Tayinat with the location of Tell Atchana Excavations and Amuq Valley Research Center (AHAM)

Many civilizations have settled in Hatay since the Bronze Age (3000 BC) such as Hittites, Assyrians, Oghuzs, Persians, Seleucians, Romans, Byzantines, Seljuqs, Crusaders, Ayyubids, Mamelukes, Ottomans and Turks (Sarı, 2009). Tell Atchana, also called as Alalakh, is located along the major branch of the Orontes River. Between 2200-1300 BC, it was the largest settlement in the region and was the capital of the Mukish Kingdom for a long time. Tell Tayinat, also called as Kunulua, is approximately 800 meters northwest to the site of Tell Atchana. After the fall of Hittites and abandonment of Tell Atchana, importance of Tell Tayinat as a settlement area had risen. This site has also hosted Neo-Hittites in the Iron Age. Tell Kurdu is located in the east of Amuq Lake and is considered as the largest Chalcolitic period settlement. As Tell Kurdu is located further to the floodplains in comparison with

Tell Atchana and Tell Tayinat, the study area can be considered as a geologically intermediate zone in this research.

Coring operations were conducted in 36 days in Tell Atchana Excavations and Amuq Valley Research Center (AHAM) in Tayfursökmen district of Hatay. The research center is located 2 kilometers northeast of Tell Atchana, and has been used for archaeological studies for the last 20 years. After obtaining cores from related study areas, core splitting and high-resolution photographing processes were held in this research center. Moreover, the region has been being studied by archaeologists of Hatay Mustafa Kemal University, Oriental Institute of University of Chicago, and University of Toronto since the early twentieth century.

Coring locations are geologically surrounded by undifferentiated Quaternary sediments ranging along River Orontes and the floodplains that consist of loose sand-sized materials (Kavuzlu, 2006). The vicinity of the study area includes clastic sediments and carbonates of various ages along with some mafic rocks. The west side of the study area is covered by mafic and ultramafic rocks of Kızıldağ (Hatay) ophiolites. Kızıldağ ophiolites consist of highly serpentinized harzburgite and dunite with high olivine and pyroxene content (Kavuzlu, 2006) along with gabbro, diabase, pillow basalts and some volcano-sedimentary formations.

There are also basaltic rocks in the northeast of Tell Kurdu, along the Turkey-Syria border, which belong to Karasu rift basalts (Figure 1.3). Rojay et al. (2001) stated that Karasu rift volcanics include quartz tholeiites, olivine tholeiites, and alkali olivine basalts. Figure 1.4 demonstrates all geological formations in the vicinity of the study area along with the coring locations.

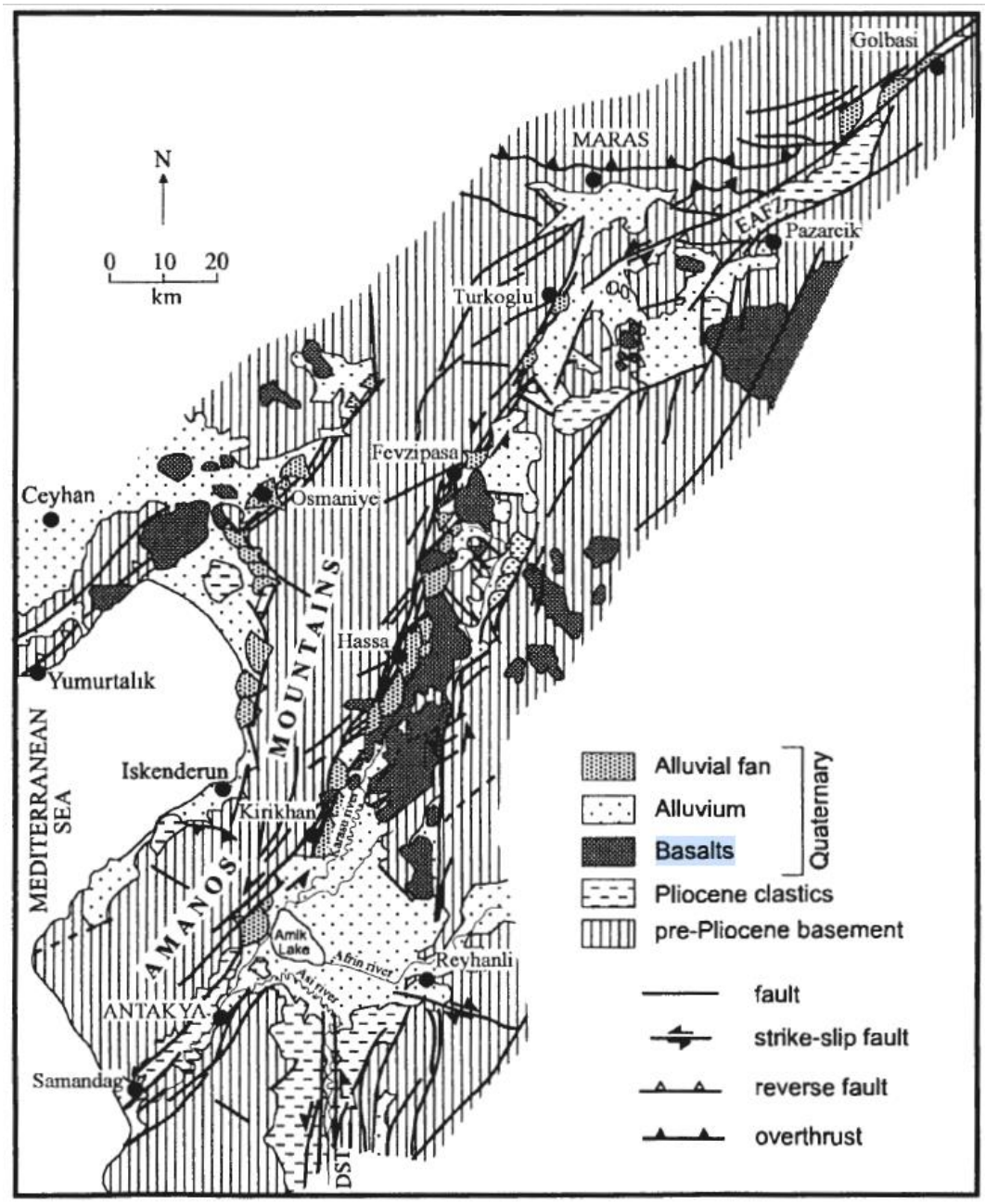

Figure 1.3. Regional geology of the Karasu rift and its vicinity (Rojay et al., 2001)

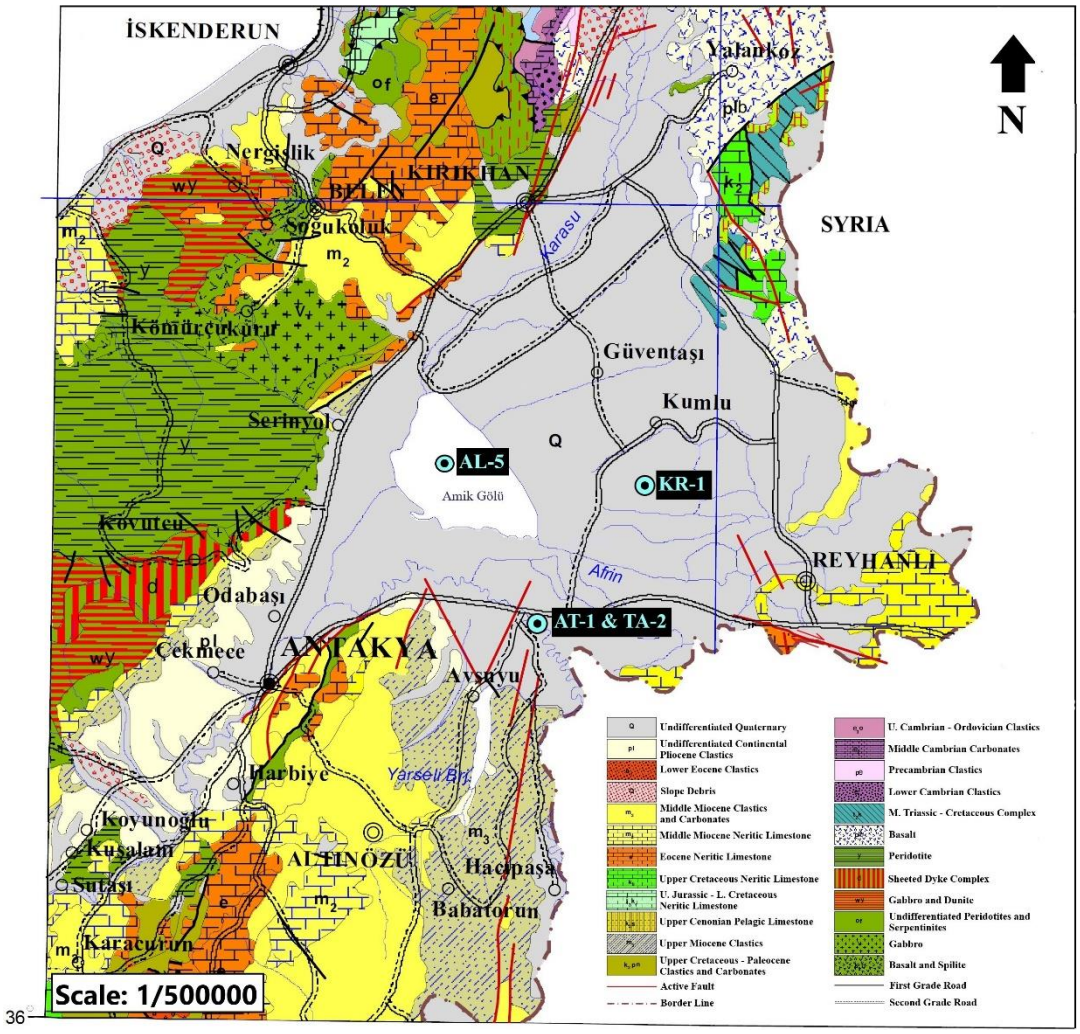

Figure 1.4. Geological map of the study area, SE Turkey (MTA, 2002)

1.3 Methods

1.3.1 Piston Coring

Undisturbed lacustrine and alluvial sediment samples were obtained by enhanced piston coring system after 36 days of fieldwork in Hatay. A total of 137.43 meters of lacustrine sediment cores were taken from 11 different locations in Amuq Lake region. Moreover, 39.15 meters of sediment cores from Tell Atchana, 15.72 meters from Tell Tayinat and 13.96 meters from Tell Kurdu were taken. The 18.88 meters

long main core of Amuq Lake (which is going to be mentioned as AL-5 thereafter), which was taken from the middle of the lake, is used in this study. AL-5 was determined as the main core as it most properly reflects the lake geology. The core samples used in this study from Tell Atchana, Kurdu, and Tayinat were named as AT-1, KR-1, TA-2, respectively.

Among all the cores obtained, these ones were specially preferred for further studies as they reflect almost all important geological features. 9.73 meters of sediments from AL-5, 10.09 m from KR-1, 8.29 meters from AT-1 and 7.57 meters from TA-2 were sub-sampled for further analyses at the Department Geological Engineering in Middle East Technical University, Ankara. Exact coordinates of the coring locations and the analysed core lengths are listed in Table 1.1.

At the very beginning, the main purpose was to obtain the most continuous and the most comprehensive cores from determined locations. By taking the topography, petrology, and structural geology into consideration, extensive literature and field surveys were conducted. Thus, coring locations, core lengths and the coring technique were specified. Piston coring, which is mostly preferred for marine and lake deposits, was determined as the most efficient technique to obtain undisturbed samples from these locations. As alluvial deposits are harder than lacustrine deposits, the piston coring system (Figure 1.5), with an inner radius of 8 centimeters, was enhanced by more durable chromium catchers and coring was operated by a slide hammer falling from a standard height just like in Standard Penetration Test (SPT).

The obtained cores were split into two (Figure 1.6) in Tell Atchana Excavations and Amuq Valley Research Center by using a fixed power saw system and wrapped up for further laboratory analyses.

Figure 1.5. Piston coring system used in the study

Figure 1.6. Split core samples

1.3.2 X-Ray Diffraction (XRD)

X-Ray Diffraction (XRD) is a non-destructive instrumentation for characterization of crystalline materials such as minerals, cements, ceramics, and polymers. It is a low-cost, semi-quantitative technique and widely used in geology, chemistry, material science, environmental science, and engineering. In geology, XRD is highly preferred for mineralogical analyses. Types, crystallinity degrees, and amounts of minerals can be identified through powdered samples. While non-clay mineral occurrences can be determined through measurements on bulk powder samples, which require less pre-treatment before measurement, clay mineral occurrences can only be identified after preparation of oriented slide samples of clay fractions. In this study, both non-clay and clay minerals were identified.

Pre-treatment procedure started with sub-sampling of wet sediments from the split cores. 2 cm thick semicircle sediment slices were taken in every 6 centimeters along the cores (Figure 1.7) and one third of these samples were packed as XRD samples.

Figure 1.7. Semicircle wet sediment slices used in pre-treatment procedure

After packing, these wet samples were put in glass beakers and dried in 60 °C for 48 hours. This temperature was fixed in order to prevent mineralogical distortions. Dried samples were carefully ground and pulverized. Then, these powder samples were sieved below 125 μm and the retained material that has larger grain size than 125 μm was packed as bulk powder samples. These powder samples (Figure 1.8) were used in determination of non-clay minerals by bulk XRD powder measurements.

Figure 1.8. Bulk X-ray diffraction powder samples

In the clay mineralogy laboratory of the Department of Geological Engineering, Middle East Technical University, 10 grams of sieved material was mixed with 800 ml of distilled water and 5 grams of sodium polyphosphate in a large glass beaker (Figure 1.9) and the clay fraction which has grain size less than 2 μm was separated by sedimentation. Sodium polyphosphate was used to prevent flocculation during sedimentation. After waiting for 8 hours considering Stokes' Law of sedimentation, the clay fraction in suspension was extracted by siphoning and enriched by centrifugation (Figure 1.10).

Figure 1.9. Mixtures of sieved powder samples, sodium polyphosphate and distilled water

Using the enriched clay fraction, four oriented slides were prepared by combining smear method with air drying technique of Nagelschmidt (1941) and Jackson (1969). All of these slices were initially air-dried at room temperature. One of the four samples remained as air-dried, the second one was saturated in ethylene glycol at 60 °C overnight, the third one was heated at 300 °C for one hour, and the last sample was heated at 550 °C for one hour. These oriented slides of clay fractions were named as AD, EG, 300 °C and 550 °C, respectively (Figure 1.11).

Figure 1.10. Centrifuge device used in oriented sample preparation for XRD

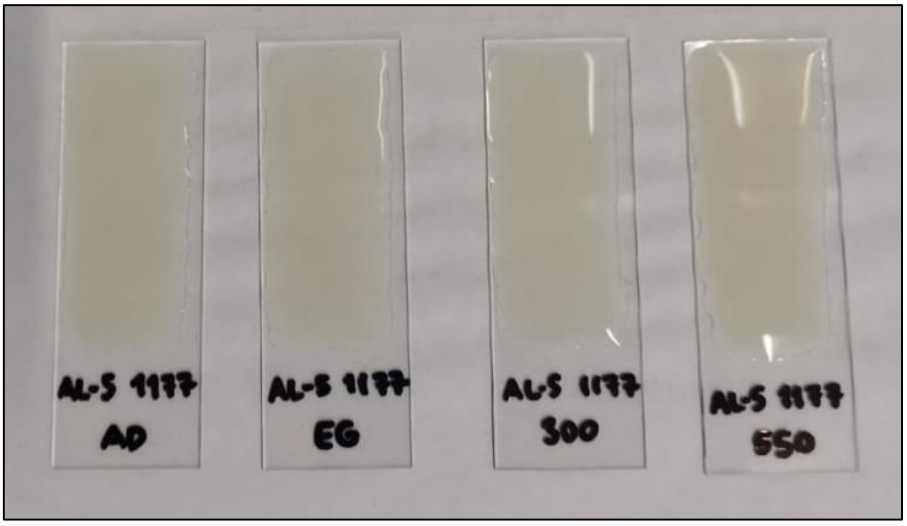

Figure 1.11. Examples of oriented slides prepared from clay fraction

While preparing oriented slides of clay fractions, using 10 grams of sieved material for mound samples (KR-1, AT-1 and TA-2) caused swelling problems. This problem

was because of high smectite content, which is going to mentioned in mineral characterization. To prevent swelling, glass slides were treated with acetone before smearing the wet clay fraction. Moreover, 200-250 ml of distilled water was added to the mixtures of these samples for dilution. This problem was solved after combined usage of dilution and acetone-treatment. After preparation of these slides, 6 grams of sieved material of AL-5 (lake sample) were used for enrichment of clay fraction by sedimentation because obtained amount of clay fraction after centrifuge was a lot more than alluvial mound samples. Efficiency of this amount was determined after few experiments. By using 6 grams of AL-5 samples, dilution part was skipped and acetone treatment was found to be unnecessary as the smectite content was relatively lower than the mound samples.

Finally, both bulk powders and oriented clay fraction slides of the samples were measured by using Rigaku Miniflex Benchtop Powder X-Ray Diffractometer (Figure 1.12) at the Department Geological Engineering, Middle East Technical University. All XRD analyses were carried out using CuK_{α} radiation (2° 2θ/min). While XRD diffractograms of bulk powder samples were measured between 2° and 70° 2θ, clay fraction diffractograms were obtained between 2° and 30°. Repeatability of these experiments were checked and confirmed over five samples after completion of all measurements.

For interpretation of bulk XRD patterns, the scientific software MDI Jade was used. Oriented clay fraction diffractograms were examined manually in order to prevent possible digital errors in clay mineral identification and statistical evaluation. All diffractograms were theta-calibrated with respect to the most dominant mineral (mostly calcite) for better mineralogical characterization and to avoid misidentification due to slight 2θ differences.

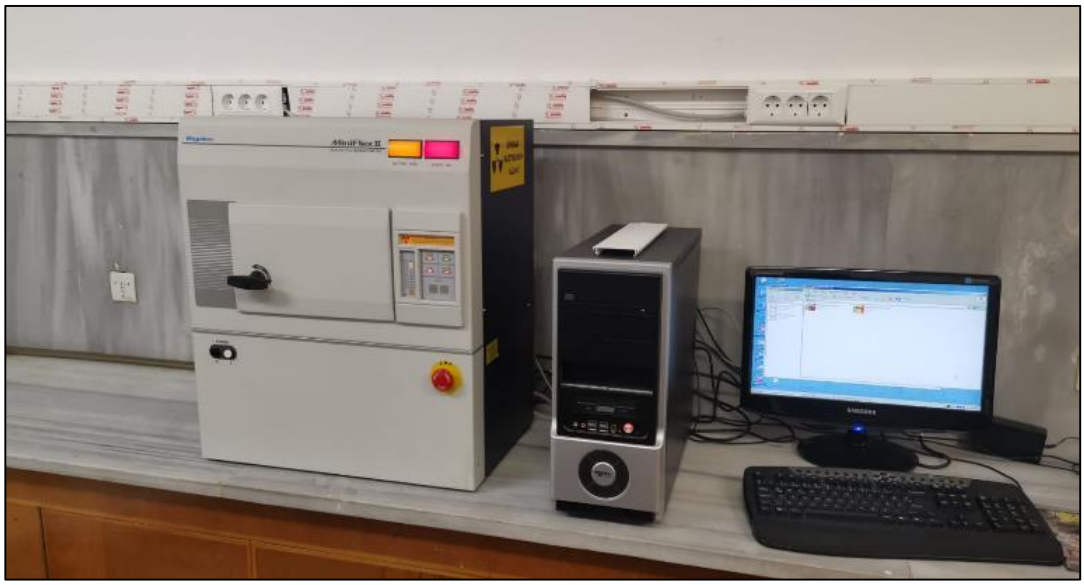

Figure 1.12. Rigaku Miniflex Benchtop Powder XRD device at the Department of Geological Engineering, Middle East Technical University

Clay minerals of the core sediment samples were identified by interpreting diffractograms of AD, EG, 300 °C, and 550 °C oriented clay fraction slides for every sample one by one (Figure 1.13).

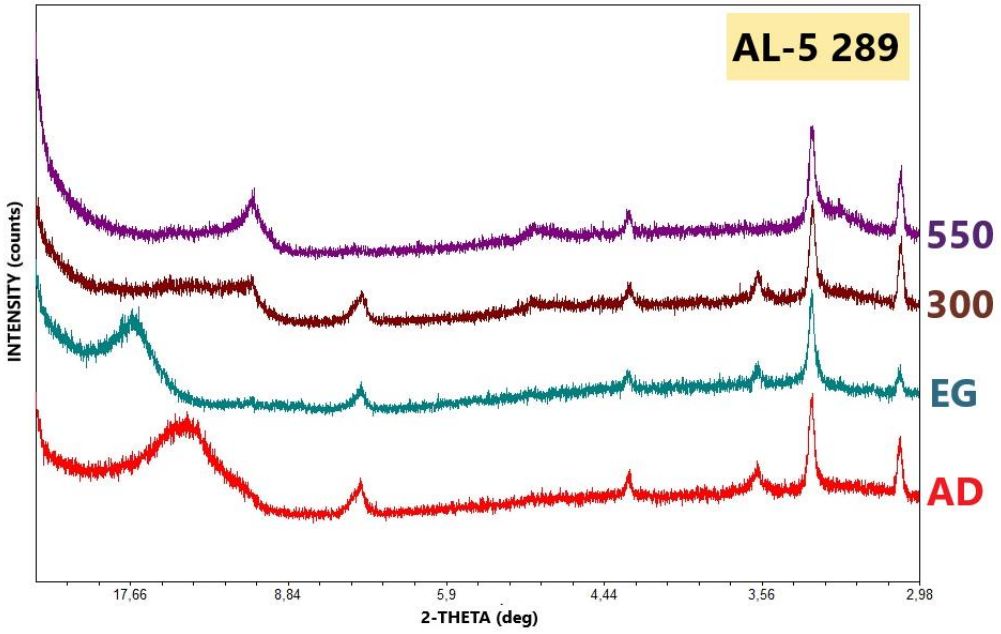

Figure 1.13. A set of oriented clay fraction XRD diffractograms for clay mineral identification

1.3.3 Scanning Electron Microscopy – Energy Dispersive X-Ray Spectroscopy (SEM-EDS)

Scanning Electron Microscopy (SEM) is an instrumental analysis technique that uses a focused beam of high-energy electrons for generation of a variety of signals at the surface of solid specimens (Swapp, 2017). These signals give information about the external morphology and crystal structure of examined materials. Energy Dispersive X-ray Spectroscopy (EDS, EDX or EDXS) is an analytical technique preferred for elemental analysis or chemical characterization (Telegdi et al., 2018). EDS is commonly used along with SEM for better characterization of samples.

SEM-EDS was used for 4 samples of Amuq Lake (AL-5 049, AL-5 433, AL-5 505, and AL-5 685) to observe and understand mineralogy of the samples in detail. While AL-5 049 and AL-5 505 were selected due to their bulk powder XRD patterns displaying presence of high amorphous material, other two samples were chosen for SEM-EDS study due to well-developed peaks of almost all minerals interpreted, and low amounts of amorphous material.

SEM-EDS studies were conducted at Hacettepe University Advanced Technologies Application and Research Center (HÜNİTEK), Ankara. Preparation process for these four samples included only drying at 60 °C for 12 hours without grinding and sieving. Then, they were analysed by TESCAN GAIA3 Triglav SEM device (Figure 1.14) equipped with Oxford X-max 150 SDD EDS. All samples were coated with 10 nm thick Au-Pt before SEM-EDS analyses. Analytical conditions during these analyses are set as follows: 10 kV accelerating voltage, 200 pA beam current, with SE (secondary electron) detector and counting times of 40 seconds.

Figure 1.14. TESCAN GAIA3 Triglav SEM Device at Hacettepe University Advanced Technologies Application and Research Center (HÜNİTEK)

1.3.4 Inductively Coupled Plasma – Optical Emission Spectrometry / Mass Spectrometry (ICP-OES/MS)

Inductively Coupled Plasma - Mass Spectrometry (ICP-MS) is a technique developed in early 1980s (Cubadda, 2007) used to analyze the elemental composition of a material. The instrument heats the material with inductively coupled plasma to convert the atoms into ions and these ions are then evaluated by a mass spectrometer. It is widely used in chemical applications, material science, medical applications, forensic field, geology, and toxicology.

Inductively Coupled Plasma - Optical Emission Spectrometry (ICP-OES) is an analytical technique that is used for determination of chemical elements and heavy metals. It is also called as Inductively Coupled Plasma – Atomic Emission Spectroscopy (ICP-AES) in literature. The instrument creates excited atoms and ions by using plasma. Since every element emits electromagnetic radiation in specific wavelengths, magnitude of emission corresponds to the element concentration within the sample. This technique is preferred for determination of undesired metal content and used in biology, food engineering, forensics, and motor oil analysis but can also be used for determination of geochemical content of samples in geology and chemistry. Both methods can be used for analysis of various elements by adjusting parameter settings and an example approach is given in Table 1.2.

As both major, minor and trace elements are important for this study, both MS and OES were used. Main reason for using both techniques was to reveal element-element and mineral-element relationships as much as possible.

The elements detected by ICP-MS/OES in this study are demonstrated in Table 1.3. The elements given in bold characters were measured both by ICP-MS and ICP-OES.

Table 1.2. Parameter settings for sediment analysis by ICP-MS and ICP-OES (Wilhelms-Dick, 2012)

	ICP-MS	ICP-OES
Resolution	1 mm	1 mm
Device	Elan6000 Perkin Elmer/Sciex	Iris Intrepid Duo, Thermo
Plasma power	1100 W	1150 W
Nebulizer gas	Cross flow nebulizer, 0.76 l min^{-1}	Cyclonic spray chamber, 27 psi
Isotopes (ICP-MS), Elements (ICP-OES)	^{7}Li, ^{9}Be, ^{45}Sc, ^{51}V, ^{52,53}Cr, ^{58,60}Ni, ^{59}Co, ^{63,65}Cu, ^{66,68}Zn, ^{69}Ga, ^{75}As, ^{78}Se, ^{85}Rb, ^{86,88}Sr, ^{89}Y, ^{103}Rh, ^{107,109}Ag, ^{111,114}Cd, ^{138}Ba, ^{139}La, ^{140}Ce, ^{141}Pr, ^{142,143,144}Nd, ^{147,149}Sm, ^{151,153}Eu, ^{159}Tb, ^{160}Gd, ^{164}Dy, ^{165}Ho, ^{166}Er, ^{169}Tm, ^{174}Yb, ^{175}Lu, ^{205}Tl, ^{204,206,207,208}Pb, ^{209}Bi, ^{232}Th, ^{238}U	Na (589.5 nm), Al (396.1 nm), Mg (285.2 nm), P (178.2 nm), S (180.7 nm), Ca (315.8 nm), K (766.4 nm), Ti (336.1 nm), Mn (257.6 nm), Fe (259.9 nm), Zn (202.5 nm, 206.2 nm), Sr (407.7 nm), Ba (455.4 nm)
No. of replicate analysis	3	3

Table 1.3. Measured elements by ICP-MS/OES analyses in this study

Analysis Technique	Detected Elements	Units
ICP-MS	Hf, Y, La, Ce, Pr, Nd, Sm, Eu, Gd, Tb, Dy, Ho, Er, Tm, Yb, Lu, Th, Ga , As, Se, Rb, Cs, Pb, U, Zr, Nb, Mo, Ta, P, **V, Cr, Mn, Co, Ni, Cu, Zn, Sc, Sr, Ba**	ppm
ICP-OES	Si, Ca, Al, Fe, K, Na, Mg, P, S, Ti,	percent

In this study, a total of 149 samples were analysed by these two characterization techniques. Samples were pre-treated before the analysis just like bulk X-ray diffraction powders. 2 cm thick semicircle sub-samples were taken in every 6 centimeters along a core and 2/9 of these samples were packed as ICP samples. After packing, these wet samples were put in glass beakers and dried in 60 °C for 48 hours. Dried ICP samples were ground to form powders and these powder samples were sieved below 125 μm, and 5-10 grams of sieved material were packed for measurements.

ICP-MS/OES analyses were conducted by using these packed powder samples at Central Laboratory (MERLAB), Middle East Technical University. The ICP-MS device used in this study is Perkin Elmer NexION 350D the ICP-OES device is Perkin Elmer Optima 4300DV. The samples were digested after a four-step procedure in Anton Paar Multiwave 3000 Microwave Digestion System (Rotor type 8SXF100). First of all, 0.3 grams of powdered sample was weighed. Then, the powder was left to ramp for a total of 20 minutes (as three steps with 200, 500, and 800 W) after addition of 4 ml HNO_3, 2 ml HCl and 3 ml HF, and held for a total of 20 minutes. In the third step, 18 ml of 5% H_3BO_3 was added to the mixture and left to ramp for 5 minutes, followed by holding it for 15 minutes in 800 W. Finally, the solution was made up to 50 ml using de-ionized water.

The analyses were performed with a detection limit of 0.01-10 ppm. Three replicates were used in the analyses. Accuracy and precision of the measurement were controlled by using the standard deviation of the mean (SD) and the relative standard deviation (RSD) of replicate unknown samples and known reference materials. Relative standard deviation ranges between 0.1-40%.

1.3.5 Statistical Evaluation Methods

As X-ray diffraction is a semi-quantitative analysis technique, quantifying the data from XRD diffractometers is not a common approach. The method is mostly used for mineral characterization and determination of relative amounts of minerals from a powder sample. The intensity values obtained from diffractograms do not exactly correspond to the amount of a mineral but it can be clearly considered as the most effective parameter. The reasons for this uncertainty can be the difference in powder preparation processes, technical errors that may be caused by the analysis device and the threshold detection limit (about 5%) of XRD technique.

One of the main purposes of this study is to reveal element-mineral and mineral-mineral correlations. Hence, all preparation processes were performed very delicately. Each powder of a coring location was prepared by considering exactly the same standards and regular maintenances for the analysis device were arranged. Performance of the analysis device and the voltage fluctuation were checked before the analyses carefully. As the most dominant minerals may shadow or reduce intensities minor peaks, some large crystals of gypsum were removed from few Tayinat samples during the powder preparation process by labelling the exact locations of existence. Characterization of these large gypsum crystals were separately conducted by XRD (Figure 1.15).

After taking care of all these processes, it can be said that the intensity peaks reflected the mineral concentrations in the least possible erroneous way possible. Thus,

intensity values could be detected by taking the background fluctuations into consideration.

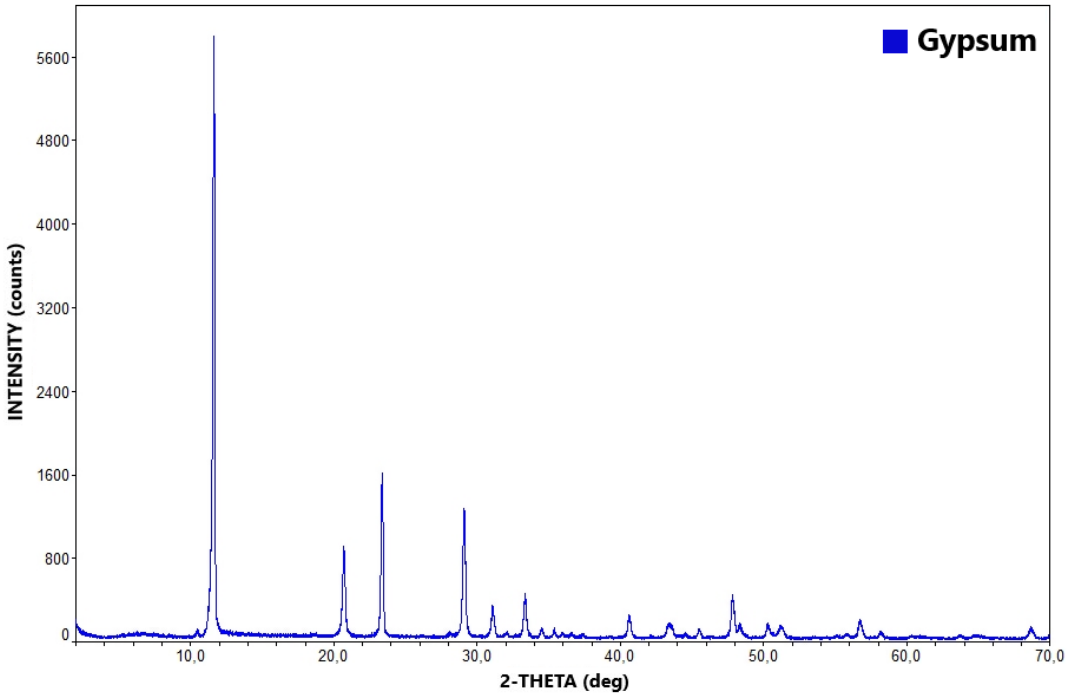

Figure 1.15. Bulk powder diffractogram of a removed large gypsum crystal from TA-2 577

As the XRD interpretation software demonstrated some important mistakes in background determination, backgrounds of each diffractogram were drawn manually using the MapInfo Pro software. MDI Jade software has drawn the backgrounds of bulk powder diffractograms mistakenly especially for 0-20° 2θ, which might cause misinterpretation of clay mineral and serpentine peaks. While intensity error range of automatically and manually obtained intensity values was determined to vary up to 250 counts for the peaks between 0-20° 2θ values, this error range decreases to a maximum of 50 counts for the peaks obtained after 20° 2θ. Diffractograms were registered as rasters to the software and y-axis coordinates were defined with respect to the intensity scale and x-axis coordinates were defined with respect to 2θ values. In order to draw backgrounds, by taking every diffractogram into consideration one by one, 15 special points of stability where no intensity or noise peaks were observed

were determined. Therefore, backgrounds were drawn below diffractograms by forming a polyline made of 15 nodes (Figure 1.16).

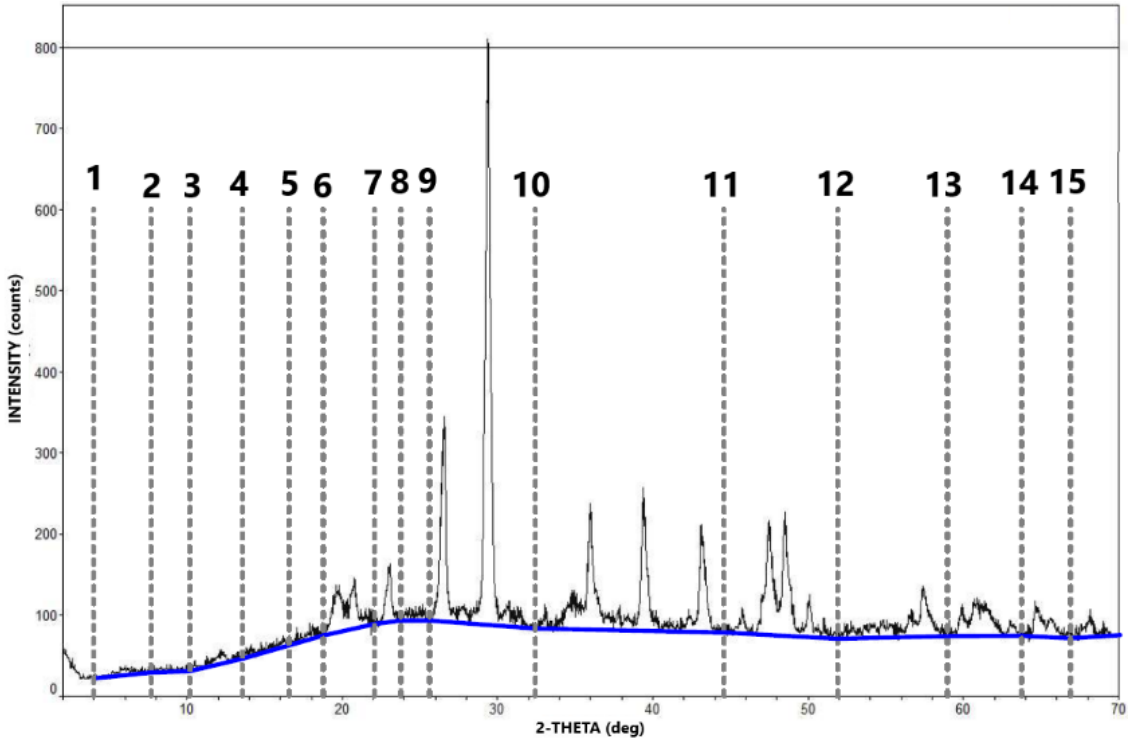

Figure 1.16. An example of background drawing by using MapInfo Professional (Grey dashed lines represent locations of 15 nodes and blue polyline is the background)

After that, intensities were quantitatively obtained by defining two points for each peak observed; one to the top of the peak and one to the intersection with the background. To perform an unbiased determination, every single peak including possible noises were taken into consideration without checking ASTM cards, and a total of 65 peak locations were defined. Later, it was revealed that 14 of these locations are noises. The numerical data were extracted by coordinate extractor tool and intensities of these 65 peaks were identified through the difference between two points defined.

After obtaining quantitative intensity data from the software, Microsoft Excel was used to observe distribution of mineral intensities. This method made mineral

characterizations easier since anomalous results were clearly observable on scatter charts (Figure 1.17).

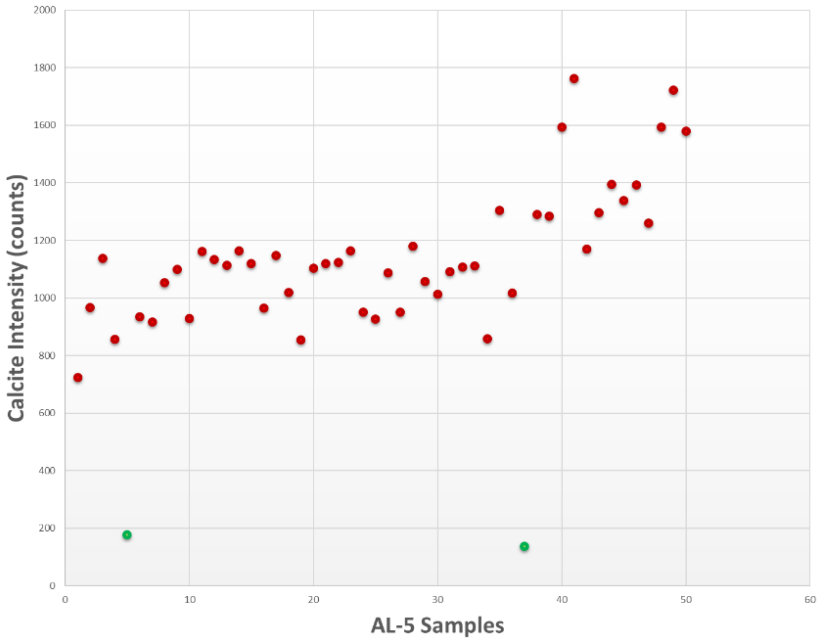

Figure 1.17. Scatter chart of calcite intensities in lake (AL-5) samples that demonstrates two scattering anomalies (shown in green) clearly

By registering these intensity values to SPSS software, correlation analyses were conducted. For correlation of both XRD and ICP-MS/OES data, correlation matrices were formed primarily. As coefficient matrices show the relation between different variables (mineral intensity data and element concentration data in this case) overtly, this statistical method was quite useful for this study.

Multivariate statistical analysis techniques were considerably beneficial for evaluation of such variable data. Principal Component Analysis (PCA), a common method for correlation of geochemical elemental data, was also used in this study. Each data were transformed into component matrices by using SPSS software and defined components were analysed for correlations. Hence, determination of noises and mineral peaks among the pre-defined 65 peak locations got easier and different PCA graphs were obtained. By using these two statistical techniques, mineralogical and geochemical variations and correlations were identified in this study.

CHAPTER 2

LITERATURE REVIEW

Amuq Valley has been an important study area for geoscientists and archaeologists as it hosts both geological and archeological records of Holocene epoch. The first archaeological studies in Amuq Valley were conducted between 1933-1938 by Robert John Braidwood (Braidwood, 1937) and James Henry Breasted and after the studies conducted between 1995-2016, existence of more than 400 archaeological sites has revealed within the study area (Yener, 2005; Gerritsen et al., 2008).

Along with many other archaeological publications about the region (Braidwood and Braidwood, 1960; Haines, 1971; Friedman and Reichel, 1995; Yener et al., 2000; Diebold, 2004; Özbal, 2006; De Giorgi, 2007; Harrison, 2009; Durusu Tanrıöven, 2010; Akar and Kara, 2018; Akar and Kara, 2020; Ingman et al., 2020), geoarcheological publications (Wilkinson, 2000; El Ouahabi, 2017; Avşar et al., 2019) have also contributed to the literature.

2.1 Literature Review on Regional Geology

In archeology, geological history plays significant role. Thus, studies on regional geology of the Amuq Valley region should be known. The area was studied by main geologists. Atan (1969) mapped the region geologically and stated the details about geological features of Amanus Mountains. He investigated Kızıldağ ophiolites structurally and petrologically. Çoğulu (1973 & 1974) studied the genesis of Kızıldağ ophiolites. He emphasized that the massive has anticlinal structure and formed after oceanic spreading. Tinkler et al. (1981) examined the structural relation between Kızıldağ ophiolite and its surroundings and prepared geological sections of

the region. Tekeli & Erendil (1986) stated that the ophiolites consist of peridotites, gabbros, dikes, and volcanic complexes. He also identified the columnar section of Amanus mountains (Figure 2.1).

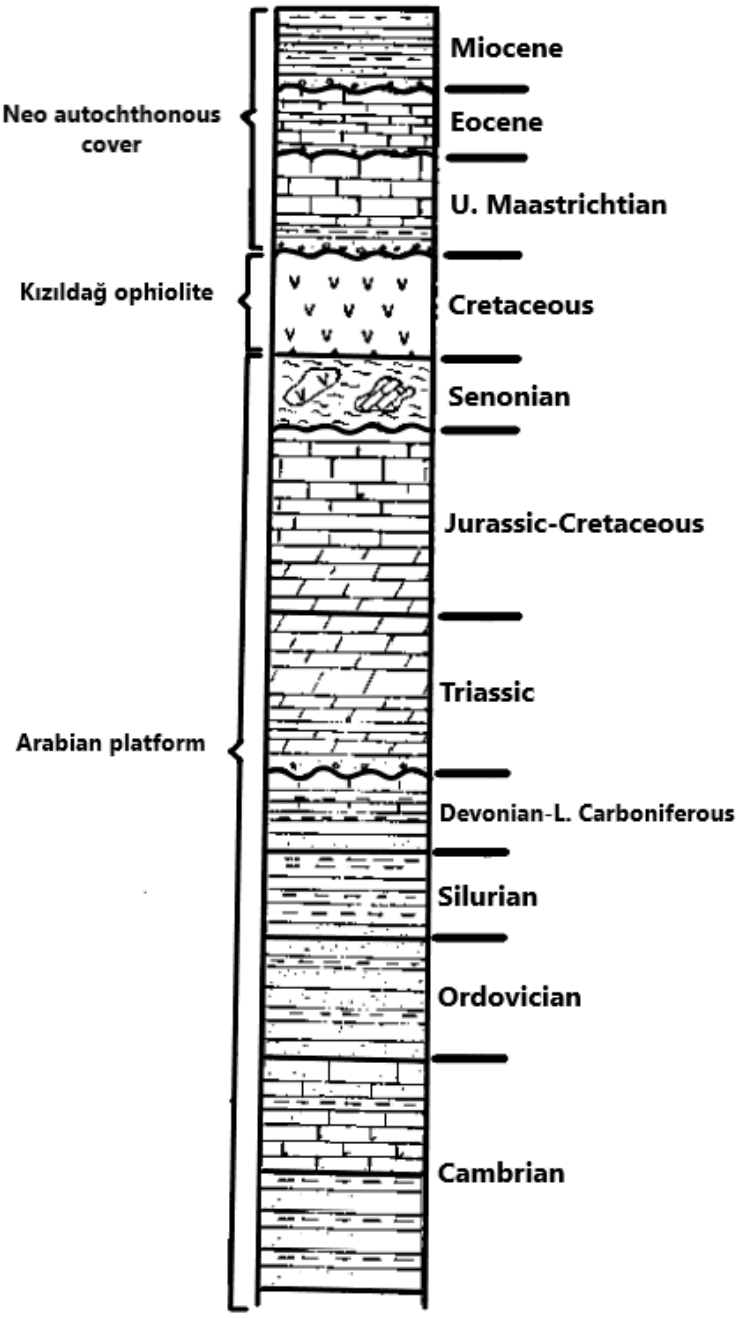

Figure 2.1. Columnar section of Amanus Mountains (Tekeli & Erendil, 1986)

Perinçek & Eren (1990) interpreted the genesis of Amuq Valley structurally. They denoted that the main reason of formation of the valley is SW-directional drift of the block of Gulf of Alexandretta. Sigal & Kafesçioğlu (1963); Sirel & Gündüz (1978); Decrouez & Selçuk (1981); Şafak (1993); Karakuş & Taner (1994) paleontologically investigated the region.

Yılmaz et al. (1988) stated that the Middle Miocene deposits around Amanus Mountains were products of complex orogenic transportation of a pre-existing marine environment. Coşkun (1994) found that Amuq Valley is not a faulted anticline but a triangular zone. Över et al. (2001) studied the tectonics in Hatay between Plio-Quaternary and Holocene. He simplified the map of major tectonic structures in Turkey and adjacent areas which was previously done by Şengör (1979) and Koçyiğit & Beyhan (1998).

Kop (1996) and Rojay et al. (2001) studied geochemistry, petrology, and genesis of Quaternary basalts of Karasu Graben and formation of northern Karasu rift. Rojay et al. (2001) visualized the distribution of Quaternary basaltic volcanics within the rift system by stating K-Ar radiometric ages (Figure 2.2). Yalangöz basalts (denoted as "4" in Figure 2.2), the southernmost volcanics in the rift, are located on the northeast of Tell Kurdu.

Mıstık (2002), Zorlu (2003), Temizkan (2003), and Kocaçiftçi (2005) examined petrology and tectono-stratigraphy of Mesozoic-Cenozoic formations in the vicinity of Antakya-Samandağ region. Kavuzlu (2006) studied the petrology, stratigraphy, and structural geology of the region.

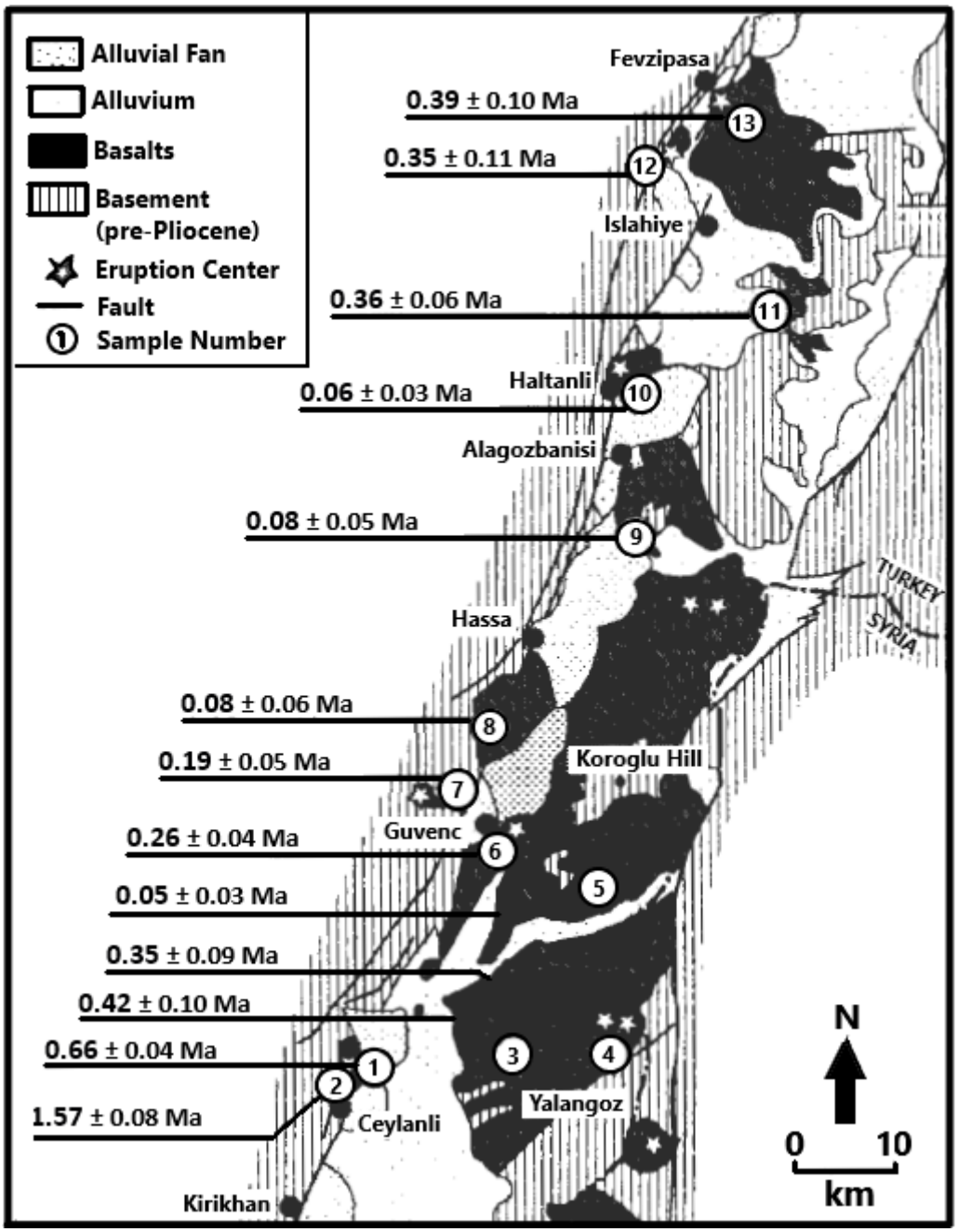

Figure 2.2. Distribution of Quaternary basalts of Karasu Rift and their K-Ar radiometric age dating (Rojay et al., 2001)

2.2 Literature Review on Analytical Methods for Sediments and Statistical Evaluation

The inorganic composition of a lacustrine deposit may be expressed in terms of either geochemistry or mineralogy (Last, 2011). However, as pointed out by others (Potter et al., 1980; Prothero and Schwab, 1996), having a knowledge about geochemistry without defining the mineralogy is not scientifically sufficient since describing a sediment using bulk chemistry may be misleading. Especially in lake studies, collecting mineralogical data is a must to reconstruct the geological history.

Elemental analyses, which can consist either of non-destructive methods like X-Ray Fluorescence (XRF) or destructive methods like Inductively Couple Plasma - Optical Emission Spectroscopy (ICP-OES), form a significant complement to mineralogical analyses (Fairchild et al., 1988; Hawthorne, 1988; Amonette and Sanders, 1994; Sawnhey and Stillwell, 1994).

In oriented slide sample preparation process for X-Ray diffraction analyses, there are many possible methods like smearing (Bradley et al., 1937; Barshad, 1960; Theisen and Harward, 1962; Gibbs, 1965; Tien, 1974) and using pipette on slide (Nagelschmidt, 1941; Jackson, 1969) in literature.

Mineralogical and geochemical data were used together in many papers of geology and material science, and the most preferred area of usage is characterization. Mineralogical studies were carried out mostly by XRD. X-Ray fluorescence (XRF) was preferred more than ICP-MS/OES for geochemical analyses because XRF is a non-destructive method unlike ICP, it is cheaper and more practical for undetailed geochemical investigations. ICP-MS/OES is mostly preferred when trace element concentrations are needed in a study.

Some researchers used both ICP and XRF techniques for elemental characterization. For instance, Yalçın & Mutlu (2012) and Gerke et al. (2009) used XRD together with both ICP and XRF for mineral characterization and identification. Moyo et al. (2016) used these three techniques for differentiation purposes, and Griggs et al. (2010)

preferred ICP-MS for differentiation analysis. Ogwuegbu et al. (2011), Zhu et al. (2019), Eren et al. (2015) and Sheppard et al. (2019) used XRD and ICP for mineral characterization. Li et al. (2016) used XRD and ICP together for determination of geological controls. Fytianos et al. (2016) used XRD and ICP for corrosion evaluation.

Kabala & Bojko (2014) used ICP-MS for determination of trace element trends in lacustrine sediments and made statistical correlations but they did not conduct mineralogical analyses. They defined two principal components, Factor 1 and Factor 2, representing the sediment texture and the organic matter respectively and demonstrated the relationship between trace elements (Cu, Ca, Na, Zn, Cd, Mg, Fe, Pb, K, Mn, Cr, and Ni) and some physicochemical properties of bottom sediments of Lake Wielski Staw in Karkonosze Mountains in Poland. Moreover, Zhu et al. (2004) preferred XRD analysis on pottery samples, and used multivariate statistical analysis techniques like cluster analysis and principal component analysis.

CHAPTER 3

RESULTS

3.1 Mineralogical Characterization

Mineralogical characterization was mainly conducted by XRD analyses in this study. Moreover, mineral contentswere also defined by SEM-EDS (in four representative lake samples) as a complementary analysis. Non-clay minerals were identified from bulk powder samples by using MDI Jade software. Search and match hits obtained from this software were also manually checked one-by-one considering the ASTM cards of minerals.

Sample displacement calibrations were done with respect to the first calcite peak (d=3.04 Å) as it was the most intense and the most common peak in almost all samples. At some depths, mostly in the samples from Tell Kurdu (KR-1), quartz gets more dominant than calcite. However, first calcite peaks are clearly observable in these samples too. Sampling depths from the cores are shown in Table 3.1.

Table 3.1. Sampling depths from the cores and total number of samples

CORE	SAMPLING INTERVAL	TOTAL SAMPLES
AL-5	1-397 cm in every 12 centimeters	50 samples
	433-973 cm in every 36 centimeters	
KR-1	1-217 cm in every 12 centimeters	41 samples
	253-1009 cm in every 36 centimeters	
AT-1	1-217 cm in every 12 centimeters	36 samples
	253-829 cm in every 36 centimeters	
TA-2	1-757 cm in every 36 centimeters	22 samples

3.1.1 Mineralogical Characteristics of Amuq Lake

In the AL-5 core samples, quartz, calcite, aragonite, serpentine, feldspar and clay minerals are present. Overall mineralogy of lake samples by XRD is given Figure 3.1. For a clear demonstration, maximum three peaks of each mineral is shown on the figure by taking the ASTM cards into consideration. All random diffractograms are smoothened by taking the Savitsky-Golay parabolic filter of 35 points as a standard for noise elimination and better visualization of peaks. IMA-CNMNC approved mineral symbols (Warr, 2021) were used in Figure 3.1.

Calcite and quartz are the most dominant minerals in the lake samples. In all depths, major peaks of these two minerals are clearly observable, and show high intensities but calcite intensity is always higher than quartz with two exceptions (AL-5 049 and AL-5 505) which will be discussed in Chapter 4.2. At some depths, aragonite was detected along with calcite. First aragonite peak (d=3.40 Å) demonstrate higher intensities in bulk powder XRD of the lake samples.

Feldspar is also common but unstable in the lake samples. As various feldspar types were observed in bulk powder diffractograms, all of them are going to be named as feldspars in general. These feldspar peaks represent all the albite, disordered albite, anorthite, orthoclase. All peaks of a feldspar mineral could not be observed clearly from bulk powder diffractograms due to probable effects of alteration. As clay minerals may form as alteration products of aluminosilicates like feldspar (Daneshvar & Worden, 2017) and gismondine may form after alteration of plagioclase feldspars (Walker, 1962), existence of such minerals may support this theory. While various clay minerals exist in all samples, gismondine peak (d=3.19 Å) was also observed in few samples.

Serpentine content is also significant throughout the core but intensity values of serpentine peaks vary more than other minerals in the lake samples. Most of the serpentine content is determined to be lizarditic (Mg-rich).

In bulk powder XRD diffractograms of the lake samples, a hump pattern distributed in a wide range of 2θ (from 10° and 40°) infer presence amorphous material, probably silica. This hump pattern in the samples AL-5 049 and AL-5 505 is so intense that may infer higher amount of amorphous material.

Moreover, clay mineral peaks in bulk powder diffractograms are significant in AL-5 with varying intensities.

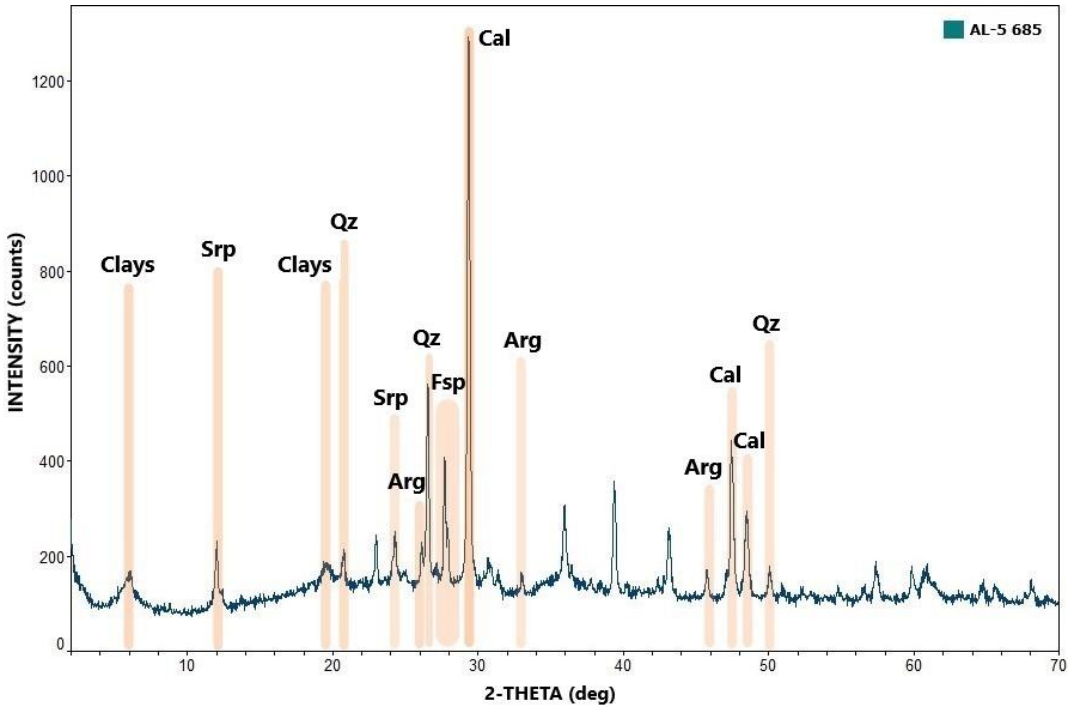

Figure 3.1. Mineralogically labelled bulk powder XRD diffractogram of AL-5 685 to reflect overall mineralogy of the lake samples (Srp: serpentine, Qz: quartz, Cal: calcite, Arg: aragonite, Fsp: feldspars)

Figure 3.2, which includes air-dried, ethylene glycolated, heated at 300 °C and 550 °C oriented clay fraction diffractograms, visualizes a representative overall clay mineralogy of the lake samples. XRD analyses on clay fraction of the lake samples from oriented slidesshowed that AL-5 samples mainly include smectites and serpentine (lizardite) with less kaolinite, illite, and chlorite as clay minerals (Figure 3.2). Smectite is the most dominant clay mineral along the core from Amuq Lake.

Since some clay peaks disappear, smoothening operation was not applied on oriented sample diffractograms. XRD diffractograms of the lake samples are given in Appendices A and B.

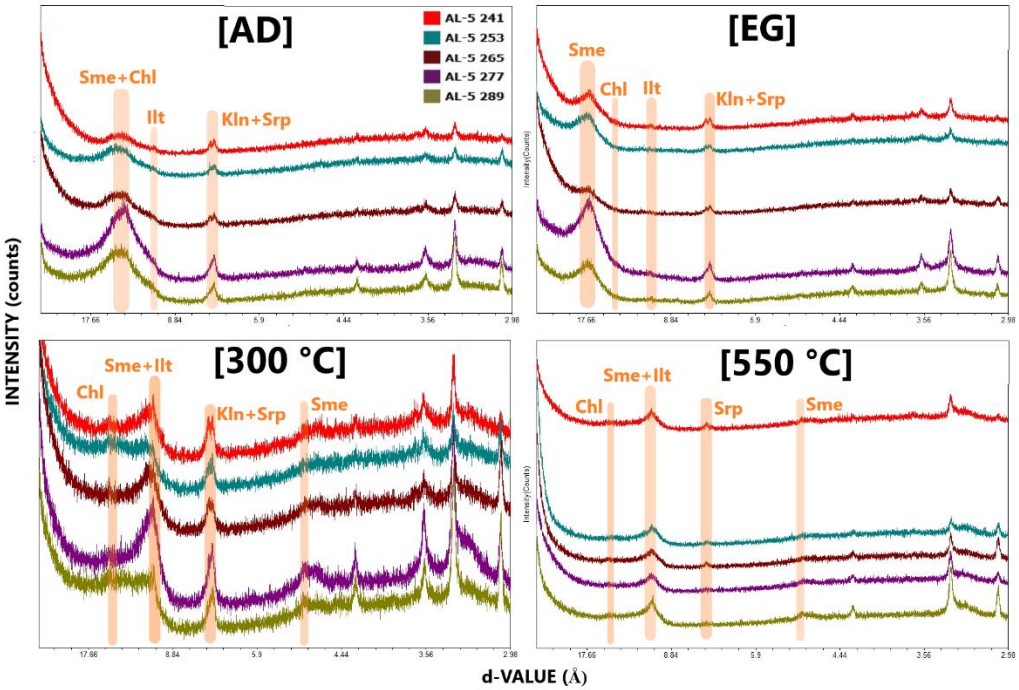

Figure 3.2. Clay fraction XRD diffractogram sets measured from oriented slides of five representative samples (Red: AL-5 241, Blue: AL-5 253, Brown: AL-5 265, Purple: AL-5 277, Green: AL-5 289) from the AL-5 core (Sme: smectite, Ilt: illite, Kln: kaolinite, Chl: chlorite, Srp: serpentine)

In addition to XRD analyses, few samples were examined by SEM-EDS technique. The SEM-EDS study displayed that smectite type is in the samples are montmorillonite (Figure 3.3).

SEM analyses on the lake samples revealed that significantly high amount of diatom is present. Many diatoms were observed in the four samples selected for SEM-EDS analyses (Figure 3.4). Especially AL-5 049 and AL-5 505 consist of extreme amounts of diatoms. Chemical composition of these diatoms were measured by EDS and showed high amounts of Si (Figure 3.5). Presence of diatom in the samples supports a hump pattern on XRD diffractograms. Moreover, large broad hump for

the samples AL-5 049 and AL-5 505 clearly explain higher abundance of diatom observed in SEM-EDS study.

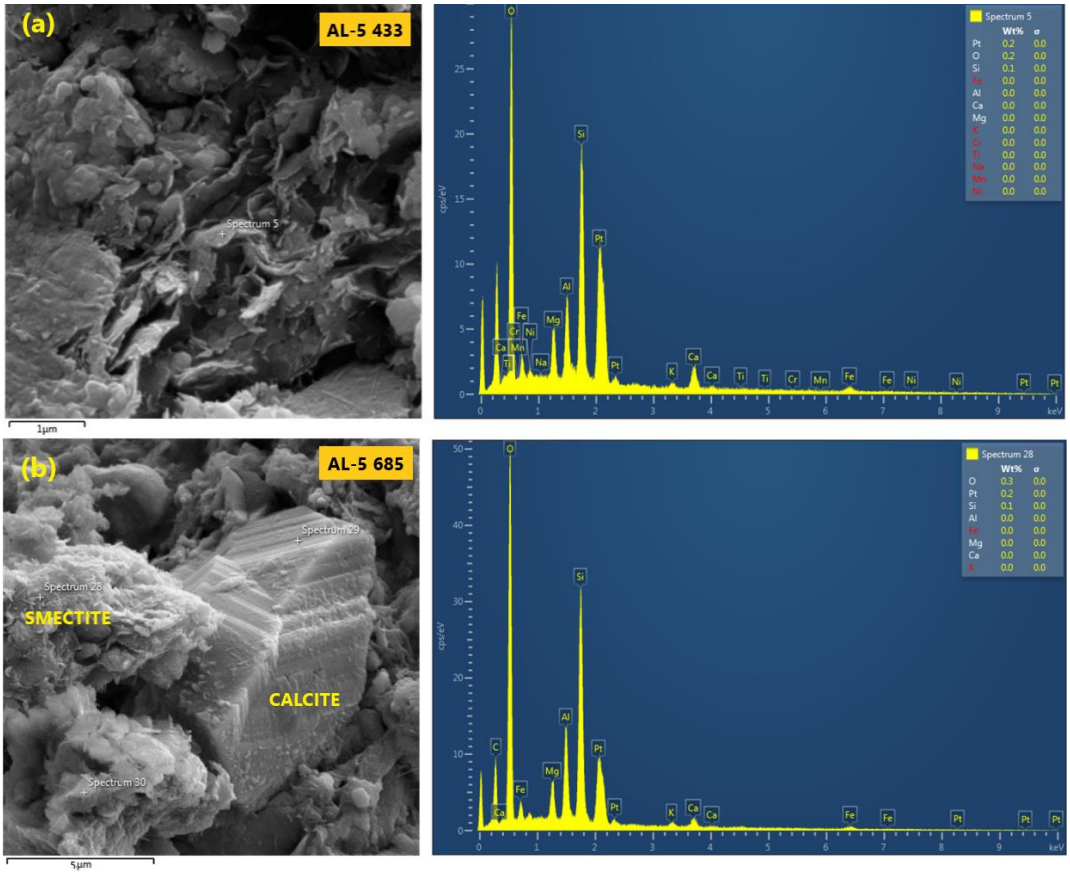

Figure 3.3. SEM images of smectite observed in (a) AL-5 433, and (b) AL-5 685 with their EDS patterns

Furthermore, SEM-EDS analyses revealed existence of dolomite within some lake samples (Figure 3.6). As bulk powder XRD diffractograms do not reflect dolomite peaks in most lake samples but they are observed in SEM images, it can be interpreted that dolomite content is too low in these samples.

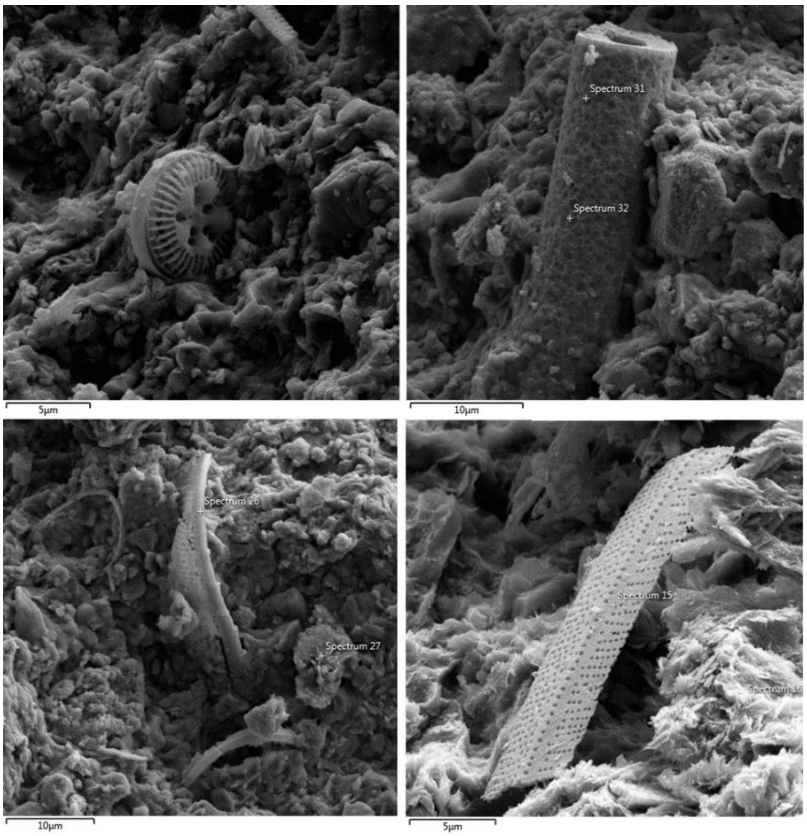

Figure 3.4. SEM images of diatoms observed in lake samples

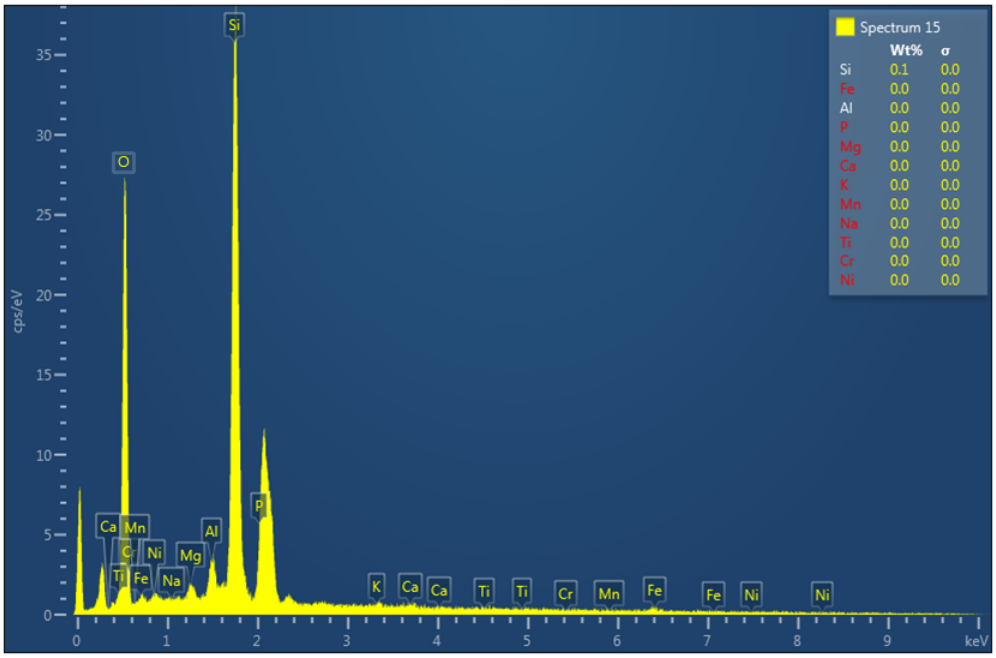

Figure 3.5. Chemical composition of a diatom in AL-5 505 measured by EDS

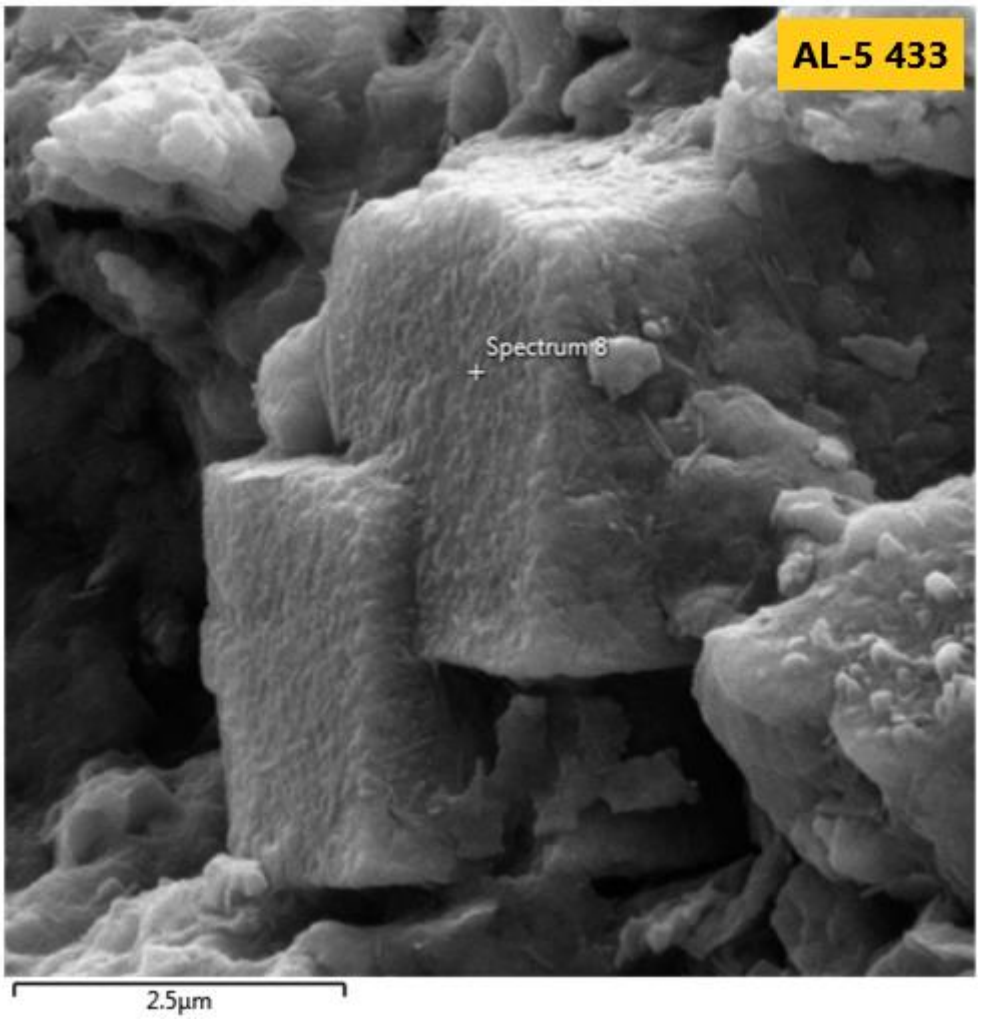

Figure 3.6. SEM image of dolomite observed in AL-5 433

3.1.2 Mineralogical Characteristics of Floodplains

3.1.2.1 Mineralogical Characteristics of Tell Kurdu

The samples from Tell Kurdu have similar mineral content. Bulk powder XRD diffractograms of five representative sample with all minerals identified are given in Figure 3.7. XRD diffractograms were smoothened and notation of sequent peaks was omitted in the same way with the lake sample diffractograms for clear-cut presentation.

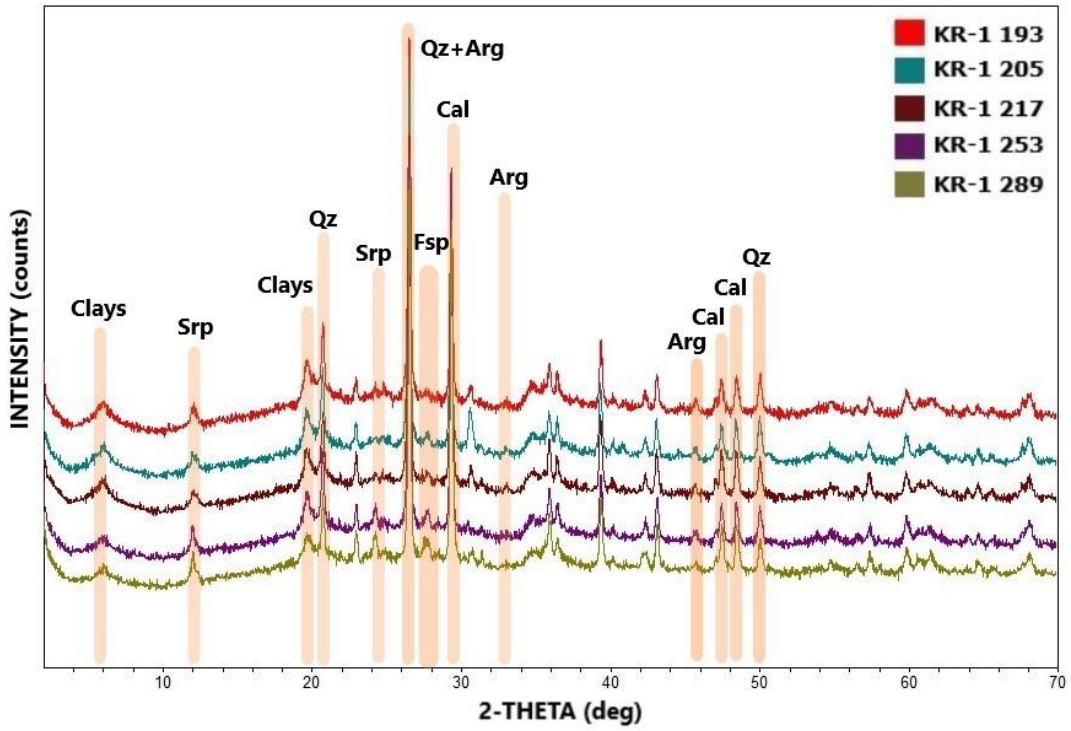

Figure 3.7. Bulk powder XRD diffractograms of five representative samples from Tell Kurdu (Red: KR-1 193, Blue: KR-1 205, Brown: KR-1 217, Purple: KR-1 253, Green: KR-1 289) to show overall mineral content of the samples (Srp: serpentine, Qz: quartz, Cal: calcite, Arg: aragonite, Fsp: feldspars)

In the KR-1 core samples, quartz, calcite, aragonite, serpentine, feldspar and clay minerals, are present. Intensities of quartz peaks are usually higher than calcite peaks along the core. Aragonite peaks are not as sharp as the lake samples, and there are many aragonite peaks observed as shoulders.

Serpentine amount seems to be higher than the lake samples in random XRD diffractograms if intensities of the serpentine peaks are considered. The peaks of serpentine in the Tell Kurdu samples reflect lizarditic (Mg-rich) type similar to that observed in the lake samples.

Various feldspar peaks such as albite, disordered albite, anorthite and orthoclase are observed in the bulk powder diffractograms of the KR-1 core samples. All these feldspars are going to be notated as feldspars. Clay mineral peaks and a few

gismondine peaks (d=3.19 Å) are also observable like the lake samples. Feldspar peaks in the Tell Kurdu samples have higher intensities than other alluvial study areas (Tell Atchana and Tell Tayinat) and Amuq Lake (see sections 3.1.2.2, 3.1.2.3, and 3.1.1, respectively).

Clay mineral intensities on the bulk powder XRD diffractograms are not as stable as in the lake sediments, and there is a significant variation among the samples.

XRD analyses on the oriented clay fraction slides displayed that the KR-1 samples include smectite (montmorillonite), illite, kaolinite and serpentine (lizardite) as clay minerals (Figure 3.8). XRD patterns of oriented clay fraction (AD, EG, heated at 300 °C and 550 °C) for the five representative samples from Tell Kurdu are given in the Figure 3.8. while patterns for the rest of samples from the KR-1 core are given in Appendices A and B. Intensity of montmorillonite peaks vary along the KR-1 core, and this variation can also be observed through clay peaks on the bulk powder XRD diffractograms.

As mentioned in the methodology section, the alluvial mound samples required extra acetone treatment in order to prevent swelling of montmorillonites on glass slides. However, it was denoted that during the preparation of oriented clay fraction glass slides, some samples from the higher depth did not swell. Nevertheless, not swelling samples were also treated with the same procedure to preserve the preparation in a standard way. It was also noted that the increase in serpentine intensities is shadowed by non-clay minerals left in the clay fractions which were smeared. It can be interpreted as a disadvantage of preferred modified slide preparation process to prevent swelling.

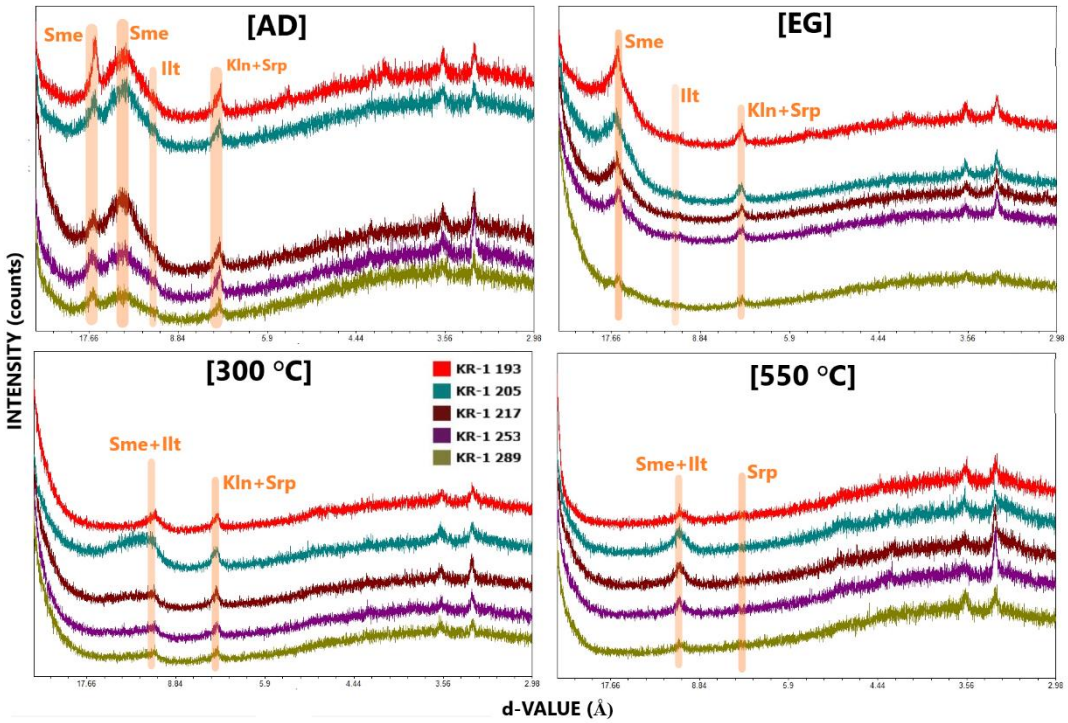

Figure 3.8. Clay fraction XRD diffractograms of five representative samples (Red: KR-1 193, Blue: KR-1 205, Brown: KR-1 217, Purple: KR-1 253, Green: KR-1 289) from the KR-1 core (Sme: smectite, Ilt: illite, Kln: kaolinite, Srp: serpentine)

3.1.2.2 Mineralogical Characteristics of Tell Atchana

The Tell Atchana mound is present on alluvial deposits like Tell Kurdu. The borehole AT-1 is from Tell Atchana. The AT-1 core samples include quartz, calcite, aragonite, serpentine, feldspar and clay minerals like the KR-1 core samples (Figure 3.9). XRD analyses on the bulk AT-1 powder samples displayed that the most dominant mineral in the Tell Atchana area is calcite. The difference between calcite and quartz peak intensities is remarkably higher than those in the core samples from the Amuq Lake and Tell Kurdu even though quartz peaks were well observed in all samples. Low intensity aragonite peaks also exists in almost all samples with only a few exceptions. Serpentine in the Tell Atchana samples are determined to be lizarditic (Mg-rich).

Moreover, intensities of clay minerals seem to be stable along the core with few exceptions. Figure 3.9 demonstrates the overall mineralogy in Tell Atchana.

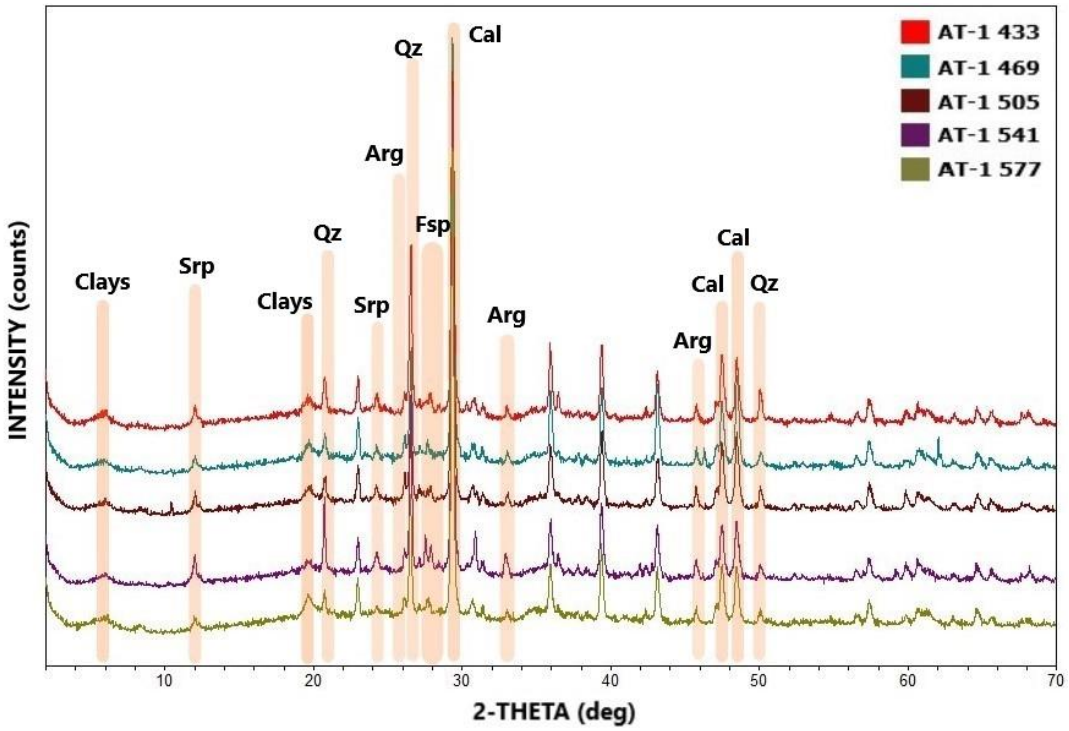

Figure 3.9. Bulk powder XRD diffractograms of five representative samples from Tell Atchana (Red: AT-1 433, Blue: AT-1 469, Brown: AT-1 505, Purple: AT-1 541, Green: AT-1 577) to show overall mineral content of the samples (Srp: serpentine, Qz: quartz, Cal: calcite, Arg: aragonite, Fsp: feldspars). Bulk powder diffractograms are smoothened and notation of sequent peaks is omitted.

XRD analyses on the oriented slide samples of clay fractions of AT-1 showed that the clay minerals are mainly smectite (montmorillonite) and kaolinite (Figure 3.10). Illite, chlorite and serpentine peaks are poorly developed in these samples. Especially, while d≈7 Å peaks, which correspond to kaolinite and serpentine, exhibit high intensity in AD, EG and 300 °C diffractograms, almost all peaks collapse in 550 °C diffractograms which proves relative absence of serpentine in the AT-1 core samples. Oriented slide preparation process is modified for these samples to avoid swelling of montmorillonite just like the ones in Tell Kurdu. XRD patterns of the

oriented clay fractions for five representative samples are given in Figure 3.10 and patterns for rest of the AT-1 samples are given in Appendices A and B.

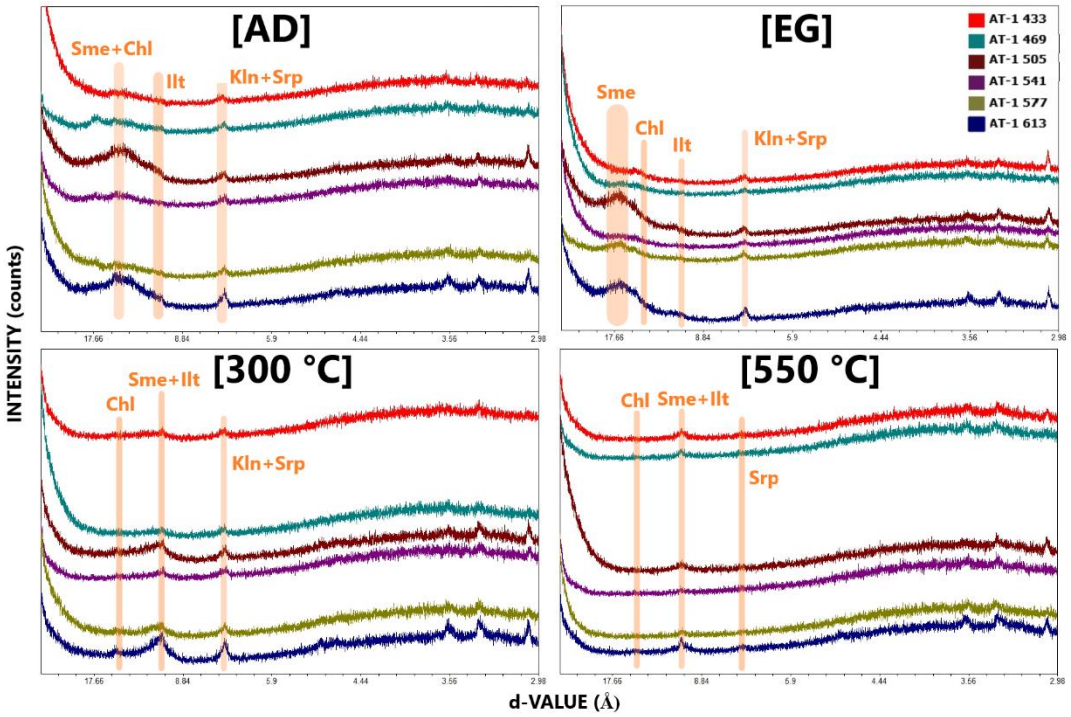

Figure 3.10. Clay fraction XRD diffractograms of six representative samples (Red: AT-1 433, Light Blue: AT-1 469, Brown: AT-1 505, Purple: AT-1 541, Green: AT-1 577, Dark Blue: AT-1 613) from the AT-1 core (Sme: smectite, Ilt: illite, Kln: kaolinite, Srp: serpentine, Chl: chlorite)

3.1.2.3 Mineralogical Characteristics of Tell Tayinat

The Tell Tayinat mound is geographically close to Tell Atchana mound that brought out close coring locations (Figure 3.11). Therefore, mineralogy of the core samples from these two locations was expected to be similar.

The TA-2 core samples have quartz, calcite, aragonite, serpentine, feldspar and clay minerals like the AT-1 core samples (Figure 3.12). Calcite is the most dominant mineral in Tell Tayinat (TA-2) like the samples from Tell Atchana (AT-1). Well-developed quartz peaks were also observed in all samples. The intensity difference

between calcite and quartz peaks are very high just as in the Tell Atchana samples. Aragonite exists within all samples with varying intensities. In this area, serpentine peaks are poorly developed which are lizarditic (Mg-rich) as the ones in other cores. On the bulk powder diffractograms, clay mineral intensities seem to be stable along the core.

Figure 3.11 Borehole locations in Tell Tayinat and Tell Atchana, and location of Tell Atchana Excavations and Amuq Valley Research Center (AHAM) (from Google Earth)

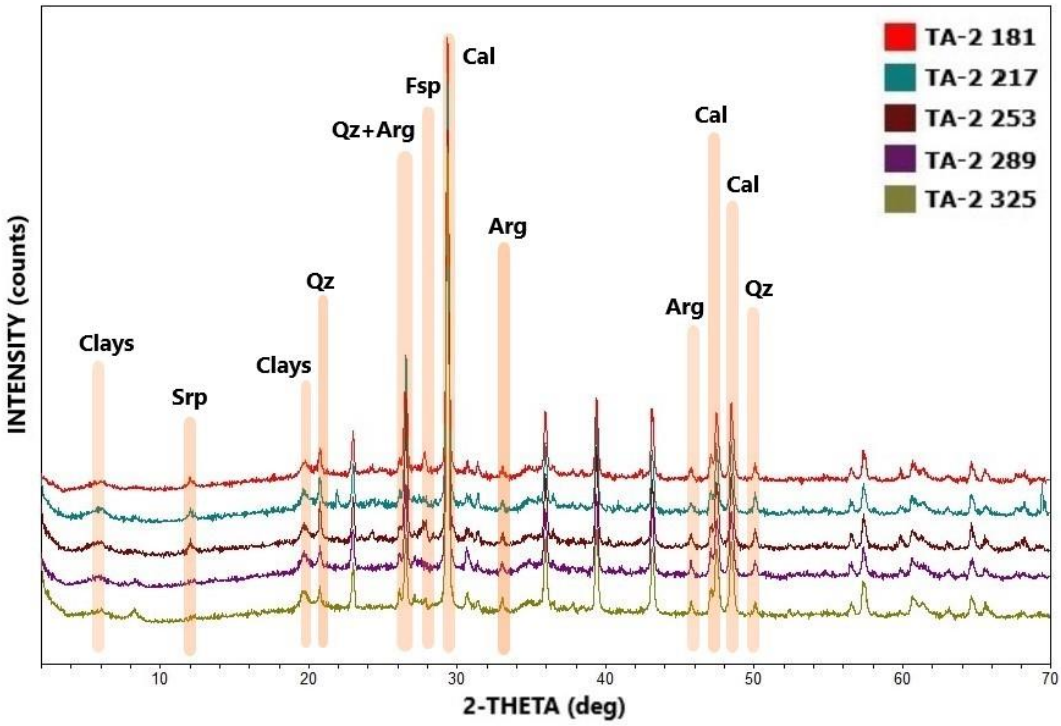

Figure 3.12. Bulk powder XRD diffractograms of five representative samples from Tell Tayinat (TA-2) to show overall mineral content of the samples (Srp: serpentine, Qz: quartz, Cal: calcite, Arg: aragonite, Fsp: feldspars). Bulk powder diffractograms are smoothened and notation of sequent peaks is omitted.

Clay minerals in the TA-2 are smectite (montmorillonite), kaolinite, serpentine (lizardite), chlorite, and illite (Figure 3.13). While montmorillonite and kaolinite demonstrate peaks of higher intensities, content of illite and serpentine seems to be low in these samples. XRD patterns of the oriented clay fractions for five representative samples are given in Figure 3.13 and patterns for rest of the TA-2 samples are given in Appendices A and B. As chlorite only exists in few samples of TA-2 core with very low intensity, it was neglected in overall clay mineralogy demonstration in Figure 3.13.

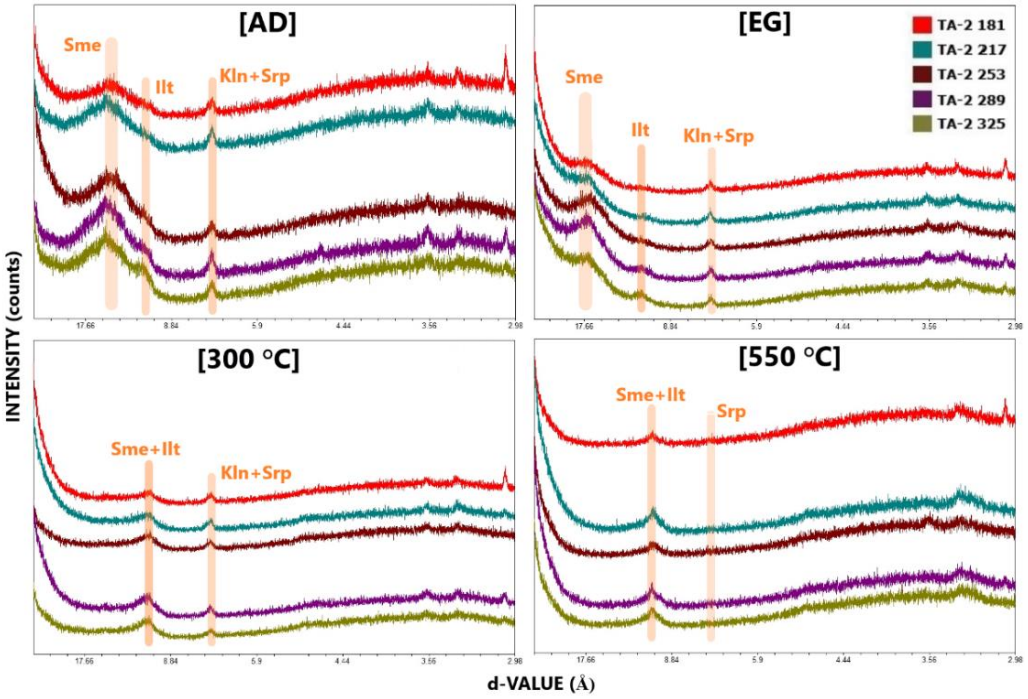

Figure 3.13. Clay fraction XRD diffractograms of five representative samples (Red: TA-2 181, Blue: TA-2 217, Brown: TA-2 253, Purple: TA-2 289, Green: TA-2 325) from the TA-2 core (Sme: smectite, Ilt: illite, Kln: kaolinite, Srp: serpentine)

The hump pattern that reflect amorphous silica also present in almost all bulk powder diffractograms of the floodplain samples (KR-1, AT-1, TA-2 cores). The amorphous silica was observed as diatom by SEM-EDS study on the lake samples as explained above. Since the floodplain samples were found to include the same minerals with the lake samples by XRD analyses in the region, no SEM-EDS analyses were conducted on the floodplain samples.

3.2 Geochemical Characterization

ICP-MS and ICP-OES analyses were conducted on the same samples of the cores taken from Amuq Lake, Tell Kurdu, Tell Atchana and Tell Tayinat (Table 3.1). Measured elements are given in Table 1.2. The main purpose of geochemical analyses is to determine overall elemental concentrations along the cores. By

determination of concentrations, statistical evaluations were done and anomalies within prepared samples were detected. Distribution of elemental concentrations along the lake and floodplain samples are visualized by scatter charts that are briefly interpreted in this chapter.

3.2.1 Geochemical Characteristics of Amuq Lake

ICP-MS/OES measurements on 50 AL-5 samples revealed that the most abundant element occurrences in the Amuq Lake samples are Ca, Si, Al, Fe, Mg, S, K, Ti, and Na (Figure 3.14). Calcium concentration along the core varies between 11-27 wt% with two exceptional samples, AL-5 049 and AL-5 505. These two samples oppositely show extreme enrichment in silicon that has range of 6 wt% and 18 wt% in general. Iron and aluminum concentrations vary in narrow ranges of 1.4-4.5 wt% and 1.5-5 wt%, respectively. It is denoted that while AL-5 505 has anomalous Al content, AL-5 049 does not. As these two samples display anomalies in some other scatter plots, the reason of discordance was examined in discussion part.

Magnesium concentration varies between 1.3-3.2 wt% with another exceptional sample, AL-5 685. When random diffractogram of this sample was examined, it was seen that peaks of serpentine, clay minerals, and feldspars are more intense than the other lake samples which explains the Mg anomaly.

Potassium concentration varies between 0.2-0.8 wt%, and only AL-5 505 shows a slight anomaly with relatively higher concentration. Titanium and sodium contents range between 0.1-0.35 wt%. AL-5 505 exhibits distinctness with respect to other lake samples in these two element concentrations too.

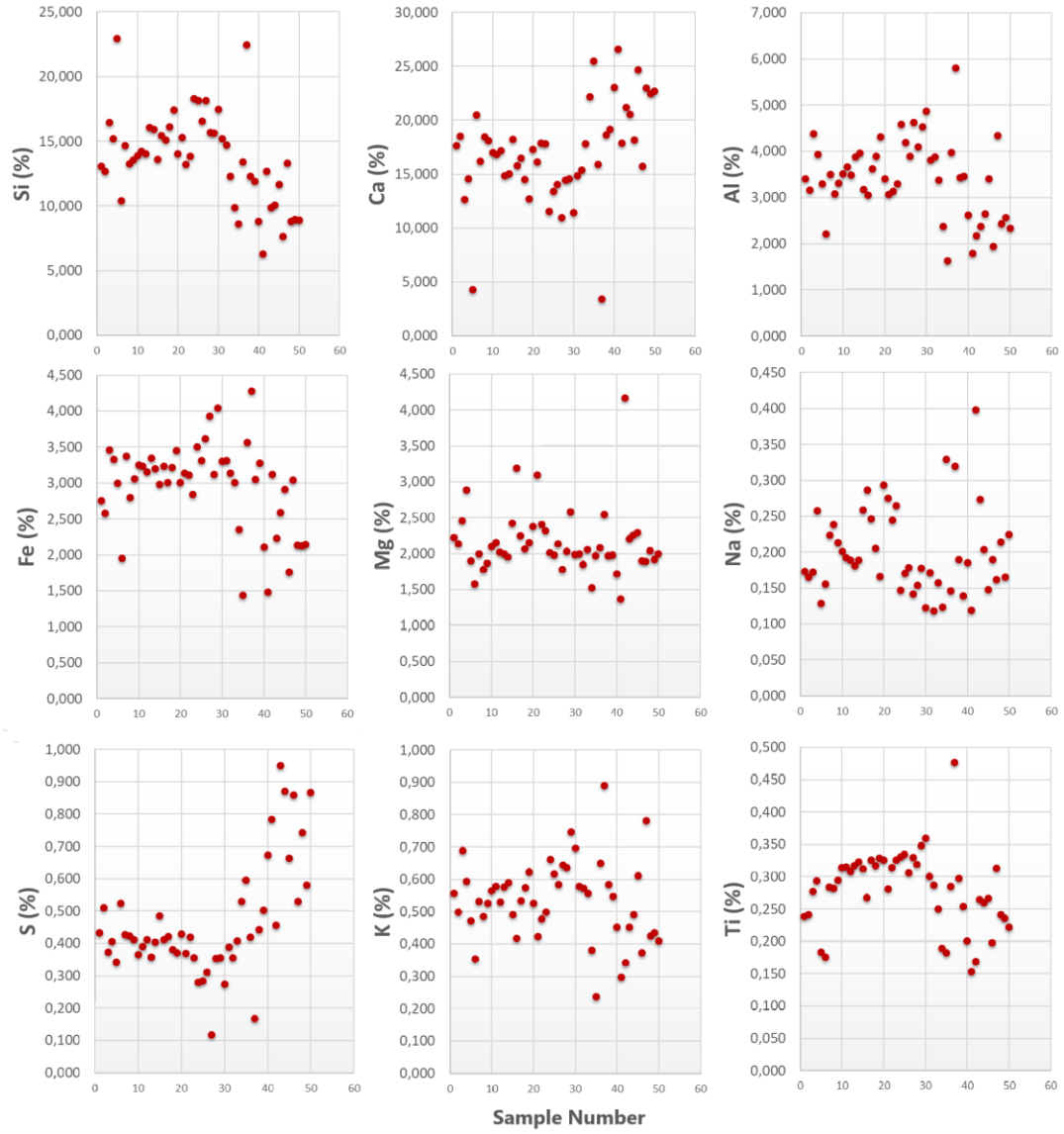

Figure 3.14. Distribution of the most abundant element concentrations (Si, Ca, Al, Fe, Mg, Na, S, K, and Ti) in AL-5

Furthermore, P, Sr, Mn, Ni, Ba, Cr, V, Zn, Cu, and Co concentrations in ppm are higher than the other trace elements measured. Phosphorus concentration ranges between 400-1200 ppm and manganese content is between 400-1000 ppm. It is denoted that both AL-5 049 and AL-5 505 have anomalous Mn concentrations. Strontium content varies between 200-1400 ppm. Nickel and chromium ranges

between 200-600 ppm. Trace element concentrations obtained from ICP-MS/OES measurements are used in statistical evaluations.

3.2.2 Geochemical Characteristics of Floodplains

ICP-MS/OES measurements on 41 samples of the KR-1 core, 36 samples of the AT-1 core, and 22 samples of the TA-2 core revealed that the most abundant elements in these 99 floodplain samples are Ca, Si, Al, Fe, Mg, K, Ti, Na, and S (Figure 3.15).

The first and most significant fact observed after plotting scatter charts is that the samples of the Tell Kurdu core generally have different concentrations than the others. Si concentration ranges between 10-18 wt% in Tell Atchana and 9-15 wt% in Tell Tayinat. However, this concentration is between 15-24 wt% in Tell Kurdu samples which infers environmental difference. Calcium ranges in the same interval in Tell Atchana but the samples of Tell Tayinat have relatively higher Ca concentration of 9-20 wt%. Two samples of Tell Kurdu, KR-1 121 and KR-1 937, have anomalous calcium concentrations. Bulk powder XRD diffractograms of these samples display a significant decrease in the intensity of calcite peaks of KR-1 937. Therefore, main reason of this anomaly is the sudden drop in calcite content within the sample. However, the diffractogram of KR-1 121 reflects no anomaly. Hence, this sample is denoted as a unique, anomalous sample. Aluminum concentration varies between 2-4.5 wt% and 1.5-4 wt% in Tell Atchana and Tell Tayinat, respectively. The Tell Kurdu samples have a wider concentration range of 2.5-7 wt% except KR-1 121. Iron concentration ranges in a narrow range of 2.5-3.5 wt% in the Atchana samples. In the samples of Tayinat, this range is between 2-4 wt%. The Tell Kurdu samples are richer in iron with concentration of 3.5-6 wt%. Distribution of magnesium concentrations is similar to iron and ranges between 1.8-3 wt%, 1.8-4.2 wt%, and 2-5.5 wt% in Atchana, Tayinat and Kurdu, respectively. Concentrations of potassium, titanium and sodium range between 0.3-1 wt%, 0.2-0.45 wt%, and 0.18-0.5 wt% in all floodplain samples.

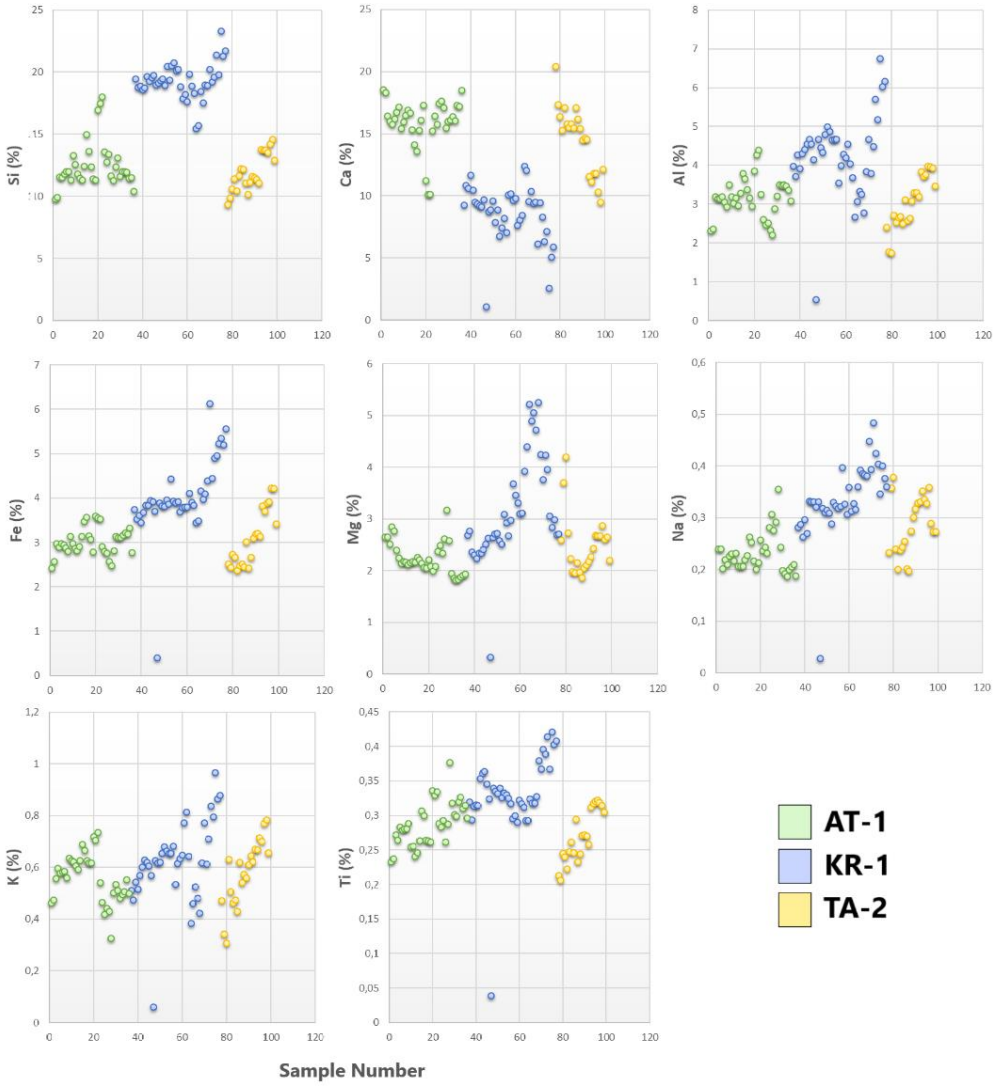

Figure 3.15. Distribution of the most abundant element elements (Si, Ca, Al, Fe, Mg, Na, K, and Ti) in the floodplain samples

The most abundant elements after the 8 elements given in Figure 3.15 are S, Sr, Mn, Cr, Ni, P, V, Cr, Ba, Zn, and Cu. Sulfur concentration ranges between 0-0.5 wt% in the floodplain samples but the scatter chart was not plotted for this element since some samples were suspiciously found to have no sulfur at all after ICP-MS/OES analyses. It is denoted that manganese concentration is relatively higher in the Kurdu samples. Furthermore, strontium and barium contents in the KR-1 samples are remarkably lower than the concentrations in the samples of Atchana and Tayinat.

CHAPTER 4

DISCUSSION

4.1 Statistical Evaluation of Mineralogical and Geochemical Data

Mineralogical and geochemical analyses for 149 sediment core samples from both Amuq Lake (AL-5) and floodplain deposits (KR-1, AT-1, and TA-2) provided huge data set. To be able to evaluate the data in a meaningful and easy way, statistical methods were used. As mentioned in Chapter 1.3.5, intensities of the bulk powder XRD patterns were converted into numerical values using MapInfo software by substracting background intensities from peak point intensities for every possible peak lines. The obtained values made it possible to have statistical evaluation in order to demonstrate all possible correlations between mineralogical and geochemical elemental data. As a first step in statistical evaluation, possible correlation for every observable peaks of each mineral identified in bulk powder XRD diffractograms. Sorting of mineral peaks were done by taking their ASTM cards into consideration. All d-values of evaluated peaks for calcite, quartz, aragonite, serpentine, feldspar, and clay minerals which were observed in bulk powder diffractograms are given in Table 4.1.

The intensity retrieval technique was also used on the XRD patterns of air-dried (AD) oriented clay fraction s to examine whether it is efficiently applicable on oriented clay fraction diffractograms. As existence of both kaolinite and serpentine can be interpreted from ≈ 7 Å peaks in air-dried diffractograms, it was impossible to distinguish these two minerals but the technique was useful for determination of the dominant clay mineral on that peak after making correlations with related elements. As no chlorite content was determined in many samples, overlapping of smectite and chlorite peaks was neglected in statistical evaluation and that overlapping d-value around 14 Å was notated as smectites. The peak at 10 Å is notated as illite. Only

these three major peaks in oriented air-dried diffractograms were taken into consideration for statistical evaluations.

Table 4.1. Evaluated mineral peak values for statistical correlations

Calcite	**Quartz**	**Aragonite**	**Serpentine**	**Feldspar**	**Clays**
d (Å)	***d (Å)***	***d (Å)***	***d (Å)***	***d (Å)***	***d (Å)***
3.04	3.34	3.40	7.24	3.21	14.50
1.88	4.25	2.70	3.63	3.19	8.44
1.91	1.82	1.98		3.16	7.16
2.28	1.54	3.27		3.13	4.48
2.09	2.46	2.37			4.05
2.49	1.37	2.11			2.59
1.60	2.13	1.74			2.56
3.85	2.24	2.87			
2.84	1.67	2.34			
1.63	1.38	1.98			
1.53		1.73			
1.47					
1.44					
1.42					

The Amuq Lake samples (AL-5) demonstrated different elemental and mineralogical fluctuations than the alluvial mound samples (KR-1, AT-1, TA-2) in results of XRD and ICP-MS/OES analyses. In the lake samples, calcite content is higher compared to clastic minerals as quartz, feldspar, serpentine, clay minerals. The most important reason for this mineralogical difference is the sedimentation environment. In alluvial environments, clastic content may be expected to be higher than lacustrine environments, and the carbonate minerals tend to be higher in lake environments. Moreover, the catchment difference affects the type of transported minerals in the depositional area. As there is an alluvial fan between Amuq Lake and the mafic-

ultramafic units of ophiolitic rocks, and serpentinites on the west side of the study area, the lizarditic serpentines might be deposited within the lake after clastic influx. Furthermore, serpentines found in Tell Kurdu may be derived from hydration of either olivine and pyroxene-bearing ultramafic rocks of Kızıldağ ophiolites (Kavuzlu, 2006) or olivine and pyroxene-bearing basalts (Rojay et al., 2011) of Karasu Rift volcanics. However, since River Orontes is fed from the south, transportation of serpentines to the study areas from Karasu Rift basalts is less likely.

It was also denoted that intensities of quartz peaks were usually higher than calcite peaks along the KR-1 core samples. Moreover, ICP-MS/OES measurements revealed that the samples of KR-1 have more different elemental concentration ranges than those of the samples AT-1 and TA-2 core samples. All these facts indicate that the content in the KR-1 core samples is more terrestrial, and this is acceptable since Tell Kurdu can be classified as an intermediate zone between lake and floodplain environments considering the geology of the area. However, this environmental difference was neglected because all floodplain study areas were considered together in statistical evaluation.

Therefore, retrieved mineral peak intensity data were categorized in terms of environment as lake and floodplain. First of all, the overall correlation was determined by correlation matrices of coefficients using all the samples within the study (Figure 4.1). Then, floodplain (KR-1 AT-1, and TA-2) and lake (AL-5) samples were evaluated separately to show environmental effect on peak correlations (Figures 4.2 and 4.3, respectively). The less correlated peaks were identified through these analyses.

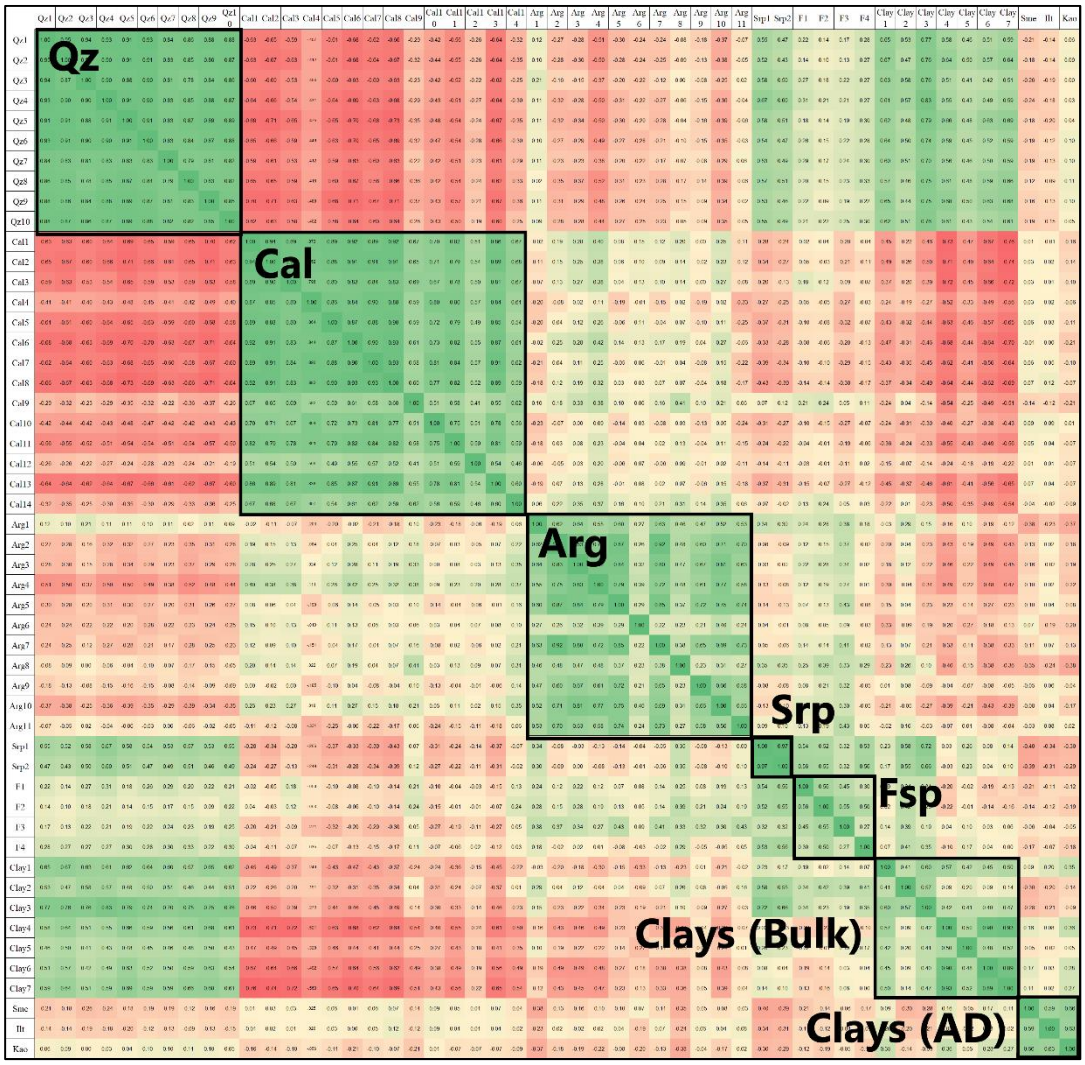

Figure 4.1. Correlation matrix showing the correlation between mineral peaks of all samples on XRD patterns from the lake and floodplain cores (Green: positive correlation, Yellow: no correlation, Red: negative correlation) (Qz: quartz, Cal: calcite, Arg: aragonite, Srp: serpentine, Fsp: feldspar, AD: air-dried)

Statistical correlation of all samples showed that there is a significant correlation among quartz peaks. In other words, all quartz peaks reflect intensity fluctuations similarly in bulk powder X-ray diffractograms. For calcite peaks, correlation is still high with two exceptional peaks of 2.84 and 1.47 Å d-values. As these two peak points are seen as shoulders in bulk powder diffractograms, they do not reflect

intensity fluctuations like other peaks of calcite. A similar discordance is observed in 2.11 Å aragonite peak due to the same reason.

It is observed that if there is more distance between peaks of mineral in other words if there is no any overlap or shoulder in peaks of different minerals, we obtain better intensity results when using this technique. Therefore, it can be stated that shoulder peaks reflect weaker correlations with other peaks in terms of intensity fluctuation. While two serpentine peaks correlate brilliantly, there is a difference in correlation of clay peaks in bulk powder diffractograms. The 8.44 Å bulk powder clay peak has relatively poor correlation with 4.48 Å, 4.05 Å, 2.59 Å, and 2.56 Å peaks. However, clay peaks of air-dried oriented clay fraction diffractograms (smectite, illite, and kaolinite-serpentine) correlate with each other in a better way.

The diagonally aligned seven squares with outside borders in Figure 4.1 reflect the positive correlation between the peaks of the same mineral. Outer zones demonstrate correlations of a mineral with another mineral. For instance, calcite shows a perfect negative correlation with quartz. Calcite represents sedimentary carbonate rich materials in the study area and quartz reflects the clastic materials. So, this negative correlation can be considered as an expected outcome. While there is a moderate to low correlation between calcite and aragonite peaks, calcite negatively correlates with other clastic minerals like serpentines, feldspars and clay minerals. However, peaks of these three clastic minerals correlate with quartz peaks that reflect environmental correlation. Since aragonite and calcite are polymorph carbonate minerals, positive environmental correlation is a normal outcome. Aragonite content may occur due to hard parts of some lake organisms, shells, and skeletons (Palache et al., 1951; Chang et al., 1996). There are many other reasons for calcite-aragonite variations in lake environments such as water column depth, lake mixing, climatic changes, organic matter, elemental concentrations, and sulphate reduction (Roeser et al., 2016). Just like calcite, aragonite negatively correlates with quartz, serpentines and clay minerals, but there is a slightly positive correlation between aragonite and feldspars.

As there are calcic feldspars within samples, fluctuations in calcium concentration affect intensity fluctuations of aragonite and feldspar peaks similarly. Lake and floodplain sediments reflect similar correlation patterns with slight differences in correlation coefficients.

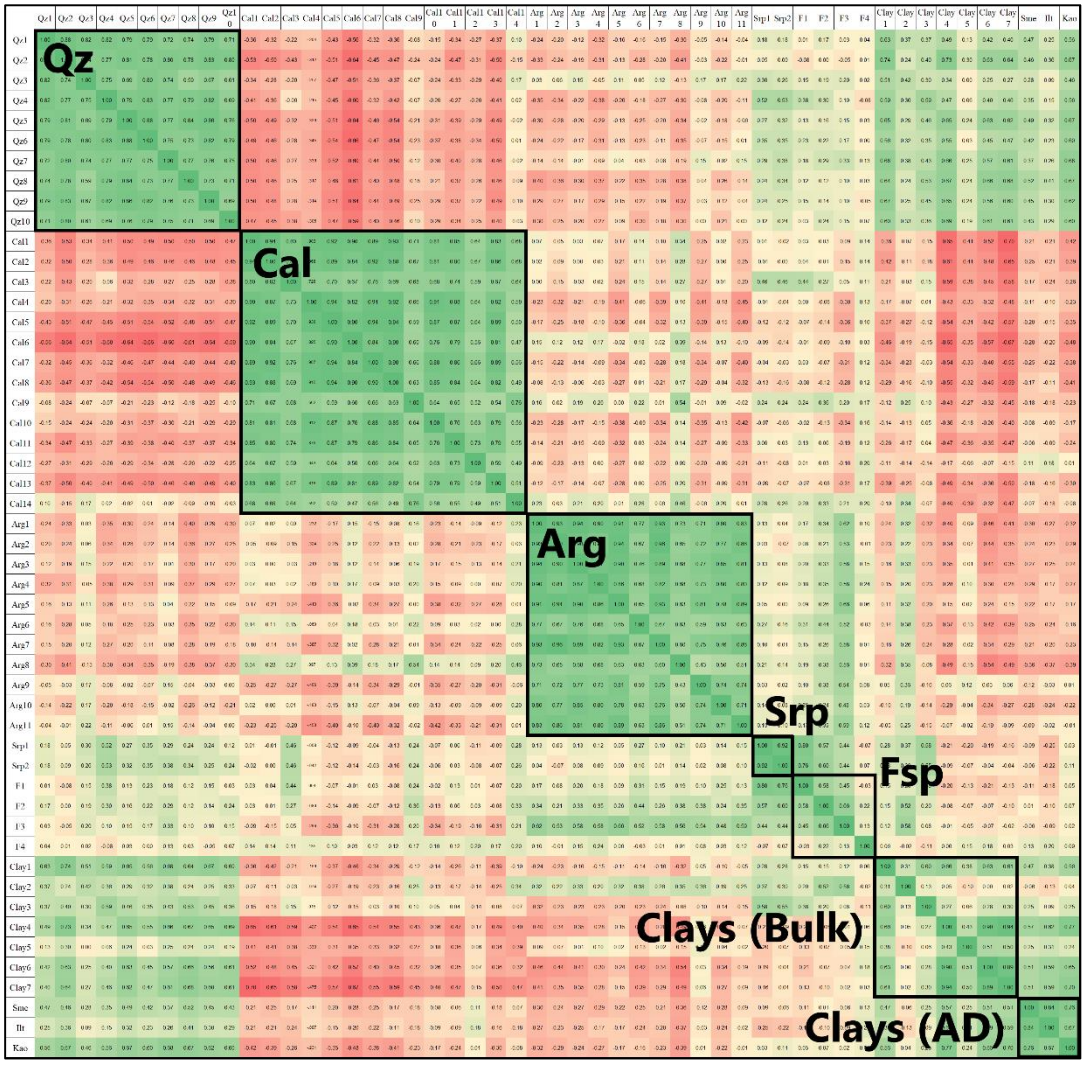

Figure 4.2. Correlation matrix displaying the correlation among mineral peaks of the lake (AL-5) samples (Green: positive correlation, Yellow: no correlation, Red: negative correlation) (Qz: quartz, Cal: calcite, Arg: aragonite, Srp: serpentine, Fsp: feldspar, AD: air-dried)

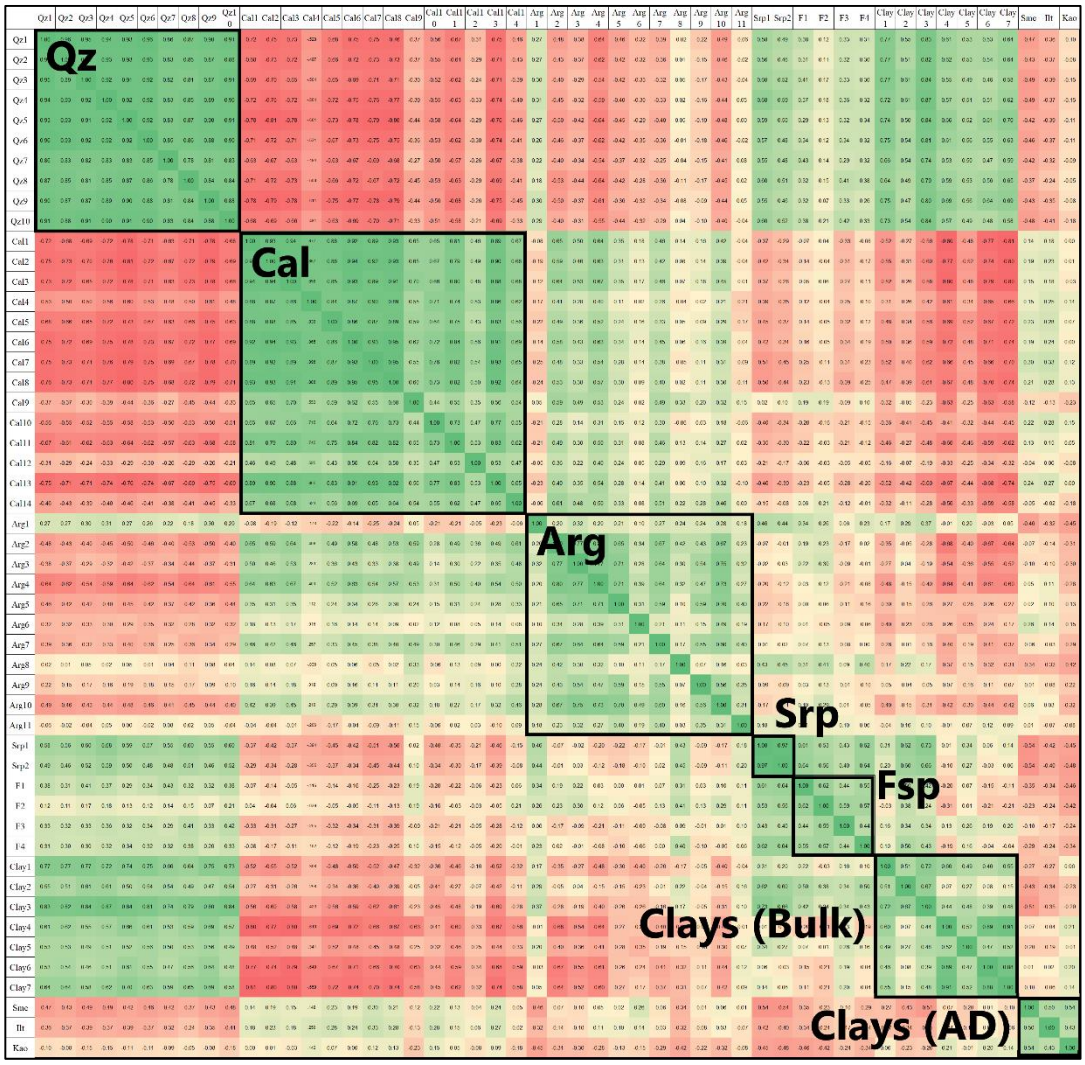

Figure 4.3. Correlation matrix visualizing the correlation between mineral peaks of floodplain (KR-1, AT-1, and TA-2) samples (Green: positive correlation, Yellow: no correlation, Red: negative correlation) (Qz: quartz, Cal: calcite, Arg: aragonite, Srp: serpentine, Fsp: feldspar, AD: air-dried)

Intensity fluctuations of quartz, serpentine, feldspar, and clay mineral peaks on bulk powder XRD patterns seem to be more coherent in the floodplain samples unlike calcite, quartz, and clays (AD), which exhibit higher correlations in the lake samples. Environmental negative correlations are higher in the floodplain samples. Intensity fluctuation correlations between aragonite peaks gets significantly lower in the floodplain samples. As observed from bulk powder XRD diffractograms, aragonite

peaks of the lake samples exhibit higher intensities which explains this significant drop in correlation coefficients. The correlation coefficients in all three coefficient matrices are summarized in Table 4.2.

Table 4.2. Overall correlation coefficients of mineral vs. mineral peaks obtained from coefficient matrices (AD: air-dried)

		Overall Correlation Coefficients		
Mineral 1	**Mineral 2**	**Lake**	**Floodplain**	**All**
Quartz	Quartz	0.79	0.90	0.88
	Calcite	-0.35	-0.61	-0.53
	Aragonite	-0.16	-0.26	-0.20
	Serpentine	0.27	0.54	0.53
	Feldspar	0.12	0.29	0.22
	Clays (Bulk)	0.45	0.58	0.59
	Clays (AD)	0.43	-0.30	-0.09
Calcite	Calcite	0.77	0.75	0.76
	Aragonite	-0.08	0.23	0.07
	Serpentine	0.02	-0.32	-0.24
	Feldspar	0.02	-0.12	-0.07
	Clays (Bulk)	-0.30	-0.51	-0.43
	Clays (AD)	-0.19	0.11	-0.02
Aragonite	Aragonite	0.79	0.46	0.61
	Serpentine	0.09	0.03	0.01
	Feldspar	0.28	0.07	0.18
	Clays (Bulk)	-0.14	-0.22	-0.18
	Clays (AD)	-0.22	-0.13	-0.11
Serpentine	Serpentine	0.96	0.99	0.98
	Feldspar	0.45	0.55	0.49
	Clays (Bulk)	0.10	0.28	0.27
	Clays (AD)	-0.08	-0.47	-0.34
Feldspar	Feldspar	0.51	0.65	0.58
	Clays (Bulk)	0.06	0.11	0.08
	Clays (AD)	0.04	-0.29	-0.12
Clays (Bulk)	Clays (Bulk)	0.48	0.57	0.55
	Clays (AD)	0.39	-0.12	0.04
Clays (AD)	Clays (AD)	0.84	0.66	0.75

After determination of mineral vs. mineral correlations, the second approach in statistical data evaluation was to show element vs. element correlations by taking the ICP-MS/OES analyses results into consideration together with element vs. minerals correlation. Weight percentage values of Si, Ca, Al, Fe, K, Na, Mg, and Ti; ppm values of V, Cr, Mn, Co, Ni, Cu, Zn, Sr, Ba, P, Hf, Y, La, Ce, Pr, Nd, Sm, Sc, Eu, Gd, Tb, Dy, Ho, Er, Tm, Yb, Lu, Th, Ga, As, Se, Rb, Cs, Pb, U, Zr, Nb, and Mo were used in this evaluation. In the correlation of element and mineral peaks, all mineral peaks was not preferred in order not to form a huge and complex correlation matrix. Therefore, first peaks of every mineral were correlated with measured element concentrations at first. As an exception, for aragonite, 2.70 Å peak was selected for this analysis since 3.40 Å peak is close to the first quartz peak, and in some samples, quartz intensity variations affect this peak slightly. For clays (bulk), peaks around 14.50 Å and 4.48 Å were used together as they showed slightly different correlations in mineral vs. mineral correlation analyses. Clay peaks of air-dried oriented clay fraction diffractograms were also used in order to reveal weaknesses of the technique. Then, the same method was applied to reveal both element vs. element and element vs. mineral correlations and a correlation matrix was formed (Figure 4.4).

As seen in Figure 4.4, correlations were not so clear from such a correlation matrix. While correlation between trace elements can be seen from this matrix, the method gets weaker for major and especially minor elements. The medhod also does not seem to be useful for element vs. mineral correlations at all. Hence, a new approach was applied. In order to have a more useful correlation matrix for element vs. mineral correlation, the first step was to form a rotated component matrix (Table 4.3) among elements to categorize them into possible principal components. Varimax method was preferred for preparation of rotated component matrices.

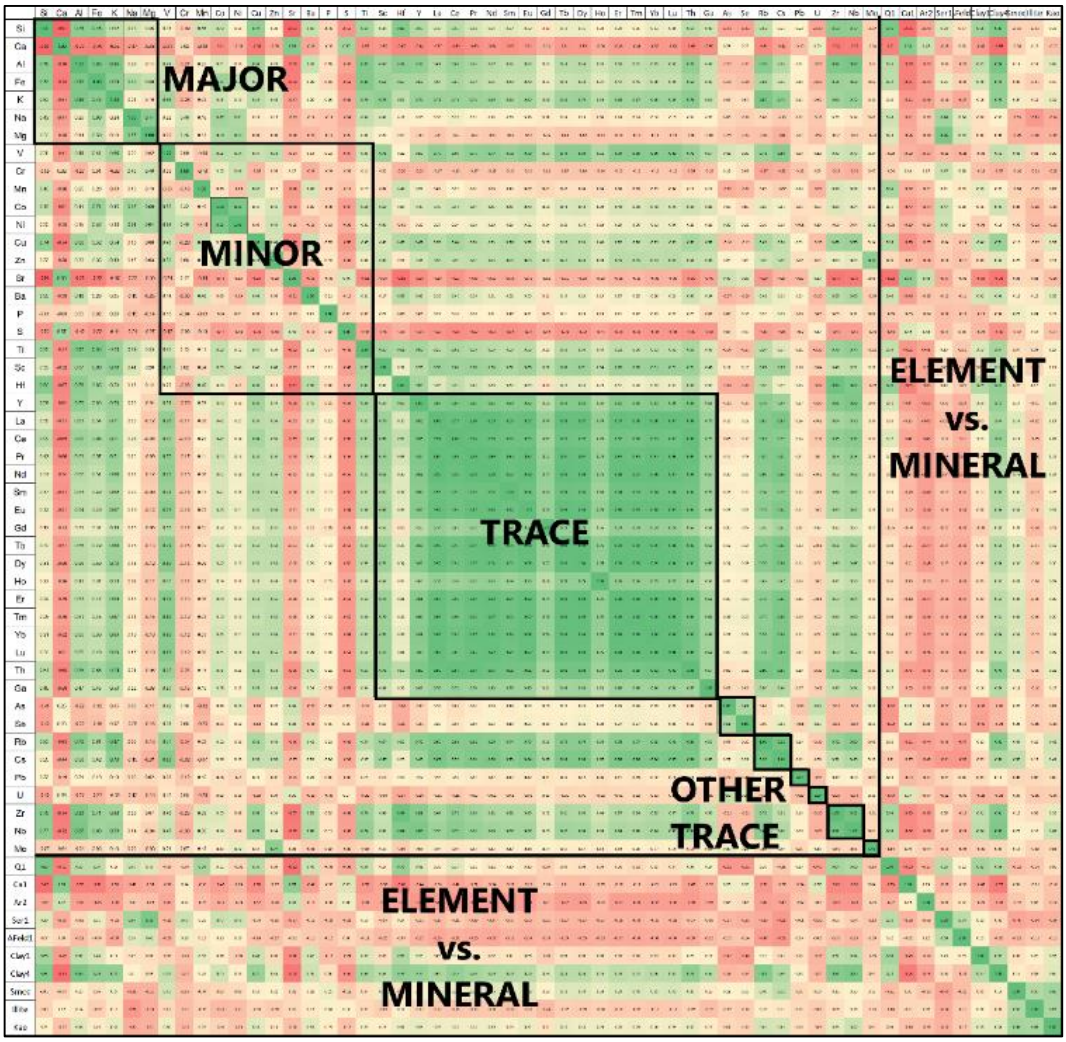

Figure 4.4. Correlation matrix visualizing element vs. element and element vs. mineral correlations in all samples (Green: positive correlation, Yellow: no correlation, Red: negative correlation)

Table 4.3. Summarized rotated component matrix used in determination of principal components of the measured elements (Green: positive correlation, Yellow: no correlation, Red: negative correlation)

PC - 1		PC-2		PC-3		PC-4		PC-5	
Er	0.975	**Si**	0.904	**Mg**	0.881	**Mo**	0.904	**U**	-0.469
Tm	0.975	**Hf**	0.889	**Na**	0.841	**Zn**	0.748	**Pb**	0.447
Yb	0.971	**Al**	0.800	**Ni**	0.818			**P**	0.775
Nd	0.970	**Zr**	0.797	**Co**	0.750				
Tb	0.969	**Nb**	0.775	**Cr**	0.684				
Lu	0.969	**Fe**	0.671						
Dy	0.968	**Cu**	0.669						
Eu	0.965	**Ti**	0.589						
La	0.958	**Ba**	0.57						
Pr	0.948	**Mn**	0.534						
Sm	0.931	**As**	-0.531						
Ce	0.888	**Se**	-0.529						
Th	0.866	**Sr**	-0.883						
Cs	0.841	**Ca**	-0.723						
Gd	0.773								
Ho	0.772								
V	0.762								
Y	0.747								
Rb	0.726								
Ga	0.679								
Sc	0.628								
K	0.584								
S	-0.531								

The correlation matrix also showed that, the first principal component (PC-1) consists of many trace elements along with potassium (weaker correlation). As sulfur does not have any positive correlation with any components but has a negative correlation with PC-1, the element was included in this component. The second principal component (PC-2) includes elements that correlate with Si and Ca. While elements of clastic environments show positive correlation, elements of carbonate

environments show negative correlation in this component. The third principal component (PC-3) includes magnesium, sodium, nickel, cobalt and chromium. The fourth principal component (PC-4) includes molybdenum and zinc, and the last principal component (PC-5) includes uranium, lead and phosphorus. As lead and uranium were the elements with least correlation in the rotated matrix and have weak correlation coefficients, they were included into the most possible component by considering their correlation coefficients with other components.

After determination of principal components, a correlation matrix was formed to show correctness of principal components and the relation between minerals and elements in all samples (Figure 4.5). The upper left part of the correlation matrix proves that the principal components were determined correctly as they have zero correlation with other principle components. While the lower right part of the matrix shows the correlation between the selected first peaks, upper right and lower left parts indicate the relation between the first mineral peaks and elemental principle components.

As PC-2 includes some elements reflecting clastic sedimentary material such as Si, Al, Fe, Cu, and Ti, the component demonstrates positive correlation with quartz and bulk powder clay minerals. Bulk powder clays also exhibit a slight correlation with PC-1. The matrix reveals that trace elements have a moderate correlation with clay minerals in all samples. Although serpentines are also clastic sedimentary materials, they correlated with PC-3 because of their magnesium-rich lizarditic nature. Feldspars demonstrate moderate positive correlation with PC-3 and moderate negative correlation with PC-1. It can be interpreted as feldspars include more sodium and potassium than calcium. This interpretation is also supported by bulk powder XRD diffractograms as most feldspar peaks were matching with sodium-rich feldspar mineral albite or disordered albite along with a few orthoclase peaks. The negative correlation between the first calcite peak and PC-2 is an expected outcome as calcium was included in PC-2 with -0.723 correlation coefficient. The most remarkable correlation is seen between aragonite and PC-2. Even though strontium

and calcite are included in PC-2, aragonite shows a moderate correlation with this component.

The main source of trace elements in these samples are clay minerals in all of the samples. As feldspars, serpentines and aragonite also show moderate correlation with PC-1, it can be said that these three minerals also contain a lesser amount of trace elements within. According to the correlation matrix obtained, PC-4 and PC-5 have no correlation with minerals in this study area, Hence, it can be suggested that the elements in these principle components probably transported and deposited from an external source.

In the lower right part of the matrix, the difference between 14.50 Å and 4.48 Å peaks of clay minerals (these peaks are going be mentioned as Clay1 and Clay4 respectively from now onward) can be observed. While 4.48 Å peak shows strong negative correlation with calcite and moderate negative correlation with aragonite, 14.50 Å peak only show moderate negative correlation peak with calcite. The reason behind this variation may be caused by calcium and strontium content of related clay minerals. Air-dried clay peaks show poor correlation with principal components in this approach. Even though illite peaks have low intensities in oriented clay fraction diffractograms, at least a moderate correlation between PC-1 and illite peaks were expected as PC-1 includes potassium. However, the matrix demonstrates no correlation between these two. The matrix revealed that while smectites contain some trace elements within, illite and kaolinite-serpentine consist of some elements within PC-3. As serpentines are Mg-rich, correlation with PC-3 is reasonable but in illite, magnesium is lower than potassium in amount. By considering these inconsistencies, it can be said that the evaluation technique used in this study has less efficiency on air-dried clay fraction diffractograms in comparison with bulk powder diffractograms.

	PC-1	PC-2	PC-3	PC-4	PC-5	PC-6	Qz1	Cal1	Arg2	Srp1	Fsp1	Clay1	Clay4	Sme	Ilt	Kln - Srp
PC-1	1.000	0.000	0.000	0.000	0.000	0.000	-0.026	-0.084	-0.388	-0.323	-0.386	-0.043	0.464	0.382	-0.147	0.258
PC-2	0.000	1.000	0.000	0.000	0.000	0.000	0.825	-0.782	-0.365	0.231	-0.003	0.700	0.773	-0.039	0.137	0.275
PC-3	0.000	0.000	1.000	0.000	0.000	0.000	0.225	-0.272	-0.104	0.743	0.382	-0.034	0.075	-0.233	-0.374	-0.314
PC-4	0.000	0.000	0.000	1.000	0.000	0.000	-0.079	-0.055	-0.061	-0.120	-0.021	-0.026	0.025	0.137	0.006	0.047
PC-5	0.000	0.000	0.000	0.000	1.000	0.000	-0.366	-0.116	-0.071	-0.310	-0.268	-0.108	0.160	0.235	0.363	0.183
PC-6	0.000	0.000	0.000	0.000	0.000	1.000	0.026	-0.088	0.043	-0.051	-0.020	-0.142	-0.025	0.149	0.205	0.085
Qz1	-0.026	0.825	0.225	-0.079	-0.366	0.026	1.000	-0.633	-0.267	0.546	0.217	0.652	0.578	-0.208	-0.140	0.056
Cal1	-0.084	-0.782	-0.272	-0.055	-0.116	-0.088	-0.633	1.000	0.187	-0.284	-0.020	-0.446	-0.734	0.010	-0.009	-0.164
Arg2	-0.388	-0.365	-0.104	-0.061	-0.071	0.043	-0.267	0.187	1.000	-0.083	0.118	-0.196	-0.430	-0.132	0.020	-0.180
Srp1	-0.323	0.231	0.743	-0.120	-0.310	-0.051	0.546	-0.284	-0.083	1.000	0.542	0.233	0.027	-0.403	-0.342	-0.304
Fsp1	-0.386	-0.003	0.382	-0.021	-0.268	-0.020	0.217	-0.020	0.118	0.542	1.000	0.185	-0.203	-0.208	-0.108	-0.116
Clay1	-0.043	0.700	-0.034	-0.026	-0.108	-0.142	0.652	-0.446	-0.196	0.233	0.185	1.000	0.566	0.092	0.203	0.346
Clay4	0.464	0.773	0.075	0.025	0.160	-0.025	0.578	-0.734	-0.430	0.027	-0.203	0.566	1.000	0.163	0.080	0.361
Sme	0.382	-0.039	-0.233	0.137	0.235	0.149	-0.208	0.010	-0.132	-0.403	-0.208	0.092	0.163	1.000	0.594	0.664
Ilt	-0.147	0.137	-0.374	0.006	0.363	0.205	-0.140	-0.009	0.020	-0.342	-0.108	0.203	0.080	0.594	1.000	0.630
Kao-Srp	0.258	0.275	-0.314	0.047	0.183	0.085	0.056	-0.164	-0.180	-0.304	-0.116	0.346	0.361	0.664	0.630	1.000

Figure 4.5. Correlation matrix showing the relationship between elemental principal components and the first XRD peaks of minerals in all samples (Green: positive correlation, Yellow: no correlation, Red: negative correlation) (Qz1: 3.34 Å quartz peak, Cal1: 3.04 Å calcite peak, Arg2: 2.70 Å aragonite peak, Srp1: 7.24 Å serpentine peak, Fsp1: 3.21 Å feldspar peak, Clay1: 14.50 Å bulk clay peak, Clay4: 4.48 Å bulk clay peak, Sme: smectite, Ilt: illite, Kln-Srp: kaolinite-serpentine)

In order to show whether overall intensities of every peak of a mineral reflect the geochemistry properly, Principle Component Analysis was also applied on mineralogical data obtained from MapInfo software (Table 4.4). This kind of

approach is preferred to examine whether the exceptional correlations like aragonite in the correlation matrix are correct or caused by chosen first peaks. This kind of approach can also be used to determine whether a peak of a mineral is shadowed by a close peak of another mineral.

Table 4.4. Summarized rotated component matrix used in determination of principal components of mineral peaks (Green: high correlation, Yellow: moderate correlation) (Qz: quartz, Cal: calcite, Arg: aragonite, Srp: serpentine, Fsp1: 3.21 Å feldspar peak, Sme: smectite, Ilt: illite, Kln-Srp: kaolinite-serpentine, Clay1: 14.50 Å bulk clay peak, Clay2: 8.44 Å bulk clay peak, Clay3: 7.16 Å bulk clay peak, Clay4: 4.48 Å bulk clay peak, Clay5: 4.05 Å bulk clay peak, Clay6: 2.59 Å bulk clay peak, Clay7: 2.56 Å bulk clay peak)

PC-A		PC-B		PC-C		PC-D		PC-E		PC-F	
Cal1	.856	Qz1	.884	Arg1	.712	Srp1	.691	Sme	.804	Clay5	.491
Cal2	.849	Qz2	.861	Arg2	.894	Srp2	.748	Ilt	.806	Clay6	.602
Cal3	.825	Qz3	.887	Arg3	.885	Fsp1	.616	Kln-Srp	.858	Clay7	.542
Cal4	.922	Qz4	.858	Arg4	.805	Fsp2	.808				
Cal5	.814	Qz5	.825	Arg5	.928	Fsp3	.531				
Cal6	.833	Qz6	.856	Arg7	.906	Fsp4	.721				
Cal7	.869	Qz7	.804	Arg9	.789						
Cal8	.849	Qz8	.759	Arg10	.795						
Cal9	.723	Qz9	.822	Arg11	.799						
Cal10	.812	Qz10	.840								
Cal11	.837	Clay1	.743								
Cal12	.696	Clay2	.550								
Cal13	.823	Clay3	.779								
Cal14	.749	Clay4	.504								

The rotated component matrix of minerals revealed some differences clearly and these are summarized in Table 4.4. The figure shows a slight difference in correlation of 14.50 Å and 4.48 Å peaks of clay minerals (bulk). This rotated component matrix displayed that the first four clay peaks (14.50 Å, 8.44 Å, 7.16 Å, 4.48 Å) correlate

better with quartz while other three peaks (4.05 Å, 2.59 Å, 2.56 Å) correlate among themselves better. Hence, it can be stated that observed clay peaks with d-values over 4.44 Å (the peaks before 20° 2θ) in bulk powder diffractograms show different correlations. However, it must be stated that correlation coefficients of 4.48 Å peak with PC-B and PC-F were really close (0.504 and 0.495, respectively). Therefore, this peak can be considered as an intermediate peak among others.

In aragonite, two exceptional peaks exhibit different correlations in contrast with other peaks of the mineral (Table 4.5). While 2.11 Å peak of aragonite is completely discordant, 2.87 Å peak moderately correlates with two different principle components. Since the correlation with PC-D which includes serpentines and feldspars is higher than PC-C that consists of aragonite, this situation can be considered as an anomaly.

Table 4.5. Correlation coefficients of exceptional aragonite peaks determined after principal component analysis (Yellow: moderate correlation, Red: poor correlation) (Arg: aragonite)

PEAK	PC-A	PC-B	PC-C	PC-D	PC-E	PC-F
Arg6 (d=2.11)	**0**	**-0.24**	**0.26**	**0.05**	**-0.16**	**0.02**
Arg8 (d=2.87)	**0.15**	**-0.06**	**0.42**	**0.44**	**-0.39**	**-0.06**

The reason behind the discordance of d=2.11 Å can be explained by the fact that the peak is located at the shoulder of calcite's 2.09 Å peak (Cal5). Since the 2.87 Å peak of aragonite is located close to the wide and sharp first calcite peak (d=3.04 Å), which is the most dominant peak in almost all samples with some exceptions in the Tell Kurdu samples, the intensity of aragonite may be shadowed by the noise of this peak. Taking all of these into account, these two exceptional peaks can be considered as a possible reason of relatively weak correlation of aragonite with other minerals and measured elements. After these two peaks and the intermediate 4.48 Å peak of clay minerals were excluded from the data, principal components of minerals were defined again and correlated with the main elemental principle components (PC-1,

PC-2, PC-3) (Figure 4.6). PC-4 and PC-5 were excluded in this analysis as they demonstrated no correlation with any minerals in the coefficient matrix formed before.

PC-A represents calcite as the component includes only calcite peaks within. This component only has a negative correlation with PC-2 that includes calcite with negative correlation. PC-B consists of quartz and clay minerals. Therefore, this component has strong positive correlation with PC-2 as the component includes related elements like Si and Al. PC-C of aragonite demonstrates weak negative correlations with PC-1 and PC-2, just like in the correlation matrix formed by the first peaks. Exclusion of two anomalous peaks did not change the correlation at all. Therefore, it can be said that excluding the discordant peaks does not work efficiently in this technique as overall mineralogy shadows minor peak fluctuations. PC-D of serpentines and feldspars correlate with PC-3 of sodium and magnesium. PC-E of air-dried clay peaks have a weak negative correlation with PC-3, too. PC-F which consists of bulk powder clay peaks after 20° 2θ correlate with PC-1 of trace elements.

	PC_A	PC_B	PC_C	PC_D	PC_E	PC_F	PC_1	PC_2	PC_3
PC_A	1.000	.000	.000	.000	.000	.000	-.051	-.511	-.286
PC_B	.000	1.000	.000	.000	.000	.000	-.056	.709	.077
PC_C	.000	.000	1.000	.000	.000	.000	-.306	-.234	-.008
PC_D	.000	.000	.000	1.000	.000	.000	-.315	-.130	.642
PC_E	.000	.000	.000	.000	1.000	.000	.135	.159	-.325
PC_F	.000	.000	.000	.000	.000	1.000	.450	.116	.186
PC_1	-.051	-.056	-.306	-.315	.135	.450	1.000	.000	.000
PC_2	-.511	.709	-.234	-.130	.159	.116	.000	1.000	.000
PC_3	-.286	.077	-.008	.642	-.325	.186	.000	.000	1.000

Figure 4.6. Correlation matrix of elemental (PC-1, PC-2, PC-3) and mineralogical (PC-A, PC-B, PC-C, PC-D, PC-E, PC-F) principle components (Green: positive correlation, Yellow: no correlation, Red: negative correlation)

Briefly, application of the first peaks and principle components for element vs. mineral correlations gave almost the same results in the technique. This proves that first peaks of minerals reflect overall mineralogy properly. Principal Component

Analysis revealed that the bulk powder clay peaks that exist before 20° 2θ has better correlation with minerals of clastic origin in contrast with the other clay peaks. It can also be interpreted that this technique has poor efficiency in evaluation of air-dried oriented clay fraction X-ray diffractogram peaks. Finally, all element-mineral correlations obtained are summarized in detail in Figure 4.7.

	Quartz	Calcite	Aragonite	Serpentine	Feldspar	Clay1	Clay4
Si	,859	-,853	-,397	,388	,074	,655	,832
Ca	-,707	,801	,469	-,346	,004	-,489	-,850
Al	,546	-,701	-,448	-,026	-,217	,507	,865
Fe	,536	-,714	-,434	,311	-,038	,399	,761
K	,204	-,513	-,458	-,182	-,372	,181	,747
Na	,451	-,406	-,121	,659	,356	,087	,224
Mg	,387	-,365	-,190	,861	,420	,061	,090
V	-,079	-,296	-,371	-,220	-,283	-,027	,507
Cr	-,042	,143	,169	,468	,280	-,175	-,272
Mn	,641	-,320	-,208	,212	,130	,328	,220
Co	,306	-,469	-,345	,474	,198	,159	,450
Ni	-,019	-,291	-,198	,450	,188	-,078	,182
Cu	,562	-,597	-,372	-,040	-,140	,465	,713
Zn	,033	-,167	-,264	-,100	-,168	,033	,358
Sr	-,817	,758	,484	-,369	-,019	-,601	-,781
Ba	,459	-,459	-,150	-,121	-,107	,418	,464
P	-,078	-,034	-,036	-,196	-,148	-,191	,056
S	-,378	,389	,303	-,212	,002	-,244	-,556
Ti	,500	-,522	-,406	,195	-,111	,392	,643
Sc	,142	-,375	-,394	-,070	-,250	,054	,537
Hf	,727	-,685	-,401	,136	-,073	,593	,744
Y	,416	-,440	-,526	-,122	-,290	,333	,721
La	,162	-,279	-,451	-,231	-,377	,091	,636
Ce	,370	-,410	-,476	-,106	-,313	,232	,733
Pr	,212	-,312	-,468	-,193	-,359	,129	,662
Nd	,123	-,239	-,451	-,241	-,373	,073	,601
Sm	,188	-,258	-,461	-,168	-,305	,115	,595
Eu	,098	-,220	-,455	-,245	-,335	,078	,564
Gd	-,045	-,094	-,309	-,209	-,297	-,080	,382
Tb	,092	-,214	-,466	-,271	-,362	,060	,563
Dy	,078	-,209	-,477	-,272	-,353	,046	,558
Ho	,041	-,148	-,253	-,273	-,332	,048	,451
Er	,060	-,184	-,470	-,283	-,368	,028	,537
Tm	,022	-,157	-,460	-,300	-,379	,004	,514
Yb	,091	-,212	-,467	-,250	-,356	,034	,558
Lu	,068	-,210	-,461	-,281	-,372	,024	,551
Th	,303	-,453	-,492	-,173	-,369	,230	,760
Ga	,268	-,317	-,395	-,092	-,229	,180	,565
As	-,524	,285	,075	-,269	-,150	-,418	-,261
Se	-,518	,284	,031	-,308	-,138	-,461	-,235
Rb	,164	-,507	-,437	-,362	-,466	,227	,814
Cs	-,111	-,266	-,400	-,509	-,521	,029	,601
Pb	,184	-,242	-,165	-,010	,059	,052	,180
U	-,426	,374	-,038	-,218	-,051	-,279	-,242
Zr	,643	-,633	-,496	,049	-,186	,512	,813
Nb	,601	-,624	-,504	-,071	-,261	,544	,852
Mo	-,142	,036	-,040	-,130	-,086	-,053	,008

Figure 4.7. Mineral-element correlation with correlation coefficients (Green: positive correlation, Yellow: no correlation, Red: negative correlation) (Clay1: 14.50 Å bulk clay peak, Clay4: 4.48 Å bulk clay peak)

Taking both lake and floodplain environments into consideration, it was determined that quartz strongly correlates with Si, Al, Fe, Mn, Cu, Ti, Hf, Zr, and Nb. While silicon is the main constituent in quartz, aluminum can be considered the prevailing impurity in this mineral (Götze et al., 2021). Götze et al. (2021) states that iron can also be incorporated into quartz in 3 different valence states (Fe^{2+}, Fe^{3+} and Fe^{4+}) and titanium is also a usual impurity in quartz as it isovalently substitutes as Ti^{4+} for Si^{4+} in the silica tetrahedra. Manganese and copper may be present in quartz because they can replace Fe^{2+}. As it is a common fact that acicular rutile crystals may also be present in quartz crystals, this correlation may be related to existence of rutilated quartz within the samples. He also stated that there are also many trace elements within quartz that have concentrations below detection limits of some analytical methods such as Nb that might be due to rutile impurity. However, rutiles may also consist of iron, aluminum and niobium as replacements (Bangaku Naidu et al., 2019). Meinhold et al. (2008) showed that Nb may exist as a trace element rutiles along with Zr. Since Ti, Zr, and Hf are group IV transition metals, they have similar chemical characteristics. Quartz has strong negative correlation with Ca, Sr, As, and Se which represent carbonate environments. As structural substitution of selenium and arsenic can be seen in calcite (Aurelio et al., 2008), considering the inverse relationship between calcite and quartz, this negative correlation is an expected outcome.

Calcite correlates positively with calcium and strontium and negatively with the elements that correlate with quartz. Aragonite has a moderate correlation with Ca and Sr when all samples are taken into consideration but the correlation coefficients of aragonite get higher in the lake samples. It may be caused by existence of hard parts of lacustrine organisms in Amuq Lake which was also observed in sub-sampling the AL-5 core.

Feldspars have moderate positive correlation with Na and Mg, and moderate negative correlation with K, Rb, and Cs. As most feldspar peaks correspond to albite and disordered albite, positive correlation with these elements can be related to the mineral chemistry.

Serpentines strongly correlate with Mg, Na, Cr, Co, and Ni. Positive correlation with Cr, Co, and Ni can be caused by the fact that serpentines derived from ultramafic rocks through deuteric and subsequent hydrothermal replacements are rich in Cr, Co, and Ni (Faust & Fahey, 1962). As serpentines within all samples are determined to be lizardites, strong correlation with Mg and Al is an expected outcome.

While the clay peaks before 20° 2θ value on the bulk powder diffractograms correlate with the same elements with quartz, other clay peaks strongly correlate with Si, Al, Fe, K, V, Cu, Ti, Rb, Cs, Zr, Nb, and trace elements. Since it was known that 20-95% of rare earth elements in argillaceous sediments were adsorbed in clay minerals (Spirn, 1965; Balashov & Girin, 1969; Roaldset, 1973; Aagaard, 1974), positive correlation between trace elements and clay minerals was expected. These clay peaks exhibit strong negative correlation with Ca and Sr due to existence of high amounts of smectite.

4.2 Amorphous Substances

The mineralogical characterization showed that two specific samples from Amuq Lake, AL-5 049 and AL-5 505, are different on bulk powder XRD diffractograms, and in geochemical scatter charts. For instance, ICP-MS/OES analyses revealed that the amount of Ca in these two samples are significantly lower than the other samples of the same environment. This intense drop in Ca content is also supported by the scatter chart that demonstrates the intensity range of the first (d=3.04 Å) calcite peak (Figure 4.8). However, results of these two analyses do not correlate each other for every element, or mineral. For instance, Si content seems to be anomalous, while the first quartz peak (d=3.34 Å) does not reflect this inconsonance (Figure 4.9).

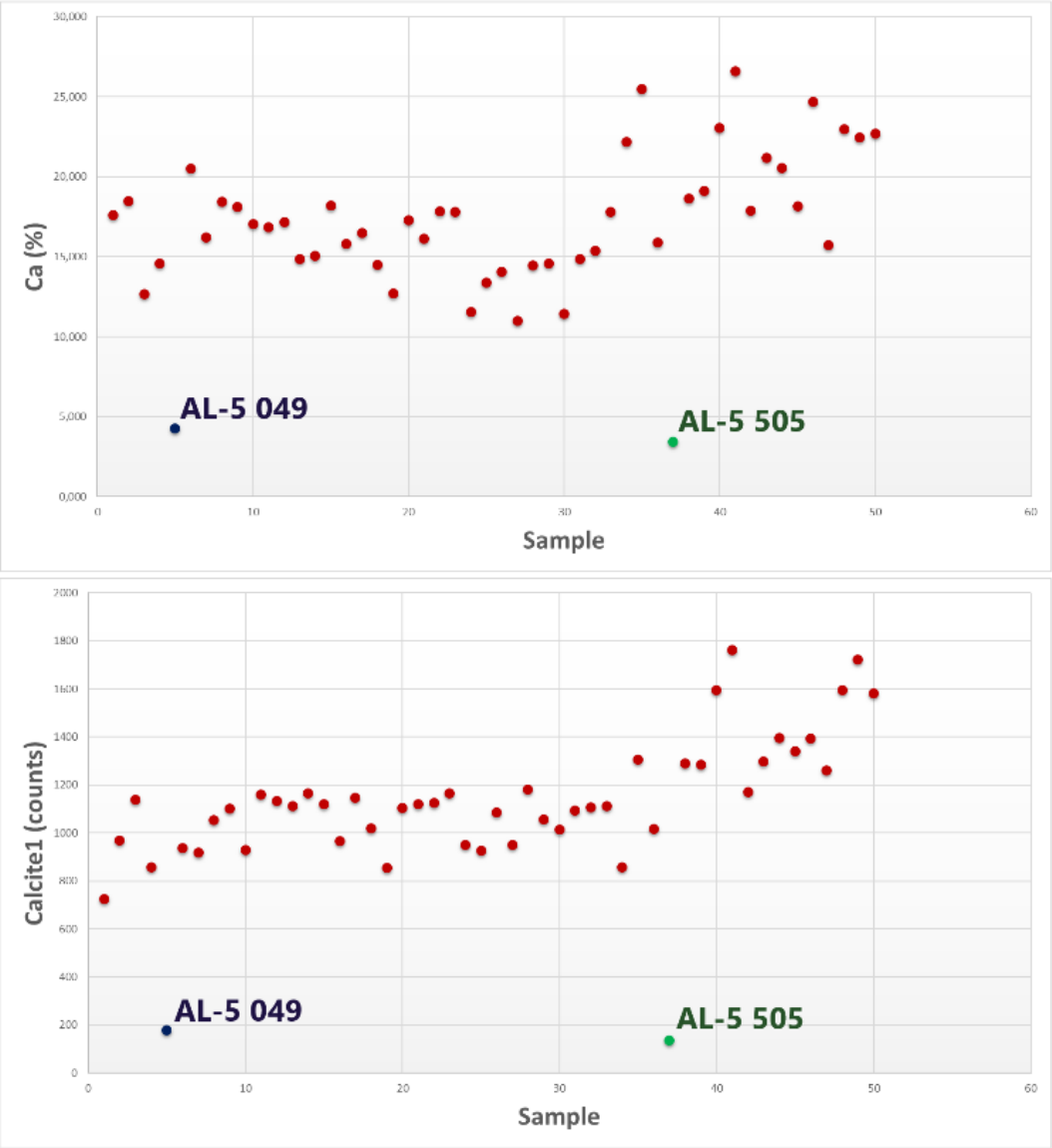

Figure 4.8. Scatter charts showing the scattering samples (AL-5 049 and AL-5 505) in calcium (wt%) content and calcite (counts) on XRD pattern, respectively

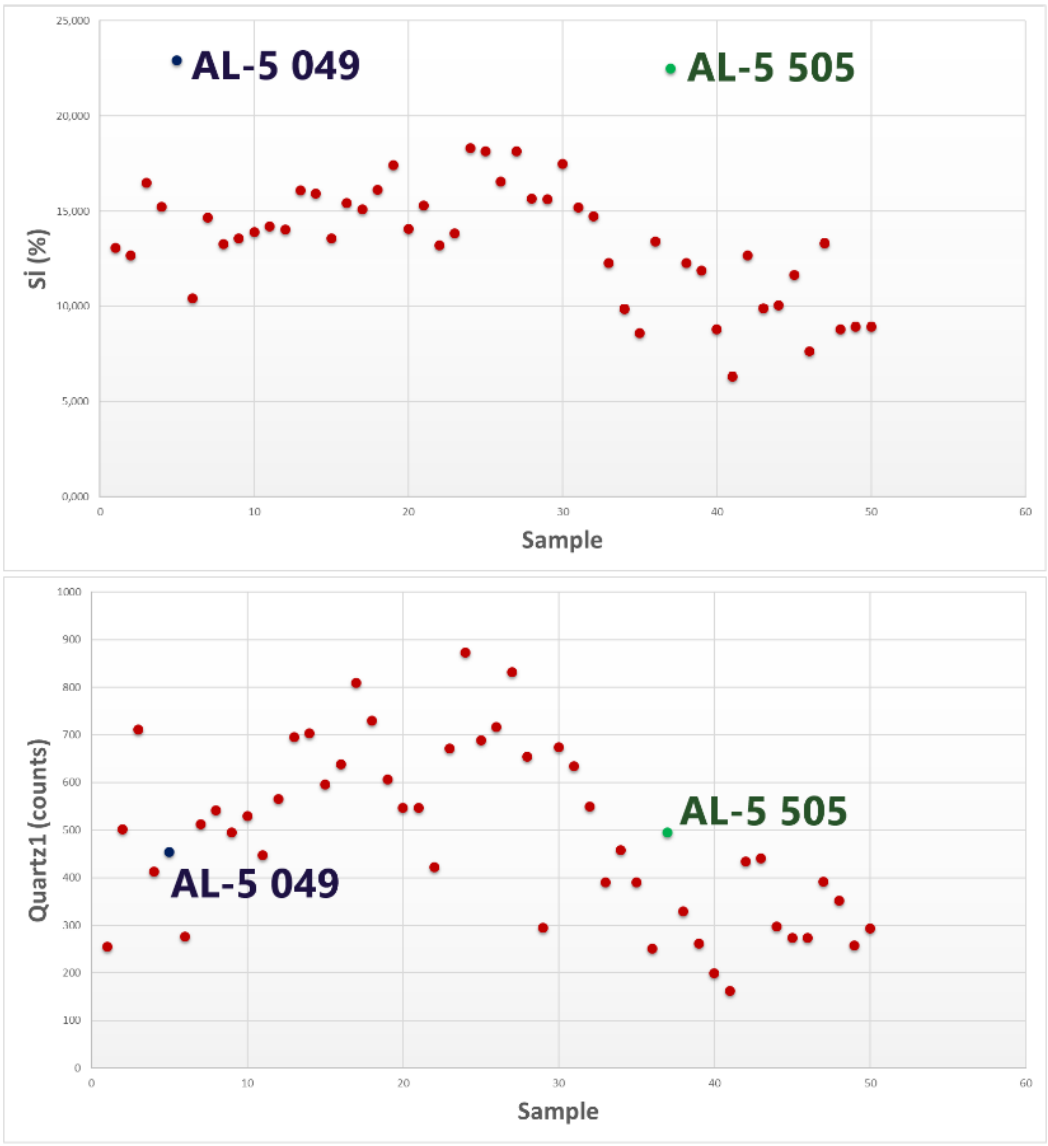

Figure 4.9. Scatter charts showing the scattering samples (AL-5 049 and AL-5 505) in Si (wt%) content and in quartz (counts) on XRD pattern

To understand the reason behind this anomaly, bulk powder X-ray diffractograms of these two samples were examined, and it was found out that these diffractograms reflect existence of high amount ofamorphous material (Figure 4.10). The diagnostic hump between 10-40° 2θ that is observed in these two samples are described as amorphous silica (Dias & Barriga, 2006; Conconi et al., 2011; Deshmukh et al., 2011; Musić et al., 2011; Brichni et al., 2016).

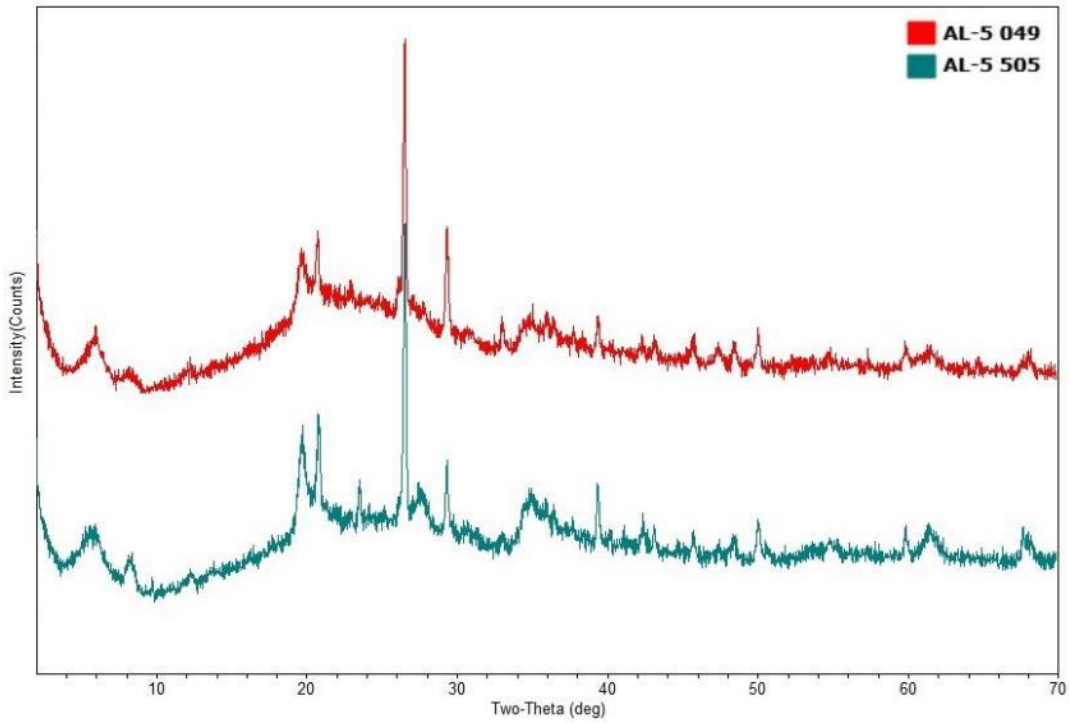

Figure 4.10. Amorphous bulk powder XRD diffractograms of AL-5 049 (red) and AL-5 505 (blue)

In order to be sure that the material is geologically different from the other samples, high-resolution photographs of split cores were examined. Photographs proved that the materials is in these two ranges (48-50 cm for AL-5 049, 504-506 cm for AL-5 505) are completely different from the rest of the sediments (Figure 4.11). To understand whether these amorphous materials belong to the same source or formed after different geological processes, ICP-MS/OES measurements were taken into consideration. While many element concentrations are similar, amounts of heavy metals such as V, Cr, and Ni are higher in AL-5 505. Furthermore, these two samples have different colors in split cores. Taking all of these into consideration, it is suggested that AL-5 049 and AL-5 505 quite likely origined from different geological processes.

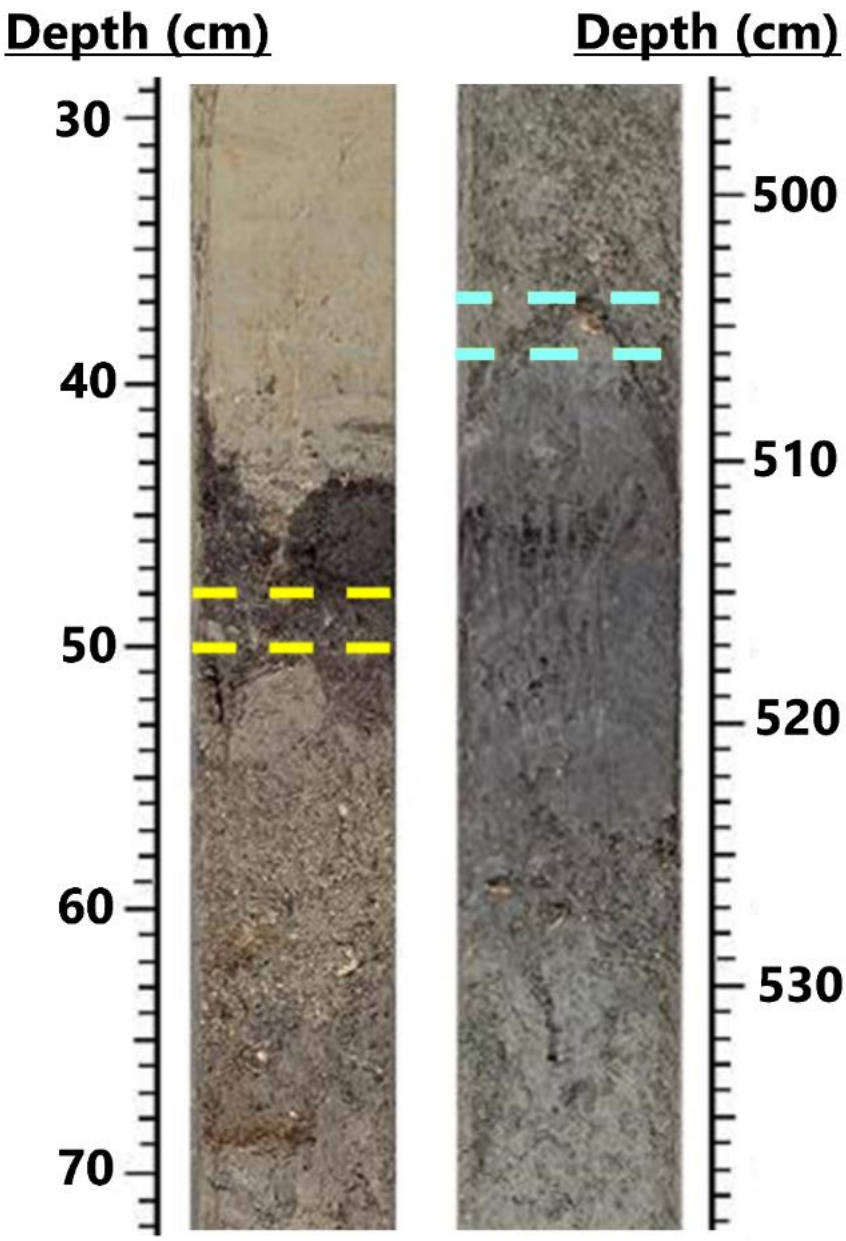

Figure 4.11. High-resolution split core photographs from AL-5 core for demonstration of where the samples AL-5 049 (between yellow dashed lines) and AL-5 505 (between blue dashed lines) were obtained

Presence of amorphous silica was suuported by SEM-EDS analyses on these two samples (AL-5 049 and AL-5 505) at Hacettepe University Advanced Technologies Application and Research Center (HÜNİTEK). The SEM images of these two

samples showed that they consist of extreme amounts of diatoms (Figure 4.12). that well explains the amorphous silica pattern on the XRD diffractograms and extreme Si concentrations in ICP results. High Si concentration of diatoms were measured by EDS (Figure 3.5 in Chapter 3.1.1). The SEM-EDS analyses, on both AL-5 049 and AL-5 505 samples clearly supported that the samples have high amounts of smectite. Representative SEM images from these two samples are given in Figure 4.12.

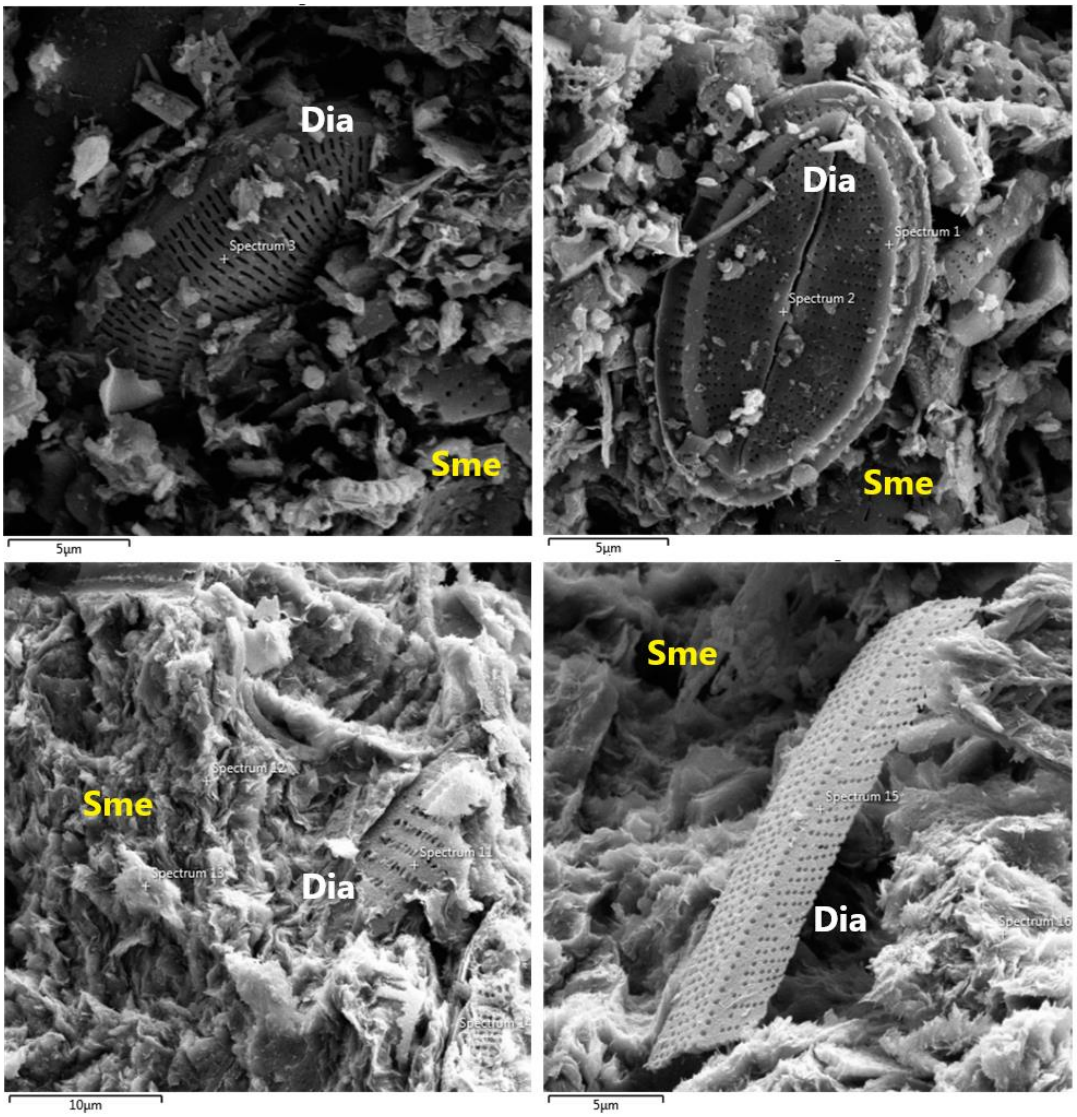

Figure 4.12. SEM images from the samples AL-5 049 and AL-5 505 showing high diatom and smectite content (Dia: diatom, Sme: smectite)

Even though in these two samples, amorphous silica material (diatom) is too high, lower amount of diatom was observed in SEM images of the other two lake samples (AL-5 433 and AL-5 685) indicating the abundance of diatoms in Amuq Lake. There is also a slight hump pattern between 10-40° 2θ (Figure 4.13) in almost all bulk powder X-ray diffractograms of floodplain samples inferring presence of low amount of diatom in both lake and floodplain deposits. However, as no SEM-EDS analyses were conducted on floodplain samples, possible existence of organic material which can also be related to this hump should also be considered.

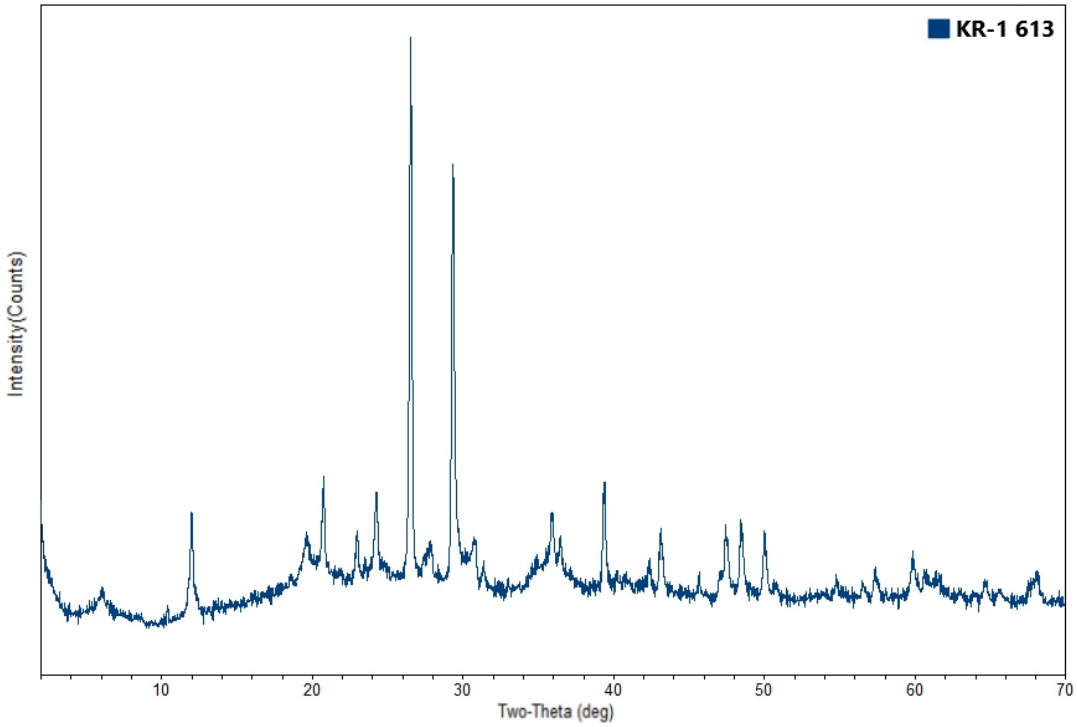

Figure 4.13. Representative bulk powder XRD pattern of a floodplain sample (KR-1 613 from Tell Kurdu) inferring low amorphous silica (diatom) content

CHAPTER 5

CONCLUSION

The following conclusions can be drawn from this study:

- The method developed by MapInfo software to convert intensities of bulk powder X-ray diffractogram peaks to numerical values and their use in statistical evaluation is applicable if XRD sample preparation procedure is conducted delicately. Correlation between element concentrations and mineral intensities proved that the retrieved intensity data reflect the mineral concentration in the sample. The statistical approach using mineral-mineral and element-mineral correlations resulted that using only Microsoft Excel and SPSS makes meaningful and easy evaluation of huge mineralogical and geochemical data set.
- The technique has poor efficiency on air-dried X-ray diffractograms of oriented clay fractions as the elemental data do not correlate with intensity distributions of the first clay mineral peaks properly.
- Mineral peaks of the same mineral correlate with each other but the correlation gets weaker if one of the peaks is a shoulder in bulk powder X-ray diffractograms or the peak location is very close to another first mineral peak. Exclusion of these peaks of low correlation do not affect geochemical correlations efficiently as the overall mineralogy shadows the exceptional peaks.
- Quartz, serpentine, feldspars and clay minerals have higher correlation coefficients in the floodplain samples while calcite and aragonite have higher correlation coefficients in the lake samples. Especially aragonite correlations are influenced by the environmental difference very much.
- Presentation of mineral-element correlations by coefficient matrices give complex results. Using Principal Component Analyses (PCA) on either all elements or all mineral peaks and forming a correlation matrix from these principal components reflect the summary of the same results.

- In statistical evaluation, the first four clay peaks (14.50 Å, 8.44 Å, 7.16 Å, 4.48 Å) exhibit higher correlation with quartz while other three peaks (4.05 Å, 2.59 Å, 2.56 Å) correlate among themselves better.
- Considering all environments together, quartz correlates with Si, Al, Fe, Mn, Cu, Ti, Hf, Zr, and Nb that infer presence of impurities like rutile. Quartz also has strong negative correlation with Ca, Sr, As, and Se. Calcite intensity correlates positively with calcium and strontium and negatively with the elements that correlate with quartz.
- Aragonite has a moderate correlation with calcium and strontium when all samples are taken into consideration but the correlation coefficients of aragonite get higher in the lake samples.
- Feldspars have moderate positive correlation with sodium and magnesium and moderate negative correlation with K, Rb, and Cs. Serpentines strongly correlate with Mg, Na, Cr, Co, and Ni.
- While the clay peaks before 20° 2θ on bulk powder X-ray diffractograms correlate with the same elements with quartz, other clay peaks strongly correlate with Si, Al, Fe, K, V, Cu, Ti, Rb, Cs, Zr, Nb, and trace elements.
- AL-5 049 and AL-5 505 are determined to include high amorphous silica from XRD and ICP-MS/OES analyses. Moreover, SEM-EDS analyses showed that this amorphous silica is due to extreme amounts of diatoms along with smectites. In the rest of the samples, amorphous silica is also present in low amounts.

REFERENCES

Aagaard, P. (1974). Rare earth elements adsorption on clay minerals. Bulletin Du Groupe Français Des Argiles, 26(2), 193–199. https://doi.org/10.3406/argil.1974.1217

Akar, M., & Kara, D. (2018). Toprakhisar höyük kazısı: MÖ 6. binyıldan 1. binyıla Amik Ovası merkezleri ve Altınözü kırsal yerleşimleri arası politik, ekonomik ve kültürel ilişkiler. Anadolu (Anatolia). 237-276. 10.1501/Andl_0000000457.

Akar, M., & Kara, D. (2020). The formation of collective, political and cultural memory in the Middle Bronze Age: Foundation and termination rituals at Toprakhisar Höyük. Anatolian Studies. 70. 1-27. 10.1017/S0066154619000139.

Amonette, J. E., & Sanders, R. W. (1994). Nondestructive techniques for bulk elemental analysis. In Amonette, J. E. & L. W. Zelanzny (eds.) Quantitative Methods in Soil Mineralogy. Soil Science Society of America, Inc., Madison, Wisconsin: 1–48.

Atan, O. R. (1969). Eğribucak-Karacaören (Hassa)-Ceylanlı-Dazevleri (Kırıkhan) arasındaki Amanos dağlarının jeolojisi: MTA Yayınları., 139, 85 s., Ankara.

Aurelio, G., Fernández-Martínez, A., Cuello, G.J., Román, G., Alliot, I., & Charlet, L. (2008). Structural Study of Selenium and Arsenic Substitution in Calcite.

Avşar, U., Akar, M., & Pearson, C. (2019). Geoarchaeological Investigations in the Amuq Valley of Hatay: Sediment Coring Project in the Environs of Tell Atchana.

Balashov, Y. A., & Girin, Y. P. (1969). on the reserve of mobile rare earth elements in sedimentary rocks. Geochem. Intern., 6, p. 649–659.

Bangaku Naidu, K., Reddy, K. S., Ravi Sekhar, C., Ganapati Rao, P., & Murali Krishna, K. N. (2019). Rutile Mineral Chemistry as a guide to provenance of red sediments and modern sands of Bhimunipatnam–konada coast, Andhra Pradesh, East Coast of India. National Academy Science Letters, 43(2), 145–152. https://doi.org/10.1007/s40009-019-00819-9

Barshad, I. (1960). X-ray analysis of soil colloids by a modified salted paste method. In Ingerson, E. (ed.) Seventh National Conf. Clays & Clay Minerals, Pergamon Press, London: 350–364.

Bradley, W. F., Grim, R. E., & Clark, G. L. (1937). A study of the behavior of montmorillonite upon wetting. Z. Kristallogr. 97: 216–222.

Braidwood, R. J., & Braidwood, L. S. (1960). Excavations in the Plain of Antioch, vol. 1. The Earlier Assemblages, Phases A-J. Chicago: Oriental Institute Publications 61.

Braidwood, R. (1937). Mounds in the Plain of Antioch. Chicago: Oriental Institute Publications 48. Cubadda, F. (2007). Inductively coupled plasma mass spectrometry. Food Toxicants Analysis, 697-751. doi:10.1016/b978-044452843-8/50020-110

Brichni, A., Hammi, H., Aggoun, S., & Mnif, A. (2016). Optimisation of magnesium oxychloride cement properties by silica glass. Advances in Cement Research, 28(10), 654–663. https://doi.org/10.1680/jadcr.16.00024

Chang, L.L.Y., Howie, R.A., & Zussman, J. (1996) Rock-forming minerals, (2nd edition), v. 5B, non-silicates, 108–135.

Conconi, M. S., Rendtorff, N. M., & Aglietti, E. F. (2011). Evaluation of non crystalline phase in AZS refractories by Xrd Methods. New Journal of Glass and Ceramics, 01(02), 28–33. https://doi.org/10.4236/njgc.2011.12005

Coşkun, B. (1994). Oil Possibility of Duplex Structures in the Amik-Reyhanlı Basin, SE Turkey. Journal of Petroleum Geology, 17. 461-472.

Cubadda, F. (2007). Inductively coupled plasma mass spectrometry. Food Toxicants Analysis, 697–751. https://doi.org/10.1016/b978-044452843-8/50020-1

Çoğulu, A. E. (1973). New data on the petrology of Kızıldağ massif (Hatay-Turkey). Congr. Earth Sciences of the 50th Anniversary of Turkish Republic, Abst. of the Papers, Ankara.

Çoğulu, A. E. (1974). Ultrabasic tectonites and layered peridotites of the Hatay area (Turkey). Bull MTA 83:139–147.

Daneshvar, E., & Worden, R. H. (2017). Feldspar alteration and Fe minerals: origin, distribution and implications for sandstone reservoir quality in estuarine sediments. Geological Society, London, Special Publications, 435(1), 123–139. doi:10.1144/sp435.17

Decrouez, D., Selçuk, H. (1981). Les Nummulites de la craie de la Formation d'Okçular (Hatay, unité téctonique des plis bordiers, sud de la Turquie). Notes du Laboratoire de Palaeontologie del'Université de Genève 8.

De Giorgi, A. (2007). The Formation of a Roman Landscape. The Case of Antioch. Journal of Roman Archaeology 20: 283-299.

Deshmukh, P., Bhatt, J., Peshwe, D., & Pathak, S. (2011). Determination of silica activity index and XRD, SEM and EDS studies of amorphous Sio2 extracted from Rice Husk Ash. Transactions of the Indian Institute of Metals, 65(1), 63–70. https://doi.org/10.1007/s12666-011-0071-z

Dias, Á. S., & Barriga, F. J. A. S. (2006). Mineralogy and geochemistry of hydrothermal sediments from the serpentinite-hosted Saldanha hydrothermal field (36°34′N; 33°26′W) at Mar. Marine Geology, 225(1-4), 157–175. https://doi.org/10.1016/j.margeo.2005.07.013

Diebold, B. (2004). Excavations at Tell Kurdu 2001: The Pottery. In: R. Özbal et al.: Tell Kurdu Excavations 2001. Anatolica 30: 52-55.

Durusu Tanrıöven, M. (2010). The transition from the Late Bronze Age to the Early Iron Age in the Upper Euphrates and the Amuq: A study of settlement patterns (Unpublished master's thesis). İhsan Doğramacı Bilkent University.

El Ouahabi, M., Hubert-Ferrari, A., & Fagel, N. (2017). Lacustrine clay mineral assemblages as a proxy for land-use and climate changes over the last 4 kyr: The Amik Lake case study, Southern Turkey. Quaternary International. 438. 10.1016/j.quaint.2016.11.032.

Eren, M., Kadir, S., Kapur, S., Huggett, J., & Zucca, C. (2015). Colour origin of Tortonian red mudstones within the Mersin area, Southern Turkey. Sedimentary Geology, 318, 10–19. https://doi.org/10.1016/j.sedgeo.2014.12.003

Fairchild, I., Hendry, G., Quest, M., & Tucker, M. (1988). Chemical analysis of sedimentary rocks. In Tucker, M. (ed.) Techniques in Sedimentology. Blackwell Scientific Publications, Oxford: 274–386.

Faust, G. T., & Fahey, J. J. (1962). The serpentine-group minerals. Professional Paper. https://doi.org/10.3133/pp384a

Friedman, E.S., & Reichel, C. (1995). Tell el-Judeidah 1995: The Amuq F and G horizons revisited. In: K.A. Yener et al.: The Oriental Institute Amuq Valley Projects, 1995. Anatolica 22: 67-70.

Fytianos, G., Ucar, S., Grimstvedt, A., Svendsen, H. F., & Knuutila, H. (2016). Corrosion Evaluation of MEA Solutions by SEM-eds, ICP-MS and XRD. Energy Procedia, 86, 197–204. https://doi.org/10.1016/j.egypro.2016.01.020

Gerke, T. L., Scheckel, K. G., & Schock, M. R. (2009). Identification and distribution of vanadinite (pb5(v5+o4)3cl) in lead pipe corrosion by-products. Environmental Science & Technology, 43(12), 4412–4418. https://doi.org/10.1021/es900501t

Gerritsen, F., De Giorgi, A., Eger, A., Özbal, R., & Vorderstrasse, T. (2008). Settlement and Landscape Transformations in the Amuq Valley, Hatay. Anatolica. 34. 241-314. 10.2143/ANA.34.0.2031568.

Gibbs, R. J. (1965). Error due to segregation in quantitative clay mineral X-ray diffraction mounting techniques. Am. Mineral. 50: 741–751.

Götze, J., Pan, Y., & Müller, A. (2021). Mineralogy and mineral chemistry of Quartz: A Review. Mineralogical Magazine, 85(5), 639–664. https://doi.org/10.1180/mgm.2021.72

Griggs, C., Larson, S., Liu, G., Felt, D., Martin, W. A., Thompson, M., & Nestler, C. (2010). Solid-phase tungsten speciation by differential digestion. Environmental Forensics, 11(3), 275–281. https://doi.org/10.1080/15275922.2010.494966

Haines, R.C. (1971). Excavations in the Plain of Antioch, vol. 2. The Structural Remains of the Later Phases. Chicago: Oriental Institute Publications 95.

Harrison, T. P. (2009). Neo-Hittites in the land of "Palistin" Renewed Investigations at Tell Taʿyinat on the Plain of Antioch, Near Eastern Archaeology, 72: 174-89.

Hawthorne, F. C. (1988). Spectroscopic Methods in Mineralogy and Geology, Mineralogical Society of America, Reviews in Mineralogy, Volume 18, 695 pp. 11

Ingman, T., Eisenmann, S., Skourtanioti, E., Akar, M., Ilgner, J., Gnecchi, G., Le Roux, P., Shafiq, R., Neumann, G., Keller, M., Freund, C., Marzo, S., Lucas, M., Krause, J., Roberts, P., Yener, K., & Stockhammer, P. (2020). Human mobility at Tell Atchana (Alalakh) during the 2nd millennium BC: integration of isotopic and genomic evidence. 10.1101/2020.10.23.351882.

Jackson, M. L. (1969). Soil Chemical Analysis - Advanced Course edition. Madison, Wisconsin, 895 pp.

Kabala, C., & Bojko, O. (2014). Trends in Trace Element Concentrations in Holocene Bottom Sediments of a Lake Wielki Staw in the Karkonosze Mountains. Polish Journal of Environmental Studies. 2014;23(2):357-362.

Karakuş, K., Taner, G. (1994). Samandağ Formasyonun (Antakya Havzası) Yaşı ve Mollusca Faunasına Bağlı Paleoekolojik Özellikleri. Türkiye Jeoloji Bülteni, C.37, Sayı 2, s.87-109, Ankara.

Kavuzlu, M. (2006). Altınözü (Antakya) ve Yakın Civarının Tektono-Stratigrafisi. Ç. Ü. Sos. Bil. Enst. (Yayımlanmamış) Yüksek Lisans Tezi. Adana.

Kocaçiftçi, P. (2005). Antakya ve Yakın Civarının Tektono-Stratigrafisi, Ç.Ü Fen Bilimleri Enstitüsü Yüksek Lisans Tezi, 56 s., Adana.

Koçyiğit, A., Beyhan, A. (1998). A New Intra Continental Transcurrent Structure: The Central Anatolian Fault Zone, Turkey. Tectonophysics, 284, 317-336.

Kop, A. (1996). Kırıkhan (Hatay) ve Kuzeyinin Tektonostratigrafik İncelemesi, Ç.Ü Fen Bilimleri Enstitüsü Yüksek Lisans Tezi, 161 s., Adana.

Korkmaz, H. & Gürbüz, M. (2013). Amik Gölü'nün Kültürel Ekolojisi. Marmara Coğrafya Dergisi, 0 (17), 1-26. Retrieved from https://dergipark.org.tr/tr/pub/marucog/issue/464/3730

Last, W.M., (2001). Mineralogical analysis of lake sediments. In: Last, W.M. and Smol, J.P. (eds), Tracking environmental change using lake sediments, Vol. 2, Chap. 6, pp. 143–187. Kluwer Academic Publishers, Dordrecht.

Li, B., Zhuang, X., Li, J., Querol, X., Font, O., & Moreno, N. (2016). Geological controls on mineralogy and geochemistry of the late Permian coals in the Liulong mine of the Liuzhi Coalfield, Guizhou Province, Southwest China. International Journal of Coal Geology, 154-155, 1–15. https://doi.org/10.1016/j.coal.2015.12.003

Meinhold, G., Anders, B., Kostopoulos, D., & Reischmann, T. (2008). Rutile chemistry and thermometry as provenance indicator: An example from Chios Island, Greece. Sedimentary Geology, 203(1-2), 98–111. https://doi.org/10.1016/j.sedgeo.2007.11.004

Mıstık, T. (2002). Samandağ (Antakya) Civarının Jeolojik İncelemesi, Ç.Ü Fen Bilimleri Enstitüsü Yüksek Lisans Tezi, 46 s., Adana.

Moyo, S., Mphuthi, D., Cukrowska, E., Henshilwood, C. S., van Niekerk, K., & Chimuka, L. (2016). Blombos Cave: Middle stone age ochre differentiation

through Ftir, ICP oes, Ed XRF and Xrd. Quaternary International, 404, 20–29. https://doi.org/10.1016/j.quaint.2015.09.041

Musić, S., Filipović-Vinceković, N., & Sekovanić, L. (2011). Precipitation of amorphous SIO2 particles and their properties. Brazilian Journal of Chemical Engineering, 28(1), 89–94. https://doi.org/10.1590/s0104-66322011000100011

Nagelschmidt, G. (1941). Identification of clays by aggregate diffraction diagrams. J. Sci. Instrum. 18: 100–101.

Ogwuegbu, M., Onyedika, G., Hwang, J. Y., Ayuk, A., Peng, Z., Bowen, L., Ejike, E. N. O., Andriese, M. (2011). Mineralogical characterization of Kuru cassiterite ore by SEM-EDS, XRD and ICP Techniques. Journal of Minerals and Materials Characterization and Engineering, 10(09), 855–863. https://doi.org/10.4236/jmmce.2011.109066

Över, S., Ünlügenç, U. C., & Özden, S. (2001). Hatay Bölgesinde Etkin Gerilme Durumları, Yerbilimleri, 23, p. 1-14.

Özbal, R. (2006). Households, Daily Practice and Cultural Appropriation at Sixth Millennium Tell Kurdu. Unpublished PhD dissertation, Northwestern University.

Palache, C., Berman, H., & Frondel, C. (1951) Dana's system of mineralogy, (7th edition), v. II, 182–193.

Perinçek, D., Eren, A. G. (1990). Doğrultu atımlı Doğu Anadolu Fayı ve Ölü Deniz Fay Zonları etki alanında gelişen Amik havzasının kökeni, Türkiye 8. Petrol Kongresi Bildiri Kitabı, 180-192.

Potter, P. E., Maynard, J. B., & Pryor, W. A. (1980). Sedimentology of Shale. Springer-Verlag, New York, 306 pp. Prothero, D. R., & Schwab. F., (1996). Sedimentary Geology. W. H. Freeman and Company, New York, 575 pp.

Prothero, D. R., & Schwab, F. (1996). Sedimentary Geology. An Introduction to Sedimentary Rocks and Stratigraphy: New York, W. H. Freeman, 575 p.

Roaldset, E. (1973). Rare earth elements in Quaternary clays of the Numedal area, southern Norway. Lithos, 6, p. 349–372.

Roeser, P., Franz, S. O., & Litt, T. (2016). Aragonite and calcite preservation in sediments from Lake Iznik related to bottom lake oxygenation and water column depth. Sedimentology, 63(7), 2253–2277. https://doi.org/10.1111/sed.12306

Rojay, B., Ariel, H., & Toprak, V. (2001). Neotectonic and volcanic characteristics of the Karasu Fault Zone (Anatolia, Turkey): The Transition Zone between the Dead Sea Transform and the East Anatolian Fault Zone. Geodinamica Acta, 14(1-3), 197–212. https://doi.org/10.1016/s0985-3111(00)01053-6

Sarı, Z. (2009). Hatay'da Tarihi ve Turistik Yerler. Antakya Belediyesi Kültür Yayını.

Sawhney, B. L., & Stilwell, D. E. (1994). Dissolution and elemental analysis of minerals, soils and environmental samples. Quantitative Methods in Soil Mineralogy, 49–82.

Sheppard, R. Y., Milliken, R. E., Russell, J. M., Dyar, M. D., Sklute, E. C., Vogel, H., Melles, M., Bijaksana, S., Morlock, M. A., & Hasberg, A. K. M. (2019). Characterization of iron in Lake Towuti sediment. Chemical Geology, 512, 11–30. https://doi.org/10.1016/j.chemgeo.2019.02.029

Sigal, J., Kafesçioğlu, İ. (1963). I. ve VII. Bölgeler stratigrafi etüdü (I.F.P. 1962-1963). TPAO. Rap. no. 300.

Sirel, E., Gündüz, H. (1978). Description of Sivasella n. gen. (Foraminifera) from the Maestrichtian of Sivas (Central Turkey).

Spirn, R. V. (1965). Rare earth distributions in the marine environment. Ph. D. Thesis, M.I.T.

Swapp, S. (2017). Scanning electron microscopy (SEM). Geochemical Instrumentation and Analysis. Retrieved January 13, 2022, from https://serc.carleton.edu/research_education/geochemsheets/techniques/SEM.html

Şafak, Ü. (1993). Antakya Havzası Planktonik Foraminifer Biyostratigrafisi. A. Suat Erk Jeoloji Simpozyumu Bildirileri , vol.1 , 143-156.

Şengör, A. M. C. (1979). The North Anatolian Transform Fault: Its Age, Offset And Tectonic Significance. Journal Geology Society of London, 136, 269-282.

Tekeli O, Erendil M. (1986) Geology and petrology of the Kızıldağ ophiolite (Hatay). Bull Miner Res Explor Inst Turk 21:21–37.

Telegdi, J., Shaban, A., & Vastag, G. (2018). Biocorrosion—Steel. Encyclopedia of Interfacial Chemistry, 28–42. https://doi.org/10.1016/b978-0-12-409547-2.13591-7

Temizkan, N. (2003). Harbiye (Antakya) Civarının Jeolojik İncelemesi, Ç.Ü Fen Bilimleri Enstitüsü Yüksek Lisans Tezi, 60 s., Adana.

Theisen, A. A., & Harward, M. E. (1962). A Paste Method for Preparation of Slides for Clay Mineral Identification by X-ray Diffraction. Soil Science Society of America Journal, 26(1), p. 90-91. https://doi.org/10.2136/sssaj1962.03615995002600010034xc

Tien, P-L. (1974). A simple device for smearing clay-on-glass slides for quantitative X-ray diffraction studies. Clays and Clay Min., 22.

Tinkler, C., Wagner, J. J., Delaloye, M., & Selçuk, R. (1981). Tectonic History of the Hatay Ophiolites (South Turkey) and their Relation with the Dead Sea Rift. Tectonophysics, 72, 23-41.

Ulu, Ü. (2002). 1:500.000 Ölçekli Türkiye Jeoloji Haritaları, No: 16 Hatay. Maden Tetkik ve Arama Genel Müdürlüğü, Ankara, Türkiye.

Varnacı, F. (2008). Kurutulan Amik Gölünün Yöresel Ekosistem Üzerindeki Etkileri, Basılmamış Yüksek Lisans Tezi, Balıkesir Üniversitesi Sosyal Bilimler Enstitüsü Coğrafya Anabilim Dalı, Balıkesir.

Walker, G. P. L. (1962). Low-potash gismondine from Ireland and Iceland. Mineral. Mag., 33, p. 187-201.

Warr, L.N. (2021). IMA–CNMNC approved mineral symbols. Mineralogical Magazine, 85(3), 291-320. doi:10.1180/mgm.2021.43

Wilhelms-Dick, D., Westerhold, T., Röhl, U., Wilhelms, F., Vogt, C., Hanebuth, T. J., Römmermann, H., Kriews, M., & Kasten, S. (2012). A comparison of MM scale resolution techniques for element analysis in sediment cores. Journal of Analytical Atomic Spectrometry, 27(9), 1574. https://doi.org/10.1039/c2ja30148b

Wilkinson, T. J. (2000). Geoarchaeology of the Amuq Plain. In K. A. Yener et al. 'The Amuq Valley Regional Project 1995-1998'. American Journal of Archaeology 104. 163-220,

Yalçın, Ş., & Mutlu, İ. H. (2012). Structural characterization of some table salt samples by XRD, ICP, FTIR and XRF Techniques. Acta Physica Polonica A, 121(1), 50–52. https://doi.org/10.12693/aphyspola.121.50

Yener, K. A., Edens, C., Harrison, P. T., Verstraete, J., & Wilkinson, J. T. (2000). The Amuq Valley Regional Project 1995-1998, American Journal of Archaeology, 104, p. 163-220.

Yener, K. A. (2005). The Amuq Valley Regional Projects, The Amuq Valley Regional Projects Volume 1: Surveys in the Plain of Antioch and Orontes Delta Turkey, 1995-2002, ed. K. A. Yener, s. 1-24. Oriental Institute Publications no 131. Chicago.

Yılmaz, Y., Gürpınar, O., & Yiğitbaş, E. (1988). Amanos Dağları ve Maraş Dolaylarında Miyosen Havzalarının Tektonik Evrimi, T.P.J.D Bülteni, 52-72, Ankara. Bull. of the Geol. Soc. of Turkey.

Zhu, J., Shan, J., Qiu, P., Qin, Y., Wang, C., He, D., Sun, B., Tong, P., & Wu, S. (2004). The multivariate statistical analysis and XRD analysis of pottery at Xigongqiao Site. Journal of Archaeological Science, 31(12), 1685–1691. https://doi.org/10.1016/j.jas.2004.05.001

Zhu, K. Y., Su, H. M., & Jiang, S. Y. (2019). Mineralogical control and characteristics of rare earth elements occurrence in Carboniferous bauxites from western Henan Province, North China: A XRD, SEM-EDS and LA-ICP-MS analysis. Ore Geology Reviews, 114, 103144. https://doi.org/10.1016/j.oregeorev.2019.103144

Zorlu, K. (2003). Samandağ-Yayladağı (Hatay) Arasının Tektono-Stratigrafik İncelemesi, Mersin Üniversitesi Fen Bilimleri Enstitüsü, Yüksek Lisans Tezi, 89 s., Mersin

APPENDICES

A. X-Ray Diffractograms of Bulk Powder Samples

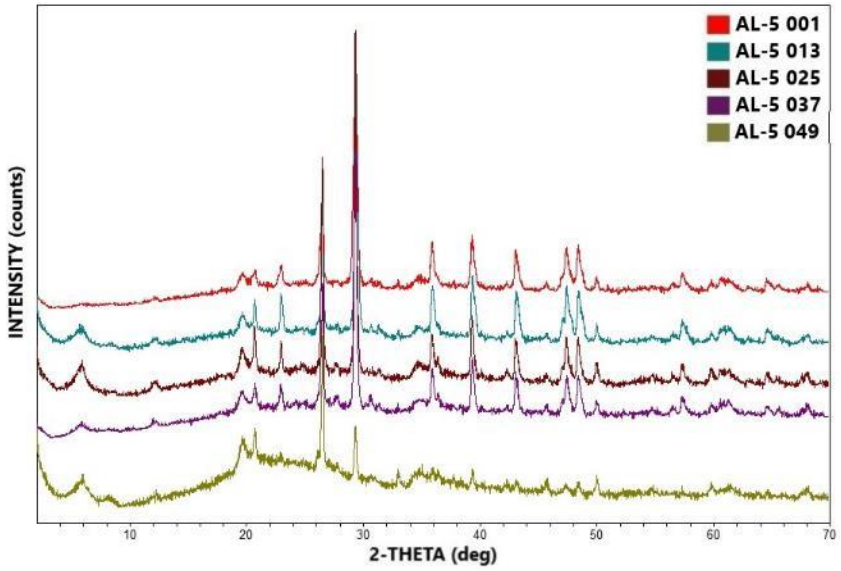

Figure A- 1. Bulk powder X-ray diffractograms of AL-5 001 (red), AL-5 013 (blue), AL-5 025 (brown), AL-5 037 (purple), and AL-5 049 (green)

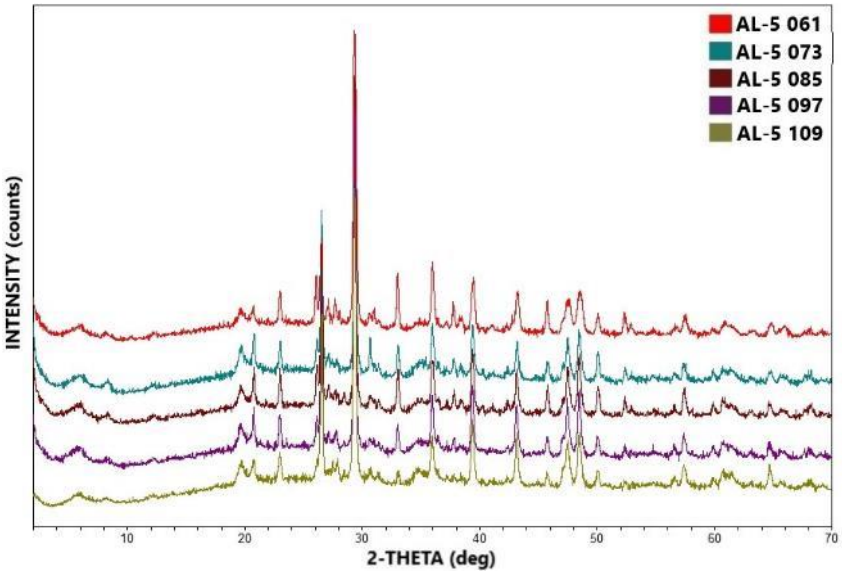

Figure A- 2. Bulk powder X-ray diffractograms of AL-5 061 (red), AL-5 073 (blue), AL-5 085 (brown), AL-5 097 (purple), and AL-5 109 (green)

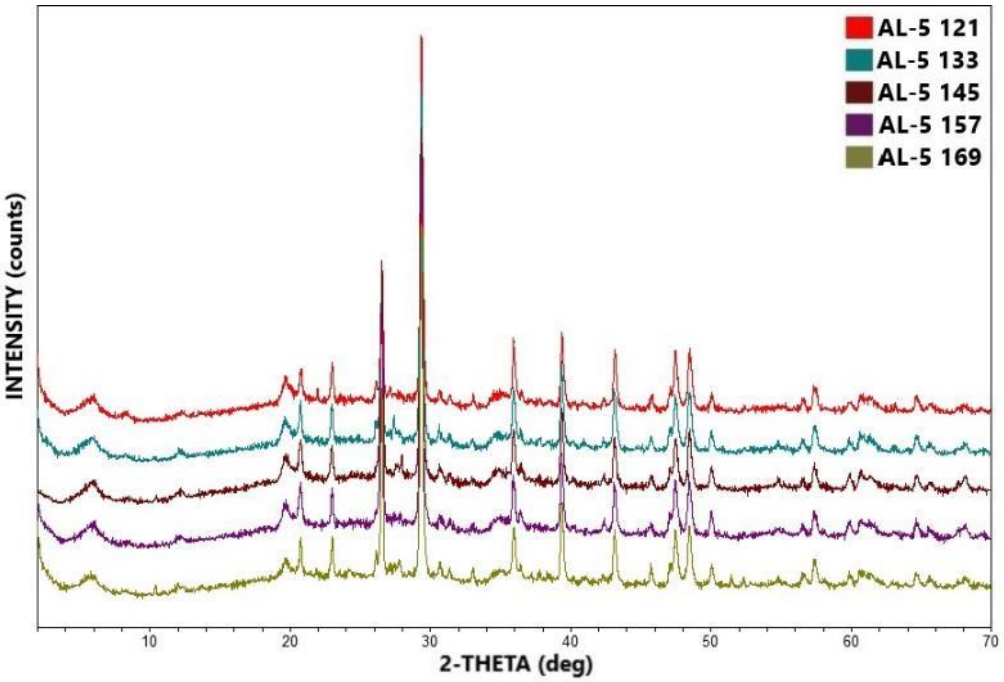

Figure A- 3. Bulk powder X-ray diffractograms of AL-5 121 (red), AL-5 133 (blue), AL-5 145 (brown), AL-5 157 (purple), and AL-5 169 (green)

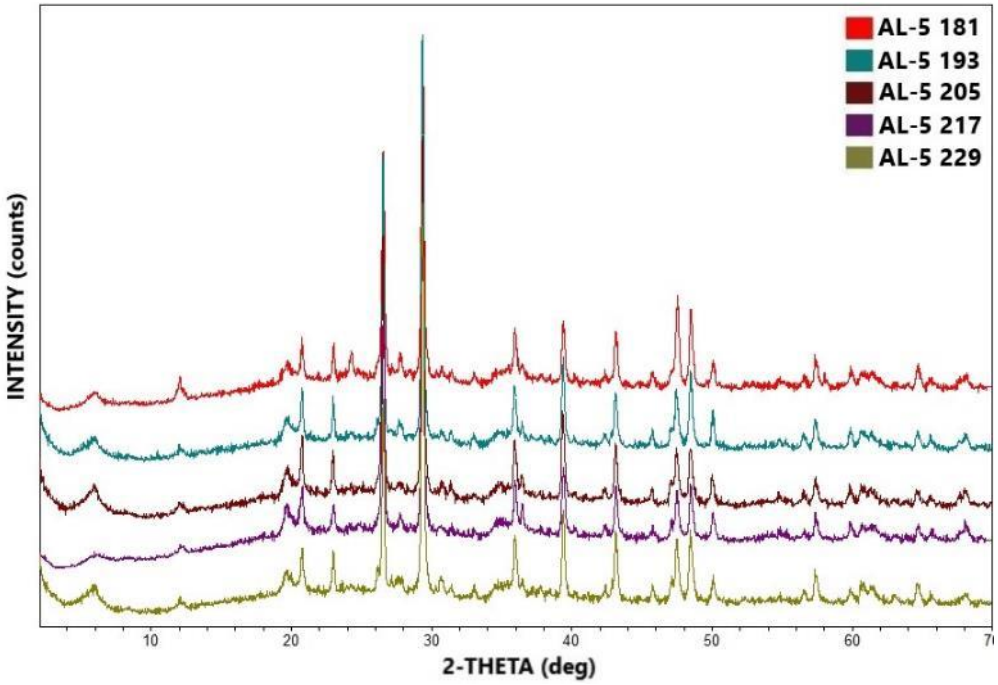

Figure A- 4. Bulk powder X-ray diffractograms of AL-5 181 (red), AL-5 193 (blue), AL-5 205 (brown), AL-5 217 (purple), and AL-5 229 (green)

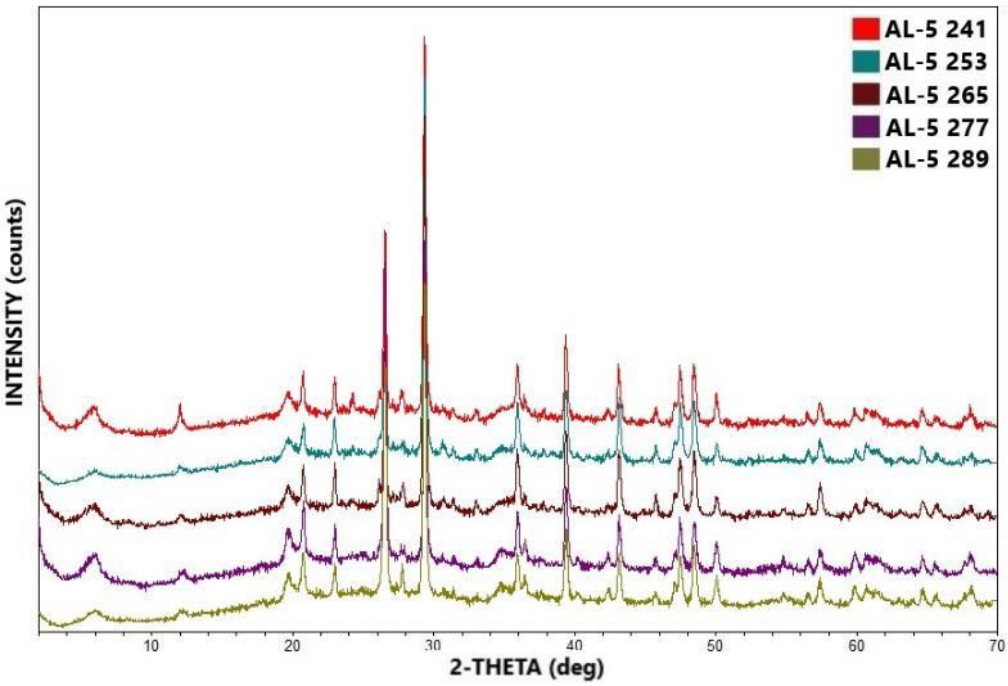

Figure A- 5. Bulk powder X-ray diffractograms of AL-5 241 (red), AL-5 253 (blue), AL-5 265 (brown), AL-5 277 (purple), and AL-5 289 (green)

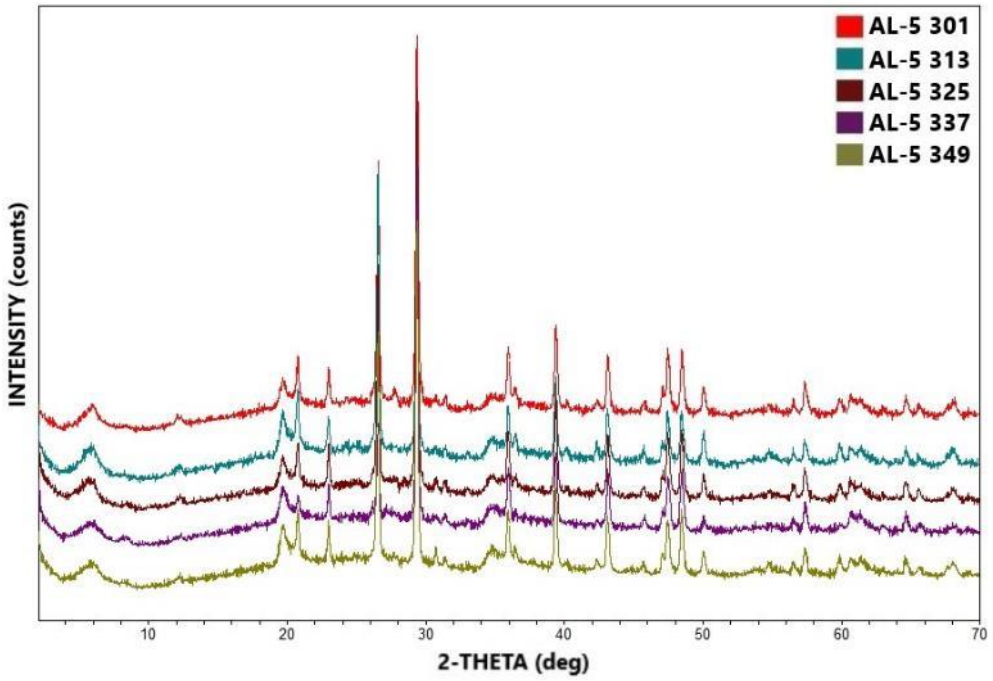

Figure A- 6. Bulk powder X-ray diffractograms of AL-5 301 (red), AL-5 313 (blue), AL-5 325 (brown), AL-5 337 (purple), and AL-5 349 (green)

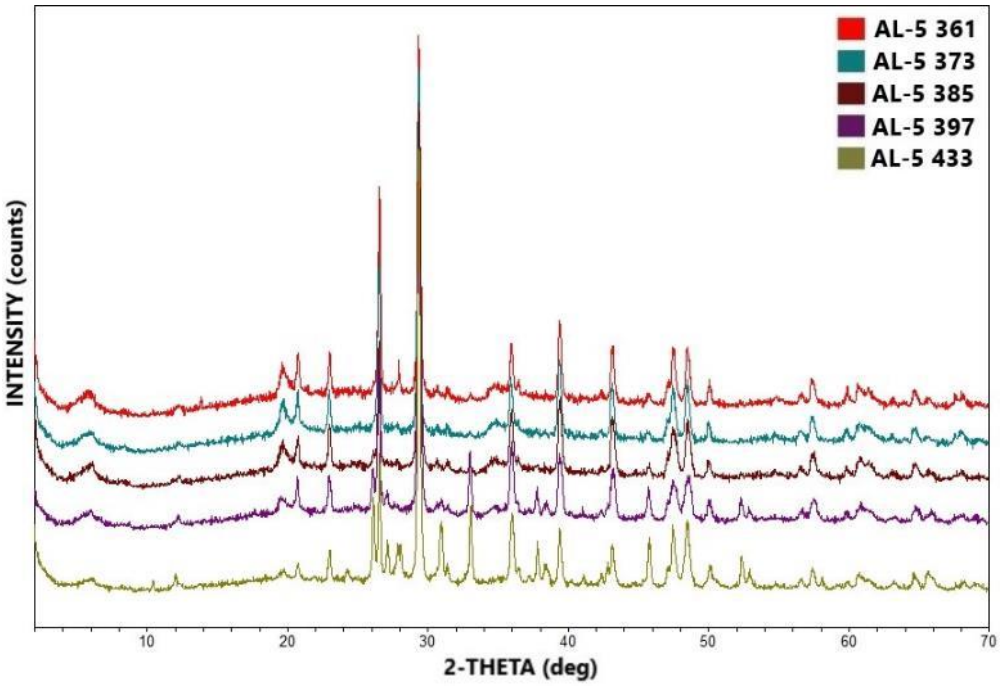

Figure A- 7. Bulk powder X-ray diffractograms of AL-5 361 (red), AL-5 373 (blue), AL-5 385 (brown), AL-5 397 (purple), and AL-5 433 (green)

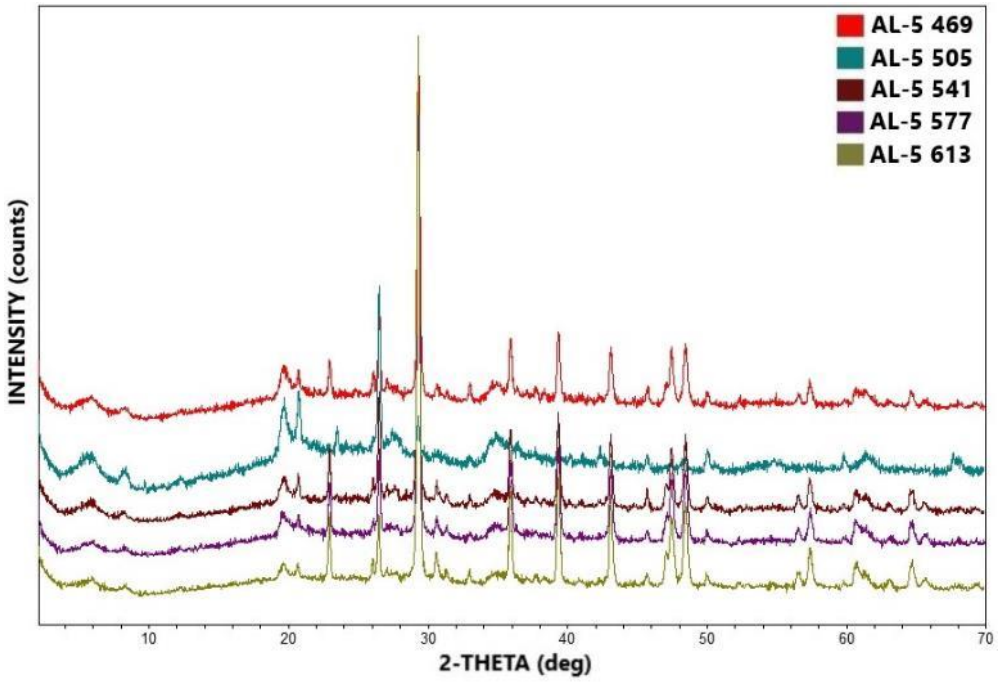

Figure A- 8. Bulk powder X-ray diffractograms of AL-5 469 (red), AL-5 505 (blue), AL-5 541 (brown), AL-5 577 (purple), and AL-5 613 (green)

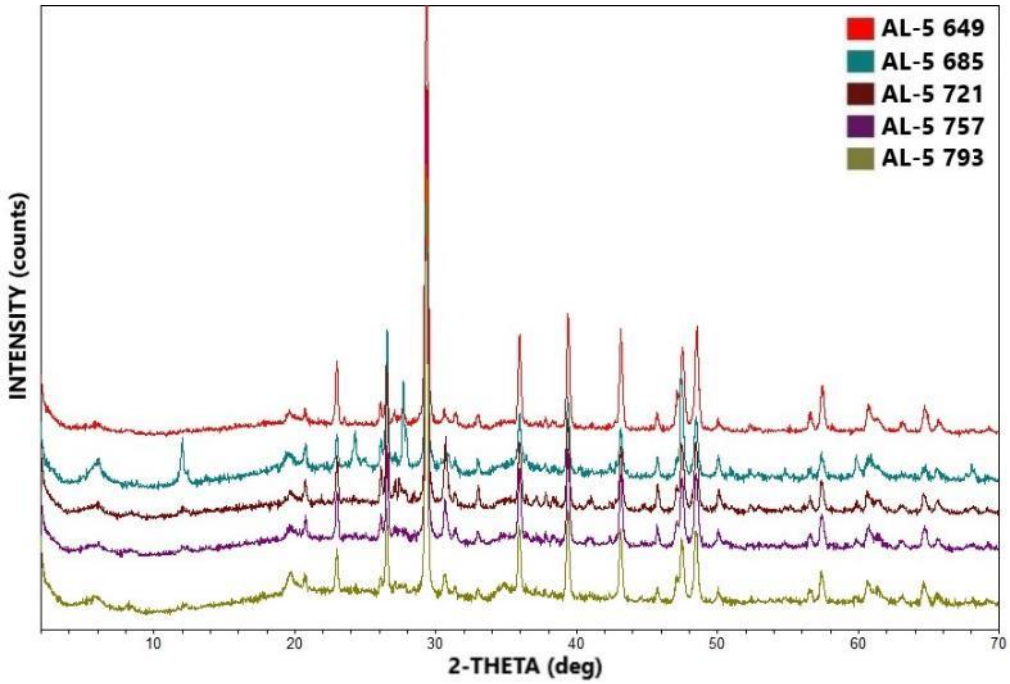

Figure A- 9. Bulk powder X-ray diffractograms of AL-5 649 (red), AL-5 685 (blue), AL-5 721 (brown), AL-5 757 (purple), and AL-5 793 (green)

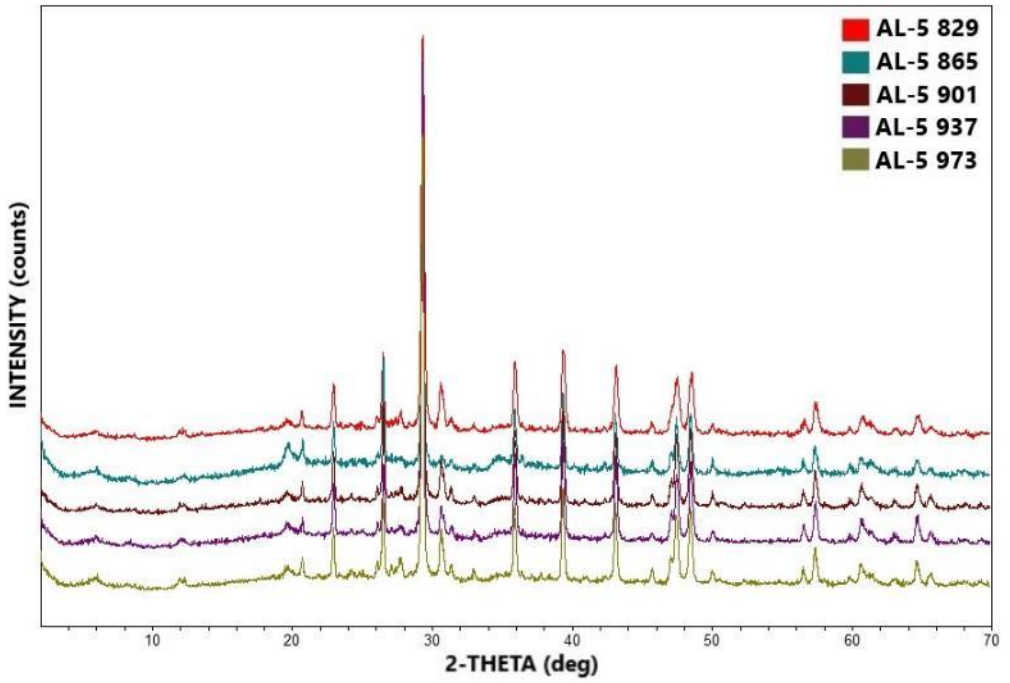

Figure A- 10. Bulk powder X-ray diffractograms of AL-5 829 (red), AL-5 865 (blue), AL-5 901 (brown), AL-5 937 (purple), and AL-5 973 (green)

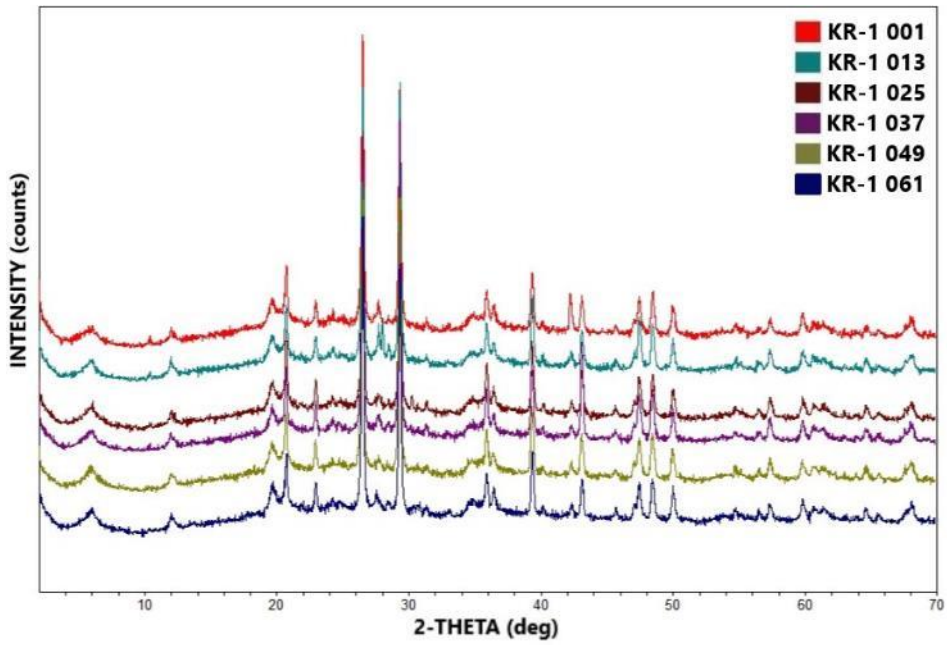

Figure A- 11. Bulk powder X-ray diffractograms of KR-1 001 (red), KR-1 013 (light blue), KR-1 025 (brown), KR-1 037 (purple), KR-1 049 (green), and KR-1 061 (dark blue)

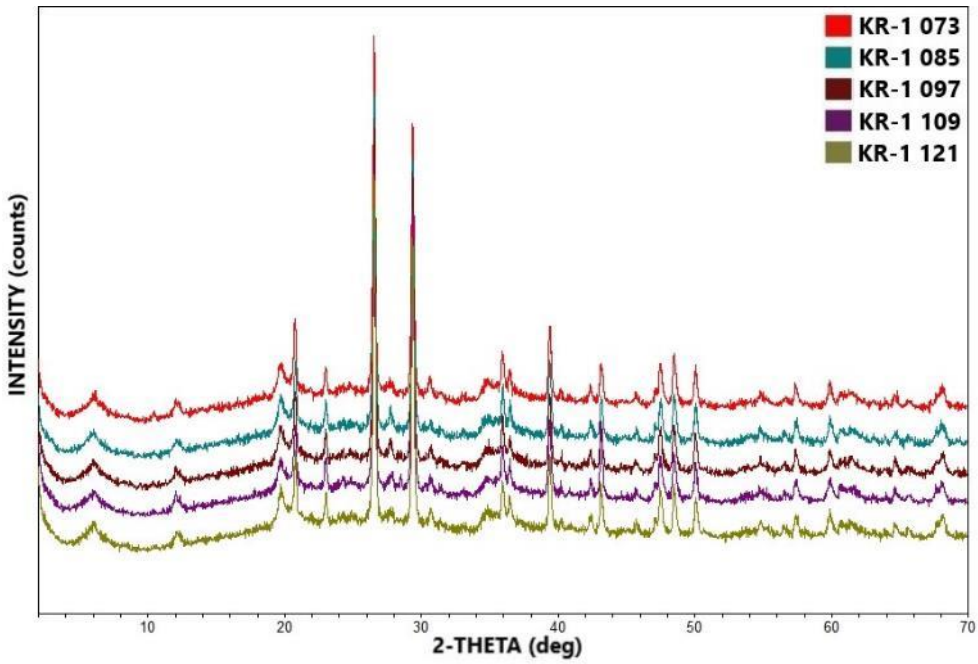

Figure A- 12. Bulk powder X-ray diffractograms of KR-1 073 (red), KR-1 085 (blue), KR-1 097 (brown), KR-1 109 (purple), and KR-1 121 (green)

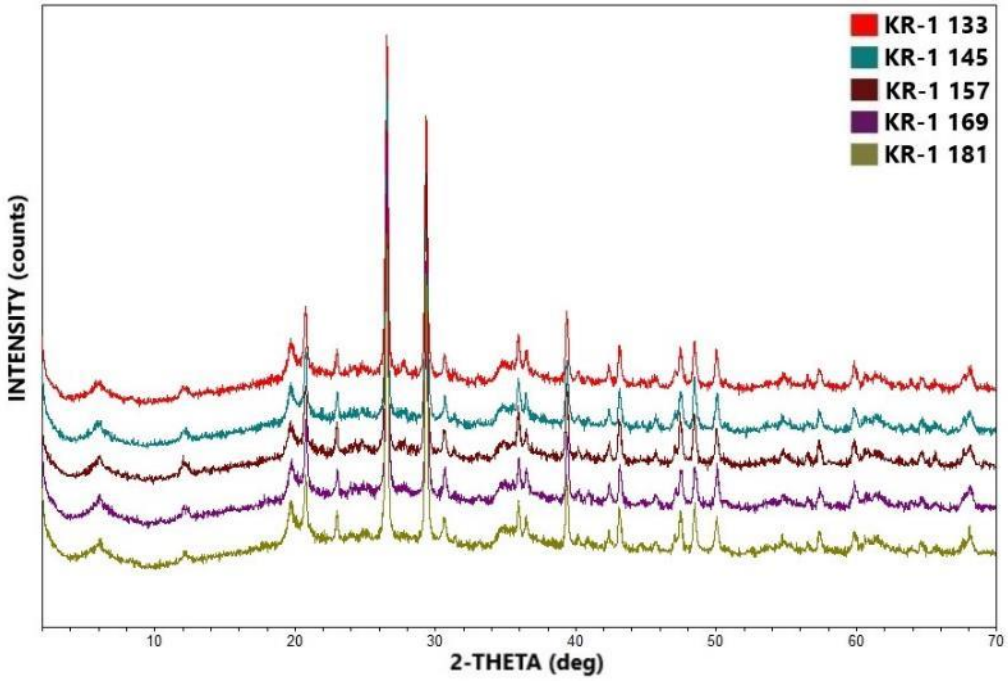

Figure A- 13. Bulk powder X-ray diffractograms of KR-1 133 (red), KR-1 145 (blue), KR-1 157 (brown), KR-1 169 (purple), and KR-1 181 (green)

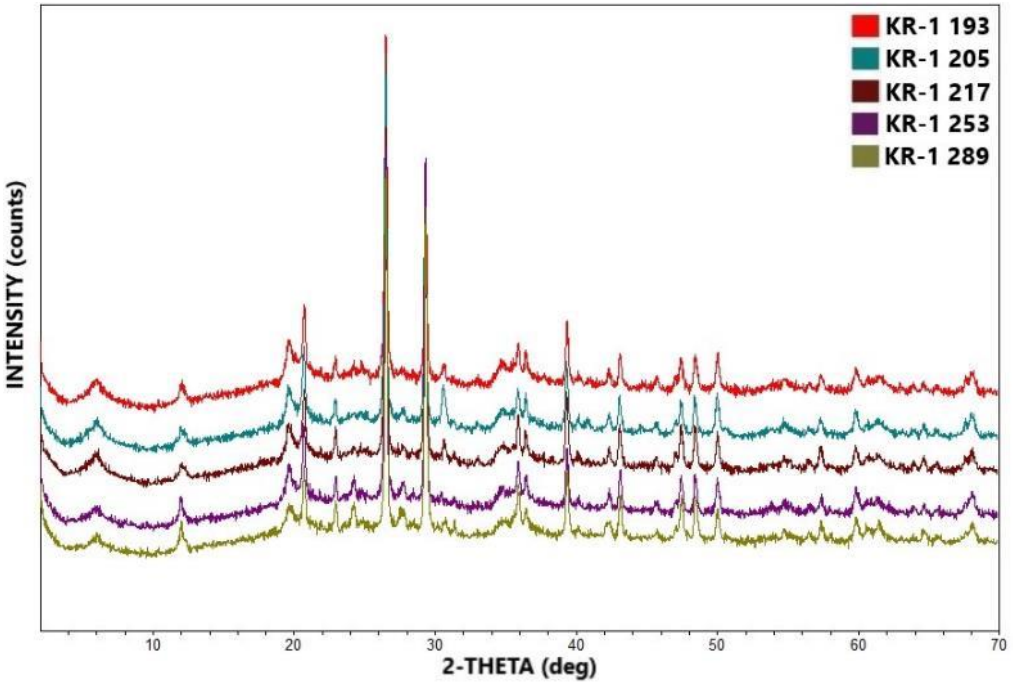

Figure A- 14. Bulk powder X-ray diffractograms of KR-1 193 (red), KR-1 205 (blue), KR-1 217 (brown), KR-1 253 (purple), and KR-1 289 (green)

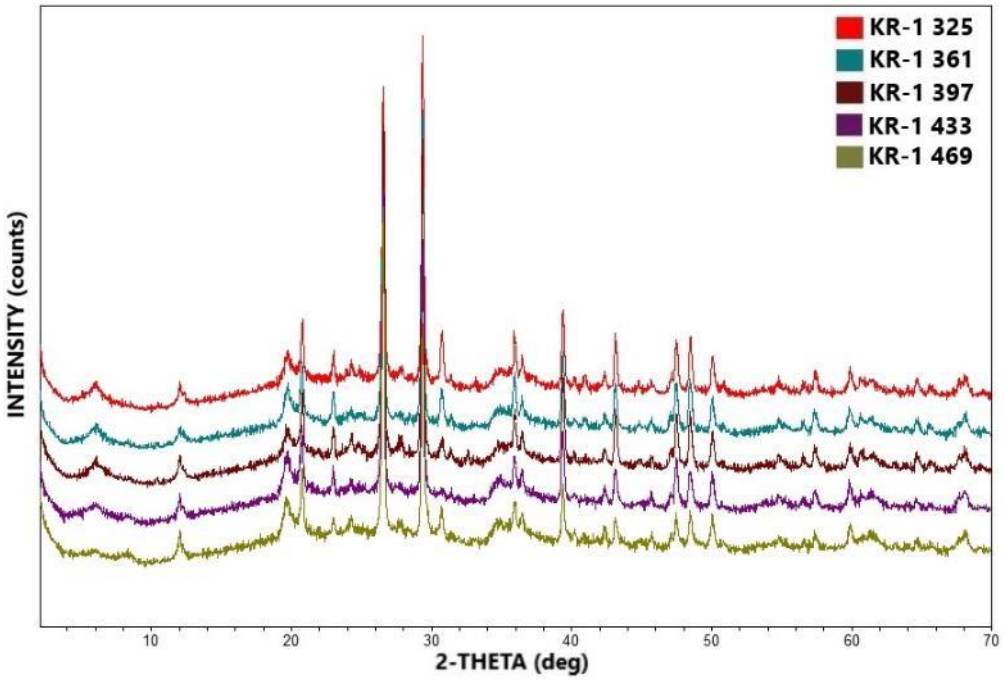

Figure A- 15. Bulk powder X-ray diffractograms of KR-1 325 (red), KR-1 361 (blue), KR-1 397 (brown), KR-1 433 (purple), and KR-1 469 (green)

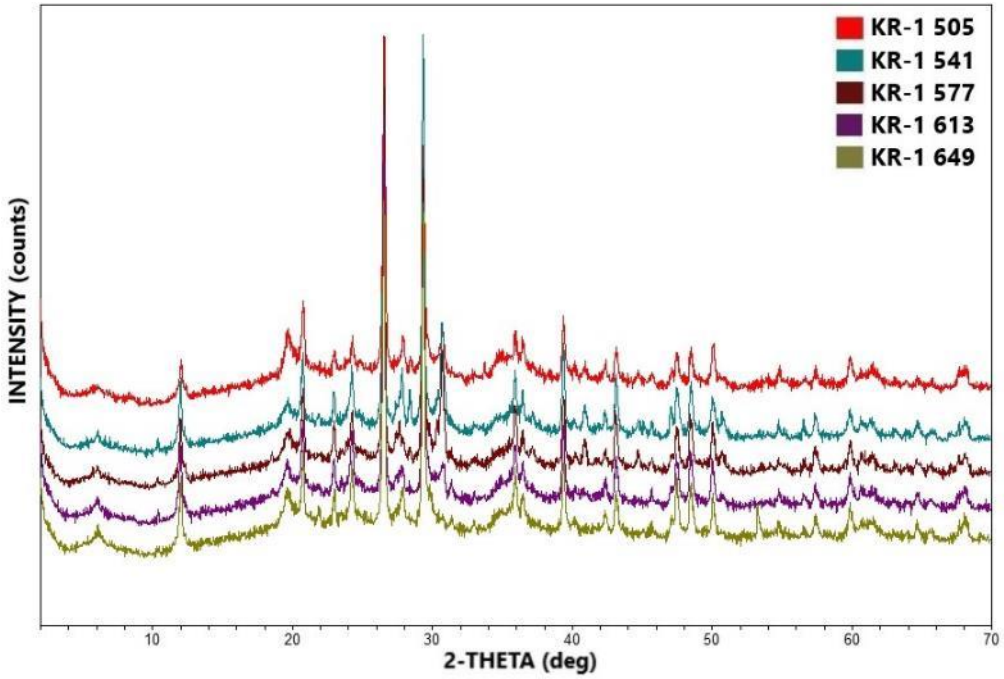

Figure A- 16. Bulk powder X-ray diffractograms of KR-1 505 (red), KR-1 541 (blue), KR-1 577 (brown), KR-1 613 (purple), and KR-1 649 (green)

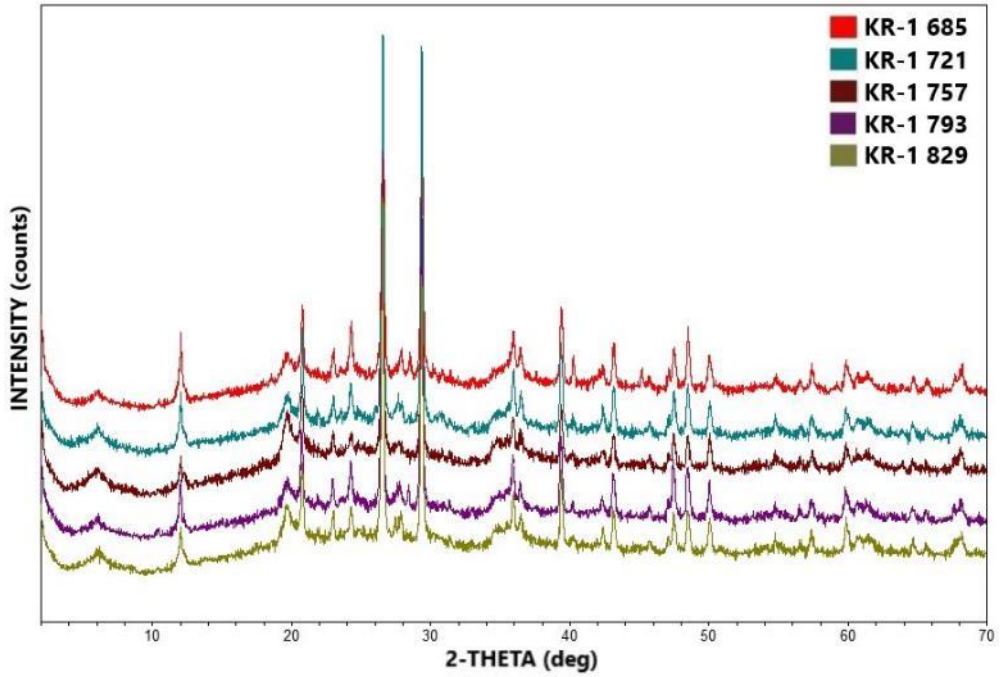

Figure A- 17. Bulk powder X-ray diffractograms of KR-1 685 (red), KR-1 721 (blue), KR-1 757 (brown), KR-1 793 (purple), and KR-1 829 (green)

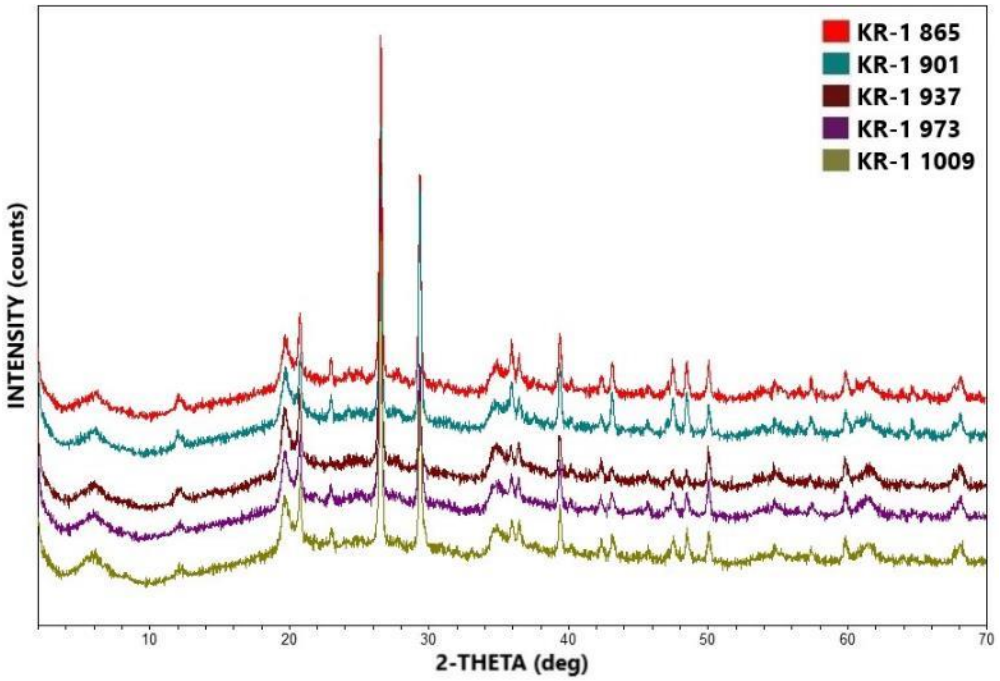

Figure A- 18. Bulk powder X-ray diffractograms of KR-1 865 (red), KR-1 901 (blue), KR-1 937 (brown), KR-1 973 (purple), and KR-1 1009 (green)

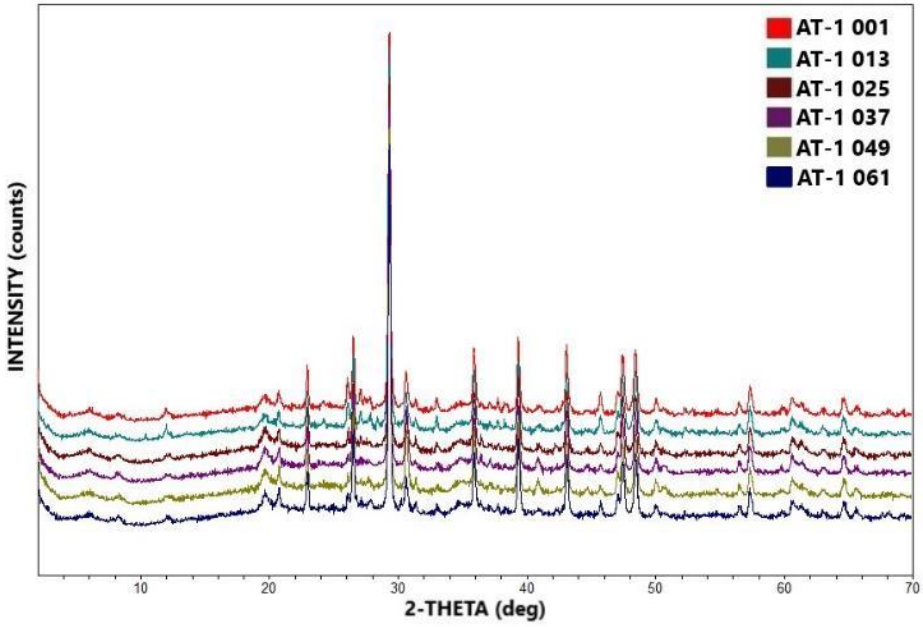

Figure A- 19. Bulk powder X-ray diffractograms of AT-1 001 (red), AT-1 013 (light blue), AT-1 025 (brown), AT-1 037 (purple), AT-1 049 (green), and AT-1 061 (dark blue)

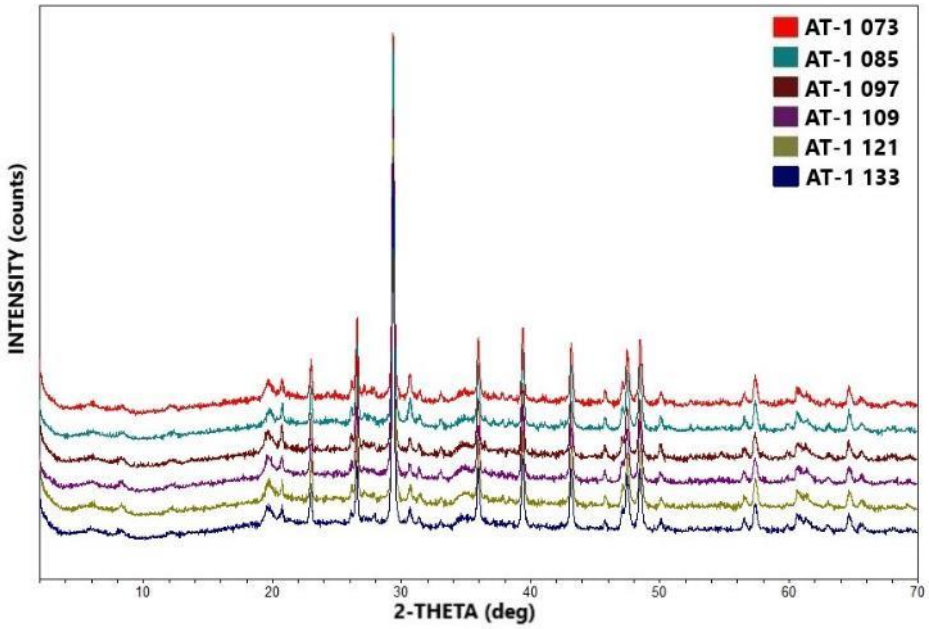

Figure A- 20. Bulk powder X-ray diffractograms of AT-1 073 (red), AT-1 085 (light blue), AT-1 097 (brown), AT-1 109 (purple), AT-1 121 (green), and AT-1 133 (dark blue)

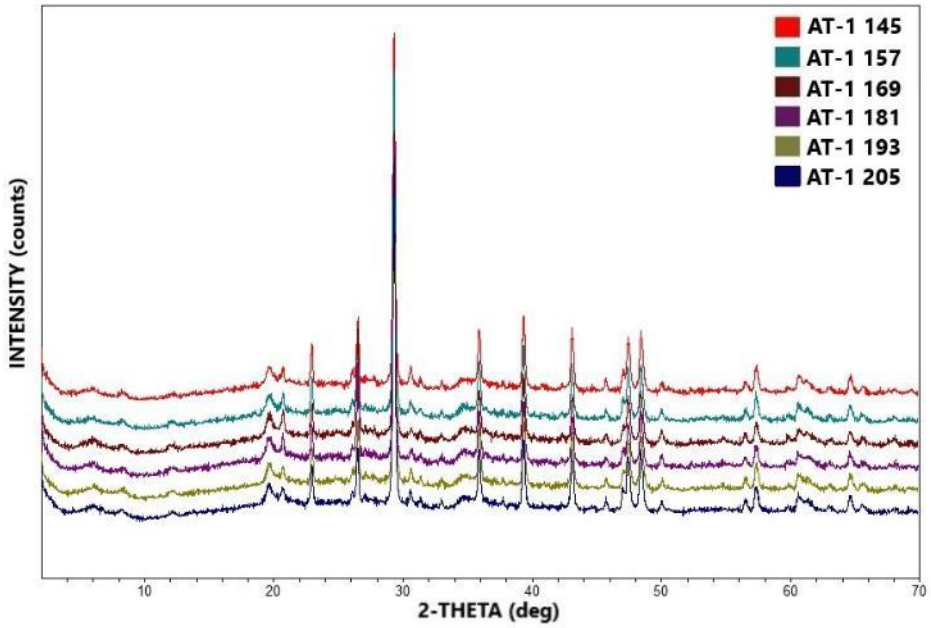

Figure A- 21. Bulk powder X-ray diffractograms of AT-1 145 (red), AT-1 157 (light blue), AT-1 169 (brown), AT-1 181 (purple), AT-1 193 (green), and AT-1 205 (dark blue)

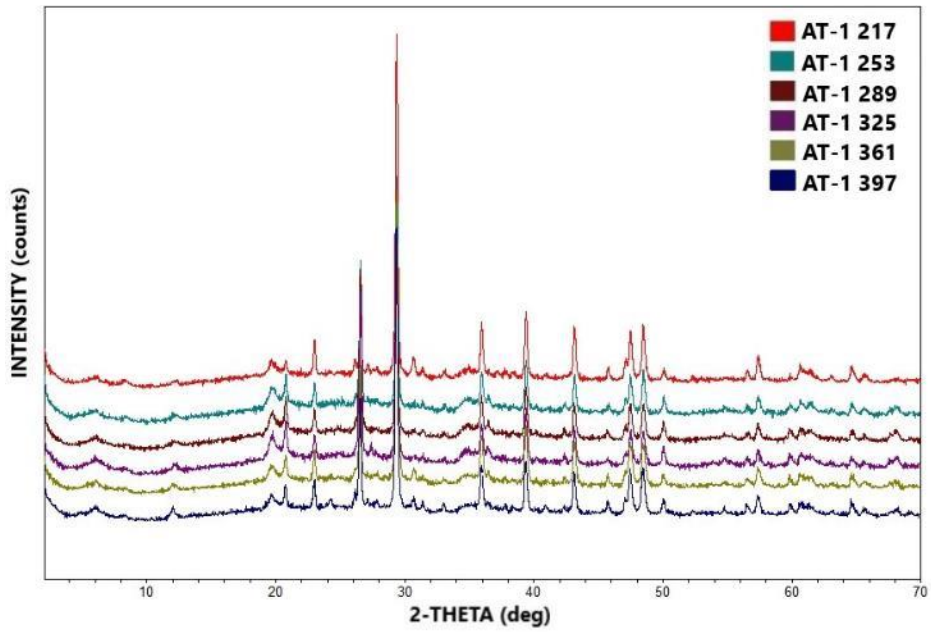

Figure A- 22. Bulk powder X-ray diffractograms of AT-1 217 (red), AT-1 253 (light blue), AT-1 289 (brown), AT-1 325 (purple), AT-1 361 (green), and AT-1 397 (dark blue)

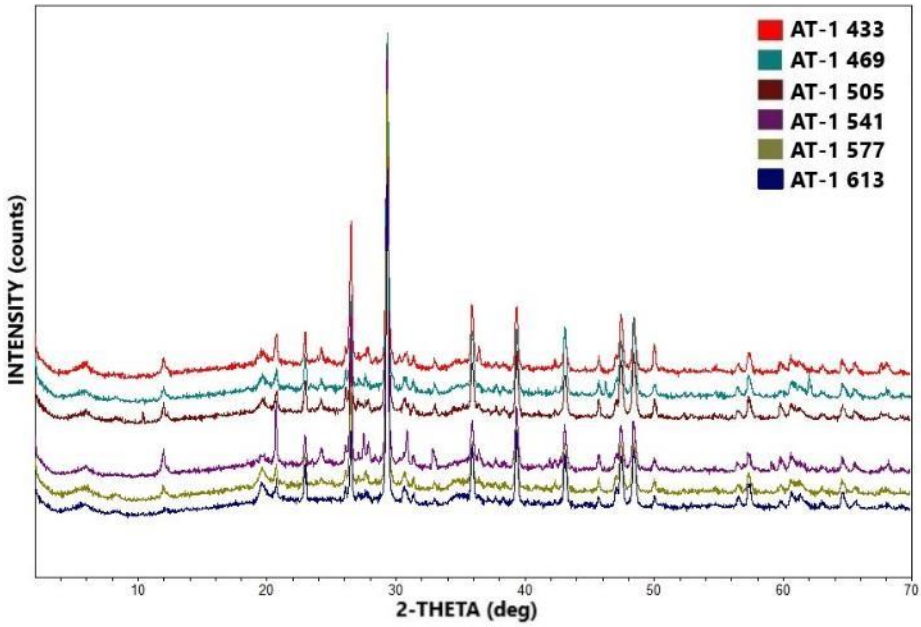

Figure A- 23. Bulk powder X-ray diffractograms of AT-1 433 (red), AT-1 469 (light blue), AT-1 505 (brown), AT-1 541 (purple), AT-1 577 (green), and AT-1 613 (dark blue)

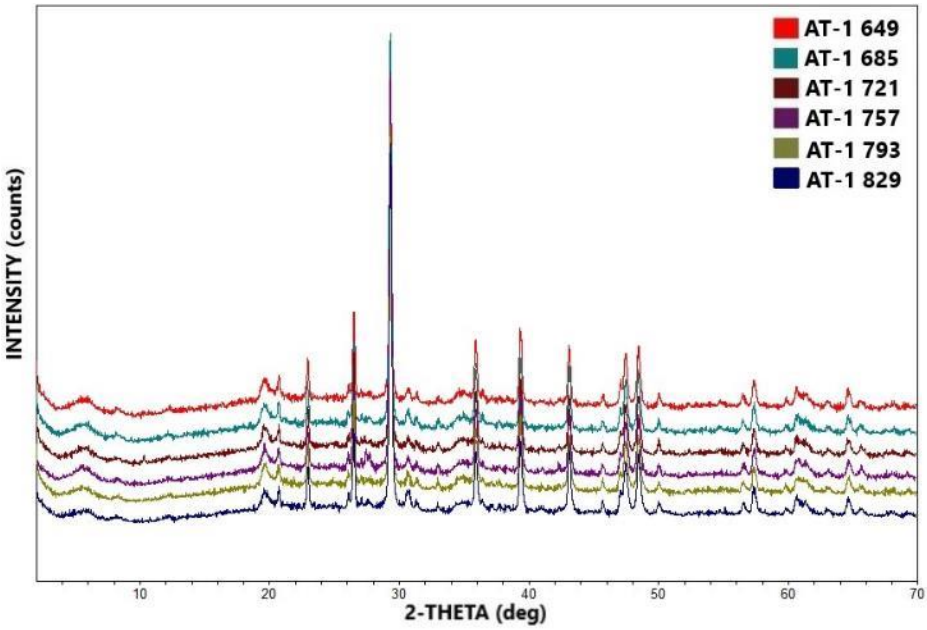

Figure A- 24. Bulk powder X-ray diffractograms of AT-1 649 (red), AT-1 685 (light blue), AT-1 721 (brown), AT-1 757 (purple), AT-1 793 (green), and AT-1 829 (dark blue)

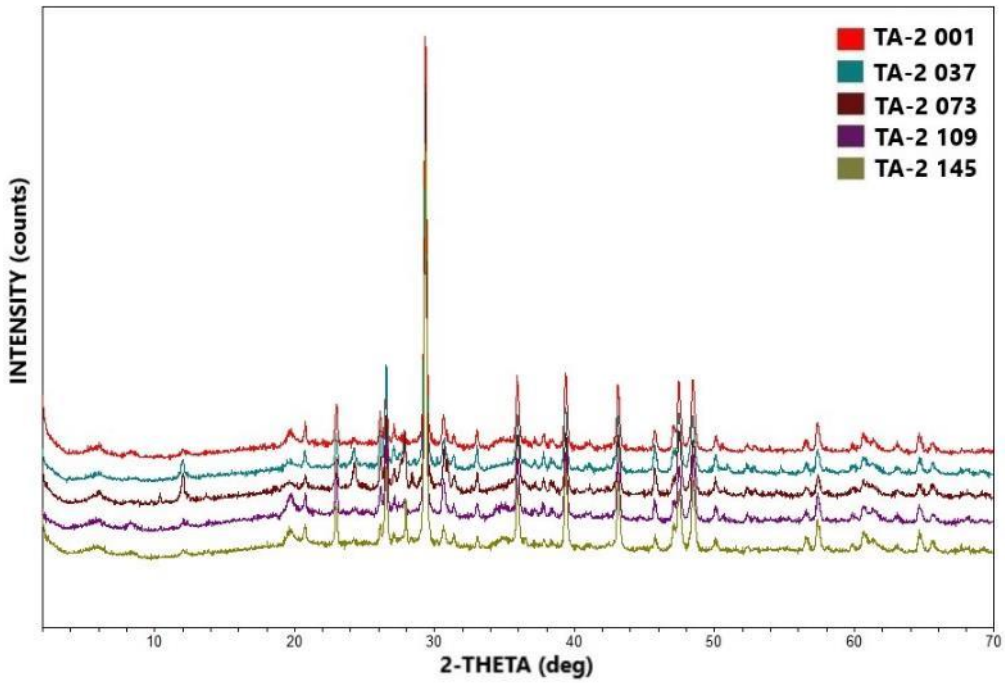

Figure A- 25. Bulk powder X-ray diffractograms of TA-2 001 (red), TA-2 037 (blue), TA-2 073 (brown), TA-2 109 (purple), and TA-2 145 (green)

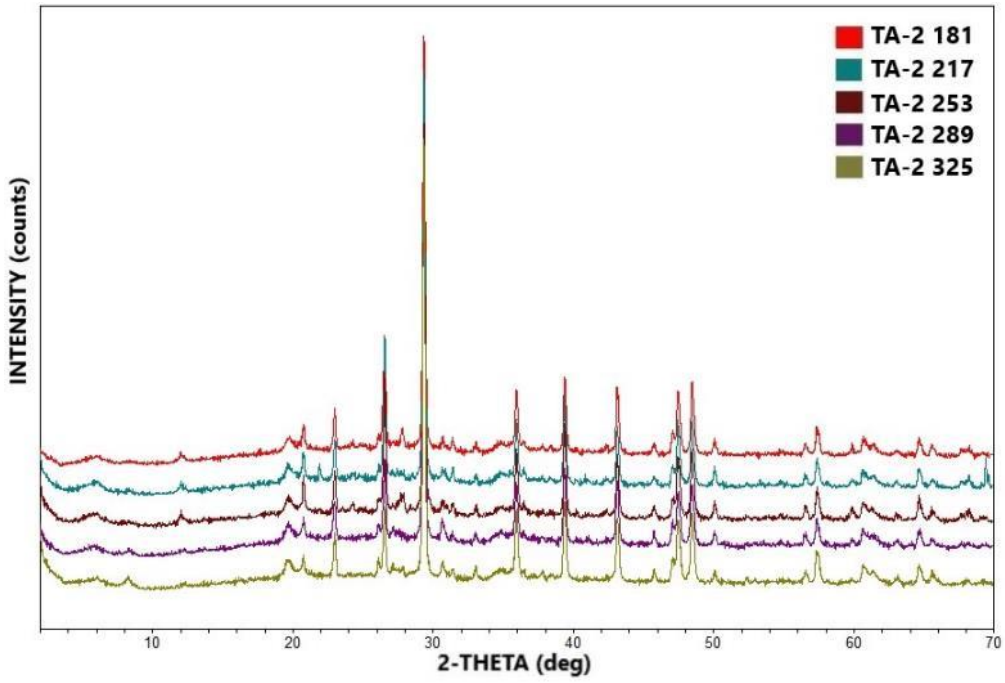

Figure A- 26. Bulk powder X-ray diffractograms of TA-2 181 (red), TA-2 217 (blue), TA-2 253 (brown), TA-2 289 (purple), and TA-2 325 (green)

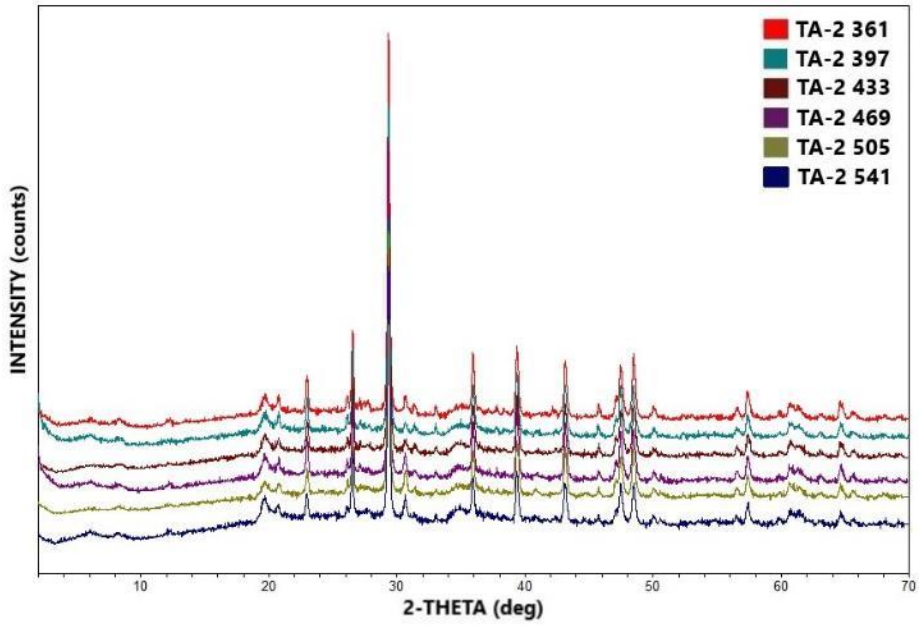

Figure A- 27. Bulk powder X-ray diffractograms of TA-2 361 (red), TA-2 397 (light blue), TA-2 433 (brown), TA-2 469 (purple), TA-2 505 (green), and TA-2 541 (dark blue)

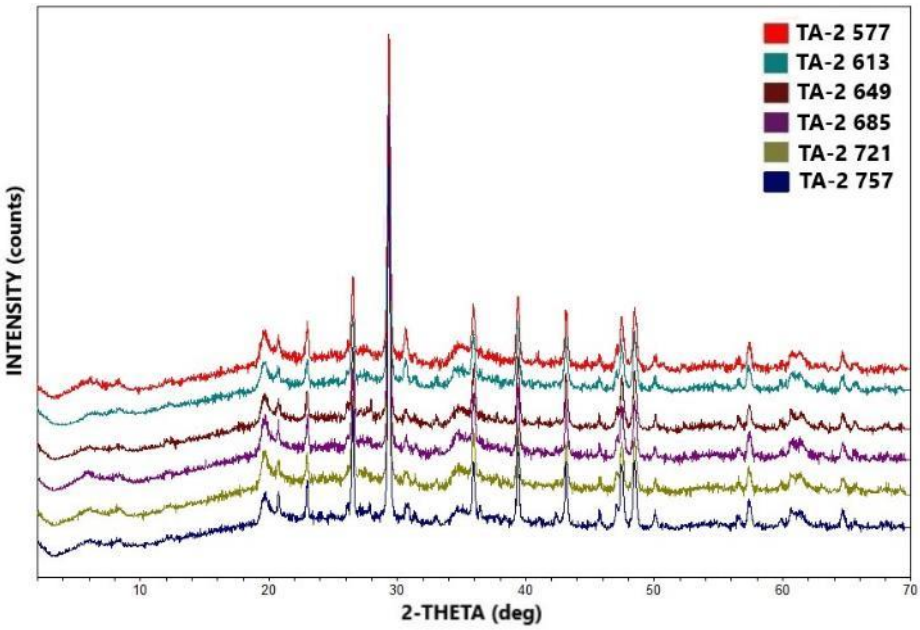

Figure A- 28. Bulk powder X-ray diffractograms of TA-2 577 (red), TA-2 613 (light blue), TA-2 649 (brown), TA-2 685 (purple), TA-2 721 (green), and TA-2 757 (dark blue)

B. X-Ray Diffractograms of Oriented Clay Fraction Slide Samples

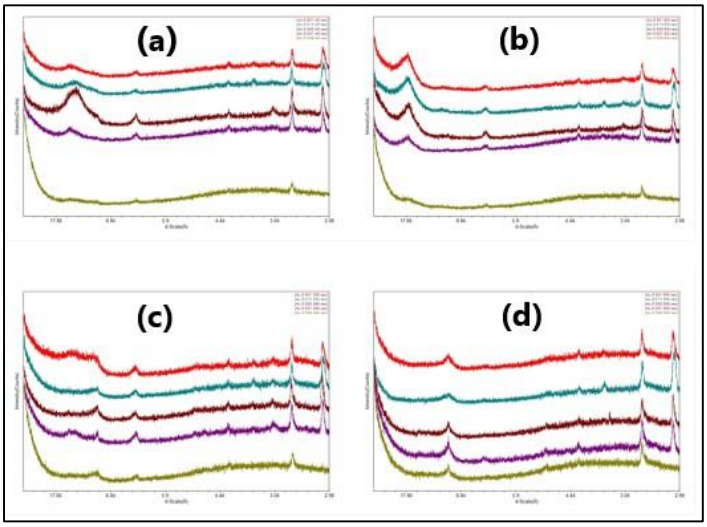

Figure B- 1. Oriented clay fraction X-ray diffractogram sets of AL-5 consisting (a) air-dried, (b) ethylene glycolized, (c) 300 °C heated, (d) 550 °C heated sample analysis results of AL-5 001 (red), AL-5 013 (blue), AL-5 025 (brown), AL-5 037 (purple), and AL-5 049 (green)

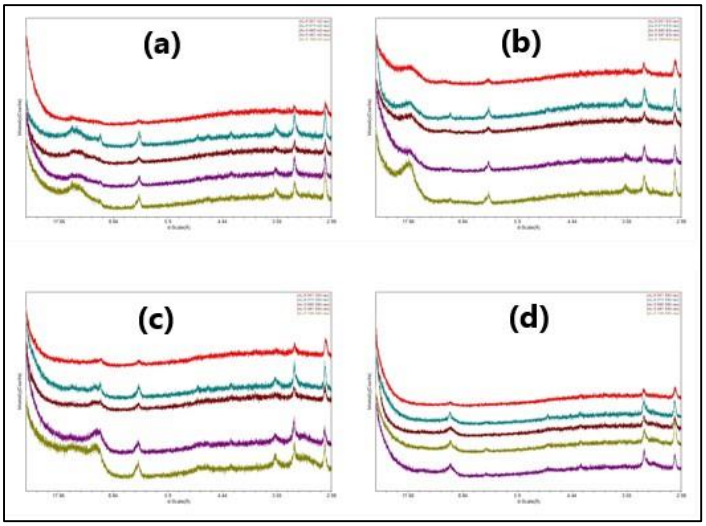

Figure B- 2. Oriented clay fraction X-ray diffractogram sets of AL-5 consisting (a) air-dried, (b) ethylene glycolized, (c) 300 °C heated, (d) 550 °C heated sample analysis results of AL-5 061 (red), AL-5 073 (blue), AL-5 085 (brown), AL-5 097 (purple), and AL-5 109 (green)

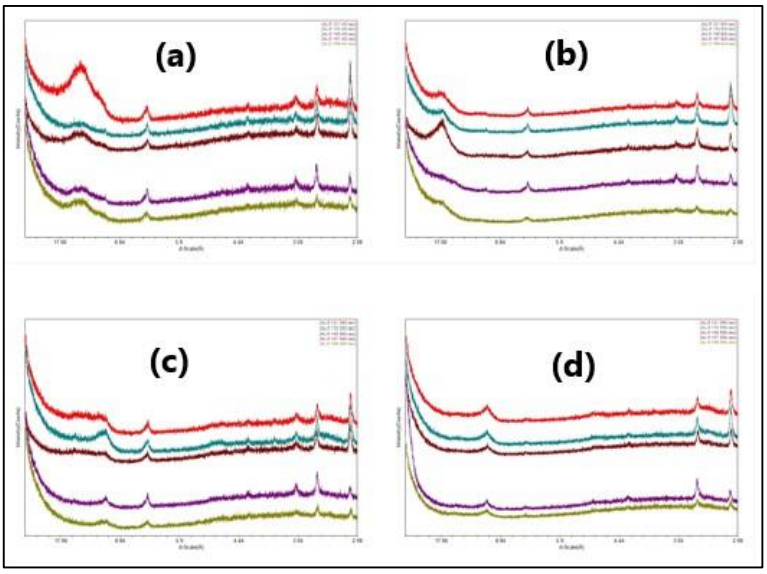

Figure B- 3. Oriented clay fraction X-ray diffractogram sets of AL-5 consisting (a) air-dried, (b) ethylene glycolized, (c) 300 °C heated, (d) 550 °C heated sample analysis results of AL-5 121 (red), AL-5 133 (blue), AL-5 145 (brown), AL-5 157 (purple), and AL-5 169 (green)

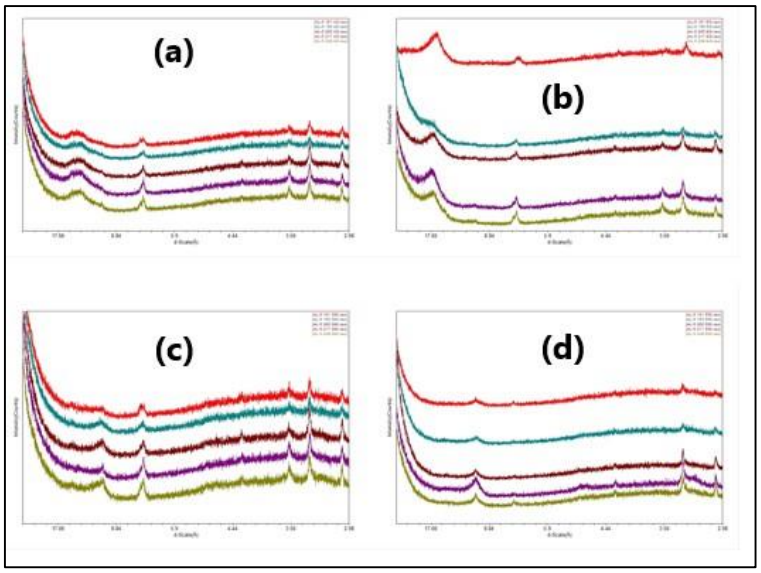

Figure B- 4. Oriented clay fraction X-ray diffractogram sets of AL-5 consisting (a) air-dried, (b) ethylene glycolized, (c) 300 °C heated, (d) 550 °C heated sample analysis results of AL-5 181 (red), AL-5 193 (blue), AL-5 205 (brown), AL-5 217 (purple), and AL-5 229 (green)

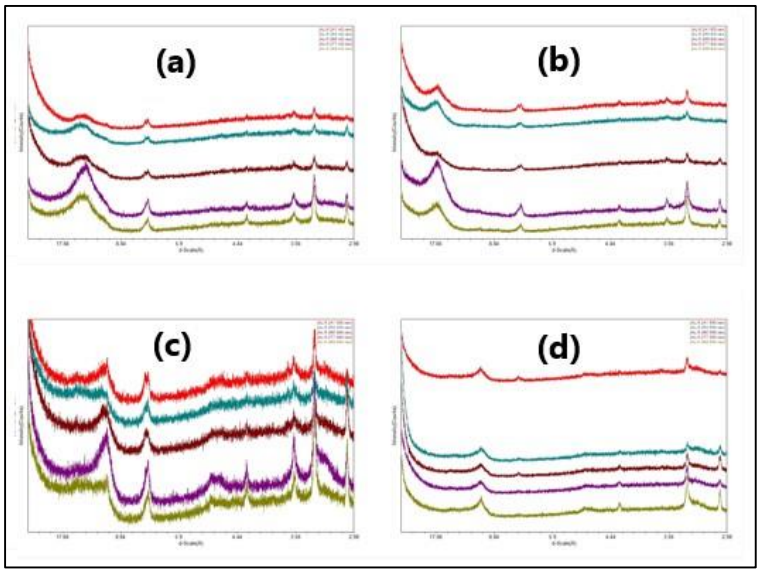

Figure B- 5. Oriented clay fraction X-ray diffractogram sets of AL-5 consisting (a) air-dried, (b) ethylene glycolized, (c) 300 °C heated, (d) 550 °C heated sample analysis results of AL-5 241 (red), AL-5 253 (blue), AL-5 265 (brown), AL-5 277 (purple), and AL-5 289 (green)

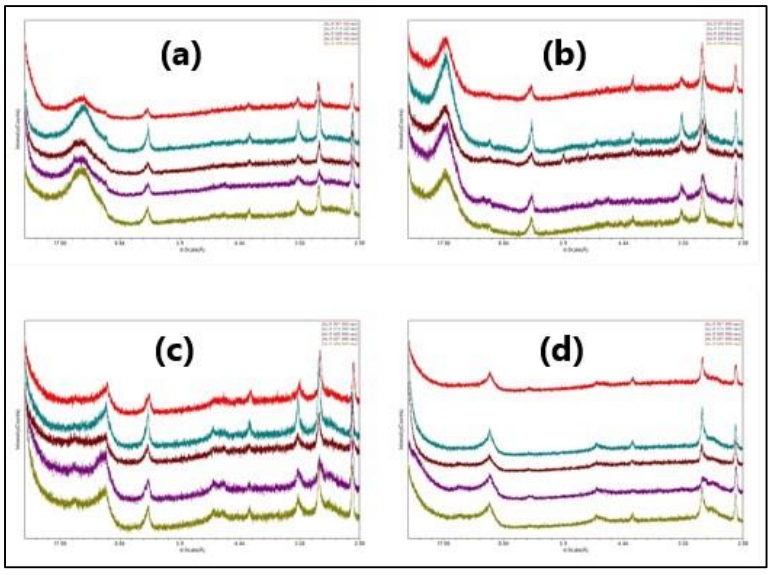

Figure B- 6. Oriented clay fraction X-ray diffractogram sets of AL-5 consisting (a) air-dried, (b) ethylene glycolized, (c) 300 °C heated, (d) 550 °C heated sample analysis results of AL-5 301 (red), AL-5 313 (blue), AL-5 325 (brown), AL-5 337 (purple), and AL-5 349 (green)

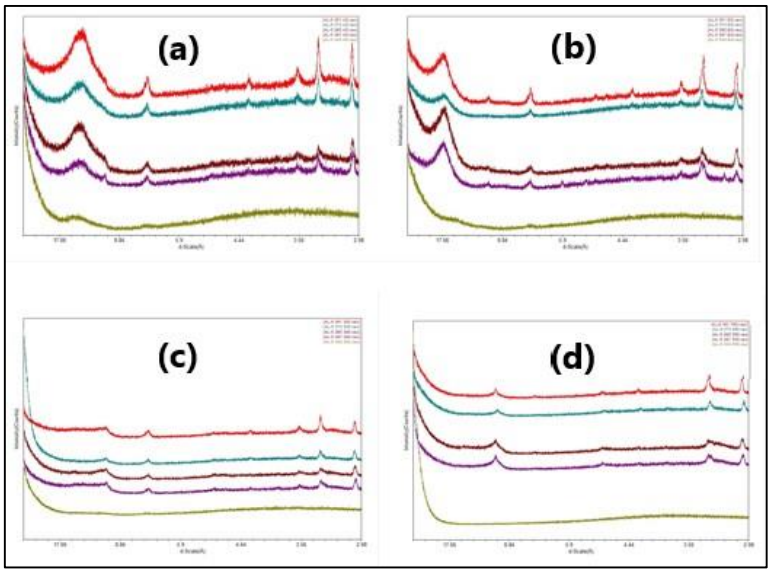

Figure B- 7. Oriented clay fraction X-ray diffractogram sets of AL-5 consisting (a) air-dried, (b) ethylene glycolized, (c) 300 °C heated, (d) 550 °C heated sample analysis results of AL-5 361 (red), AL-5 373 (blue), AL-5 385 (brown), AL-5 397 (purple), and AL-5 433 (green)

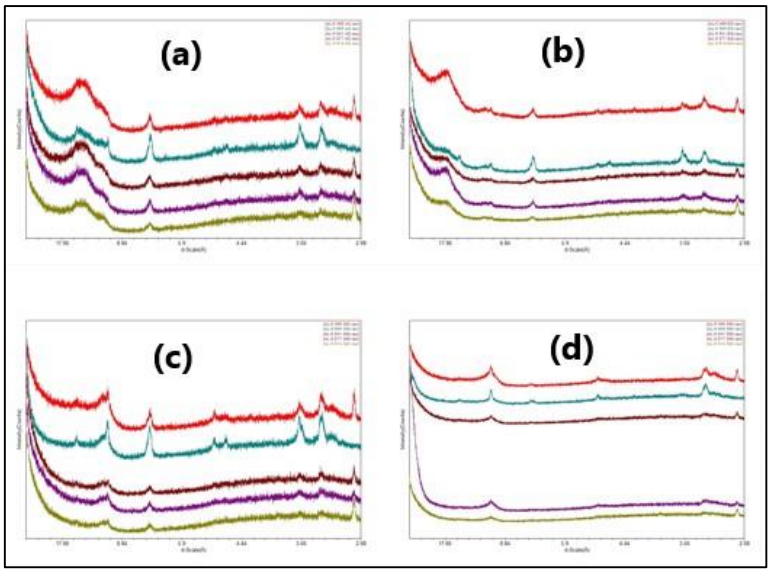

Figure B- 8. Oriented clay fraction X-ray diffractogram sets of AL-5 consisting (a) air-dried, (b) ethylene glycolized, (c) 300 °C heated, (d) 550 °C heated sample analysis results of AL-5 469 (red), AL-5 505 (blue), AL-5 541 (brown), AL-5 577 (purple), and AL-5 613 (green)

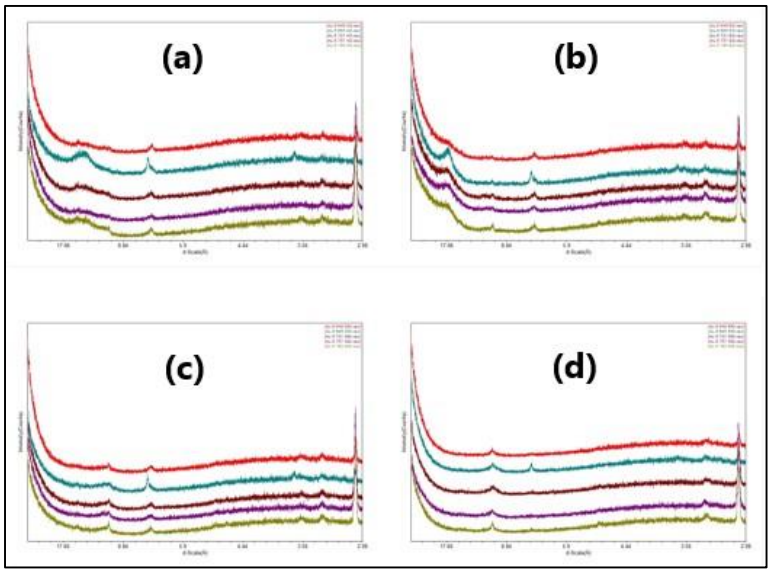

Figure B- 9. Oriented clay fraction X-ray diffractogram sets of AL-5 consisting (a) air-dried, (b) ethylene glycolized, (c) 300 °C heated, (d) 550 °C heated sample analysis results of AL-5 649 (red), AL-5 685 (blue), AL-5 721 (brown), AL-5 757 (purple), and AL-5 793 (green)

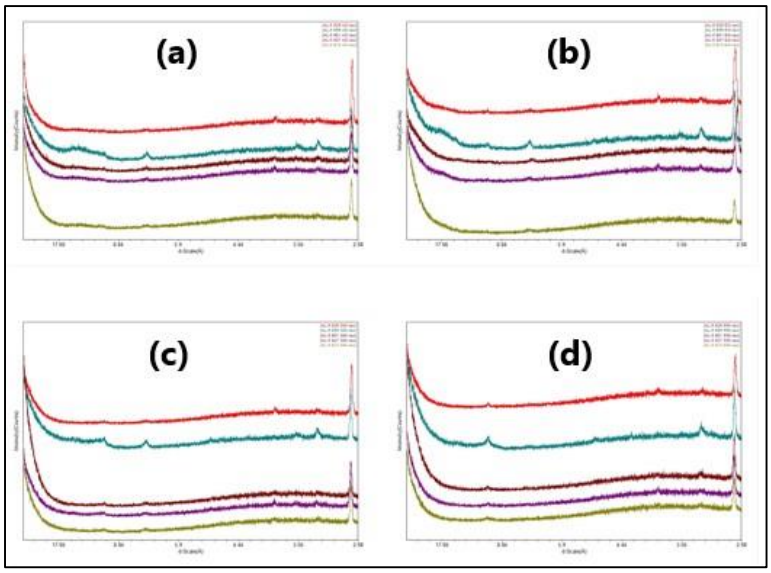

Figure B- 10. Oriented clay fraction X-ray diffractogram sets of AL-5 consisting (a) air-dried, (b) ethylene glycolized, (c) 300 °C heated, (d) 550 °C heated sample analysis results of AL-5 829 (red), AL-5 865 (blue), AL-5 901 (brown), AL-5 937 (purple), and AL-5 973 (green)

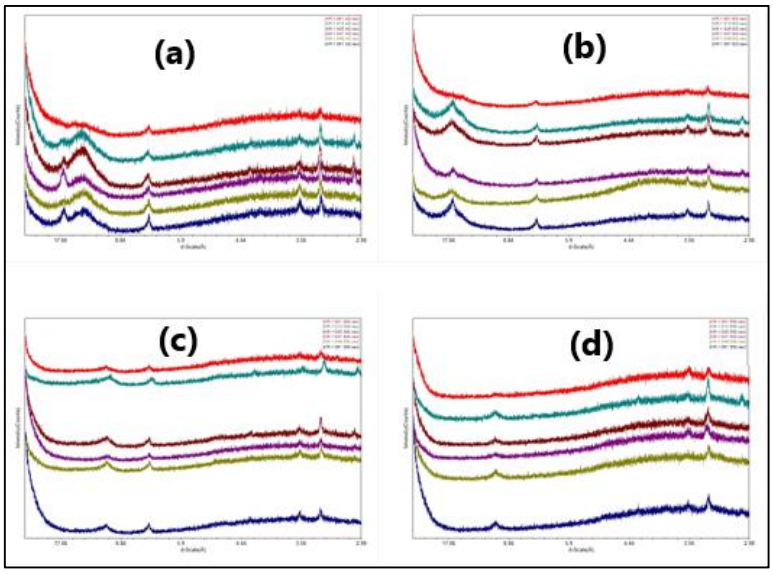

Figure B- 11. Oriented clay fraction X-ray diffractogram sets of KR-1 consisting (a) air-dried, (b) ethylene glycolized, (c) 300 °C heated, (d) 550 °C heated sample analysis results of KR-1 001 (red), KR-1 013 (light blue), KR-1 025 (brown), KR-1 037 (purple), KR-1 049 (green), and KR-1 061 (dark blue)

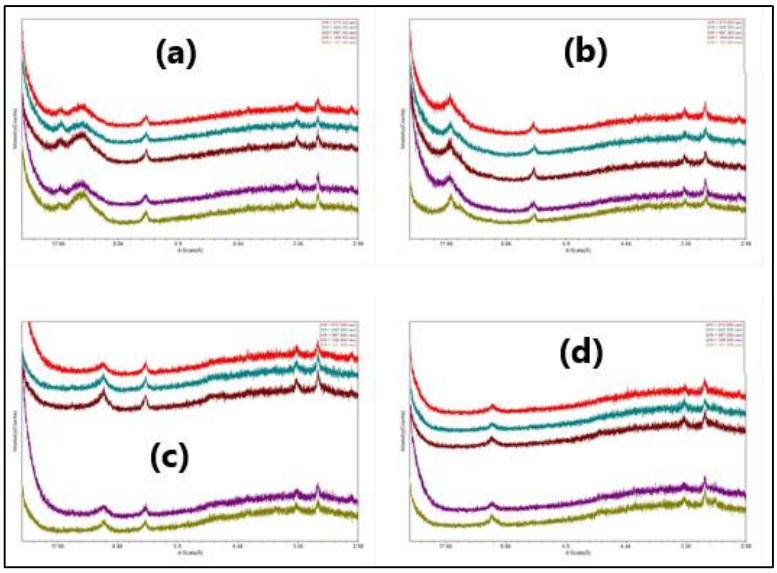

Figure B- 12. Oriented clay fraction X-ray diffractogram sets of KR-1 consisting (a) air-dried, (b) ethylene glycolized, (c) 300 °C heated, (d) 550 °C heated sample analysis results of KR-1 073 (red), KR-1 085 (blue), KR-1 097 (brown), KR-1 109 (purple), and KR-1 121 (green)

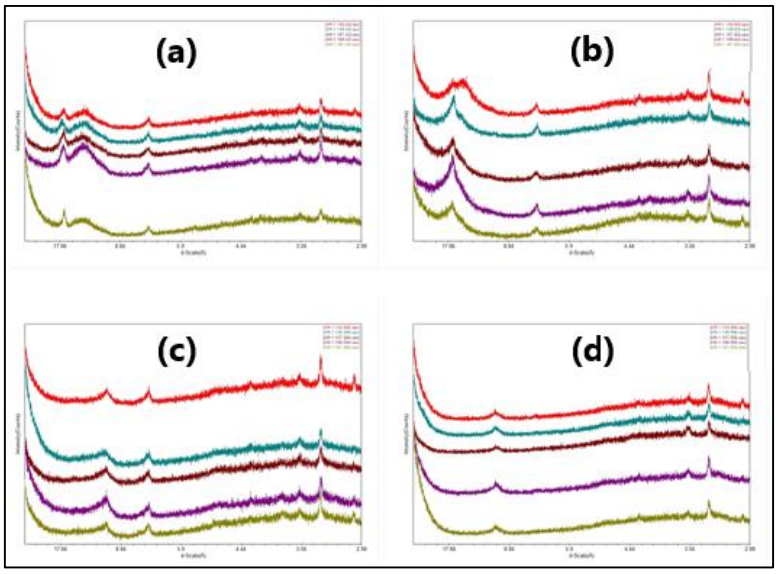

Figure B- 13. Oriented clay fraction X-ray diffractogram sets of KR-1 consisting (a) air-dried, (b) ethylene glycolized, (c) 300 °C heated, (d) 550 °C heated sample analysis results of KR-1 133 (red), KR-1 145 (blue), KR-1 157 (brown), KR-1 169 (purple), and KR-1 181 (green)

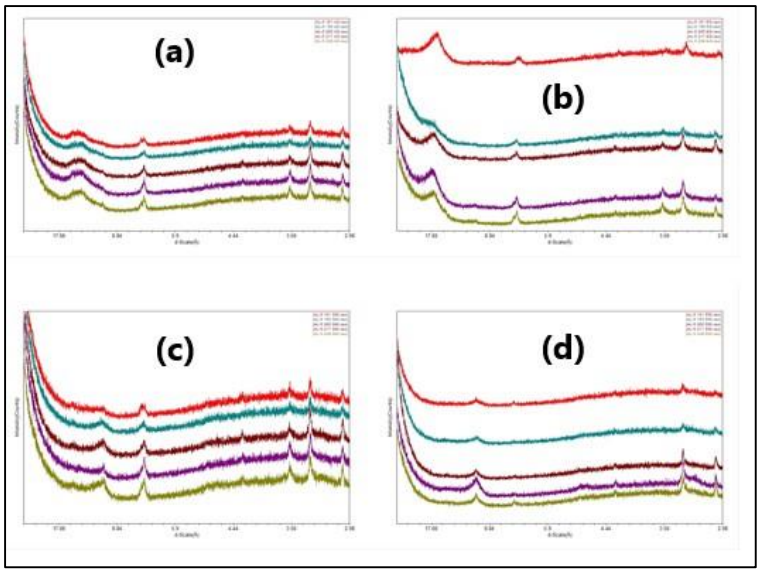

Figure B- 14. Oriented clay fraction X-ray diffractogram sets of KR-1 consisting (a) air-dried, (b) ethylene glycolized, (c) 300 °C heated, (d) 550 °C heated sample analysis results of KR-1 193 (red), KR-1 205 (blue), KR-1 217 (brown), KR-1 253 (purple), and KR-1 289 (green)

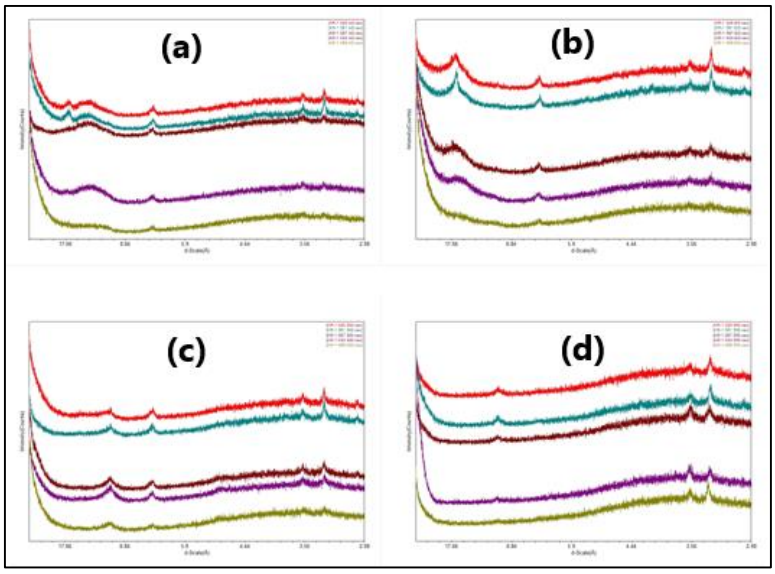

Figure B- 15. Oriented clay fraction X-ray diffractogram sets of KR-1 consisting (a) air-dried, (b) ethylene glycolized, (c) 300 °C heated, (d) 550 °C heated sample analysis results of KR-1 325 (red), KR-1 361 (blue), KR-1 397 (brown), KR-1 433 (purple), and KR-1 469 (green)

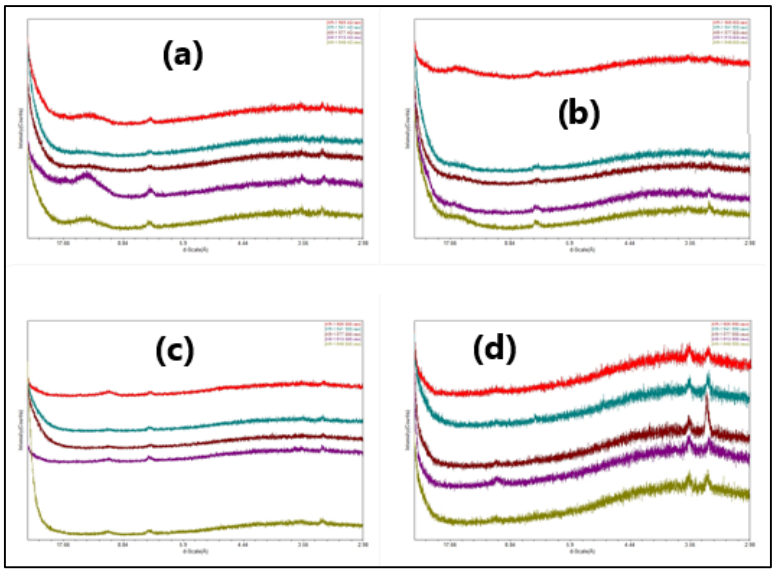

Figure B- 16. Oriented clay fraction X-ray diffractogram sets of KR-1 consisting (a) air-dried, (b) ethylene glycolized, (c) 300 °C heated, (d) 550 °C heated sample analysis results of KR-1 505 (red), KR-1 541 (blue), KR-1 577 (brown), KR-1 613 (purple), and KR-1 649 (green)

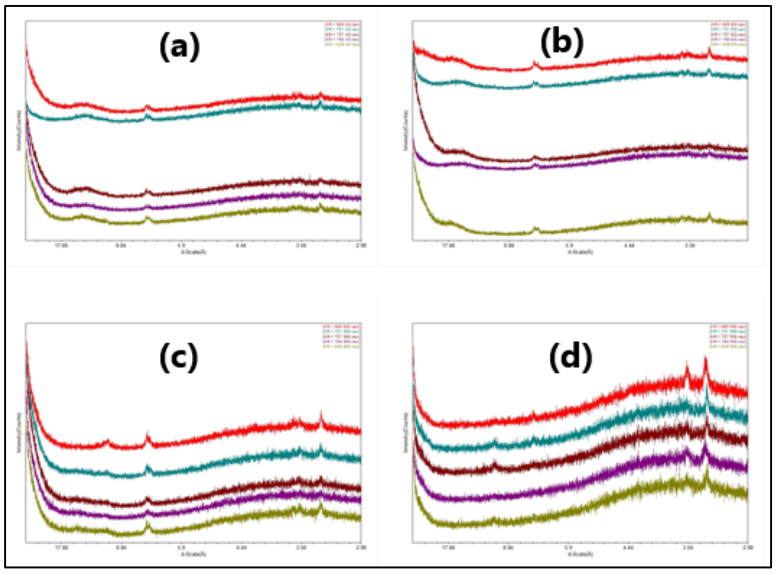

Figure B- 17. Oriented clay fraction X-ray diffractogram sets of KR-1 consisting (a) air-dried, (b) ethylene glycolized, (c) 300 °C heated, (d) 550 °C heated sample analysis results of KR-1 685 (red), KR-1 721 (blue), KR-1 757 (brown), KR-1 793 (purple), and KR-1 829 (green)

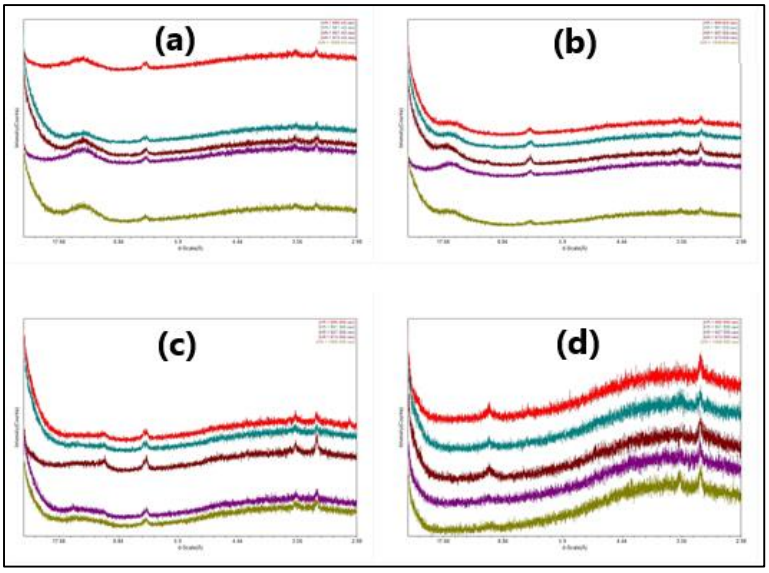

Figure B- 18. Oriented clay fraction X-ray diffractogram sets of KR-1 consisting (a) air-dried, (b) ethylene glycolized, (c) 300 °C heated, (d) 550 °C heated sample analysis results of KR-1 865 (red), KR-1 901 (blue), KR-1 937 (brown), KR-1 973 (purple), and KR-1 1009 (green)

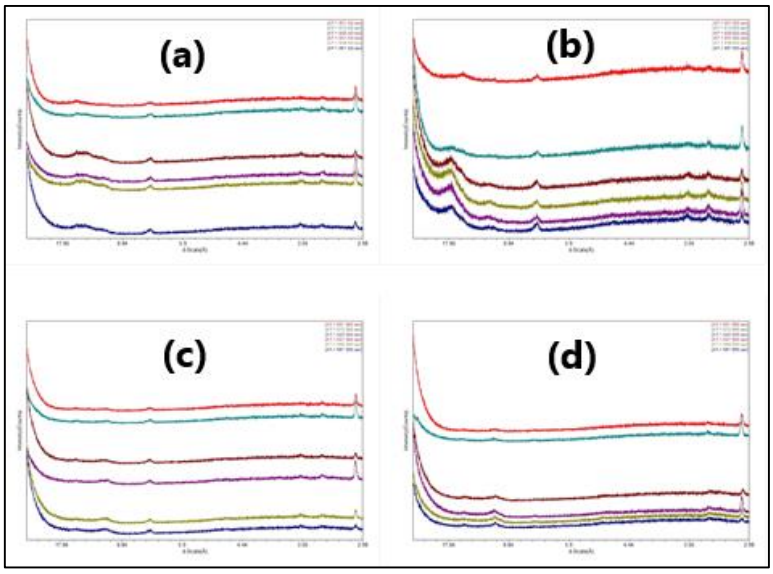

Figure B- 19. Oriented clay fraction X-ray diffractogram sets of AT-1 consisting (a) air-dried, (b) ethylene glycolized, (c) 300 °C heated, (d) 550 °C heated sample analysis results of AT-1 001 (red), AT-1 013 (light blue), AT-1 025 (brown), AT-1 037 (purple), AT-1 049 (green), and AT-1 061 (dark blue)

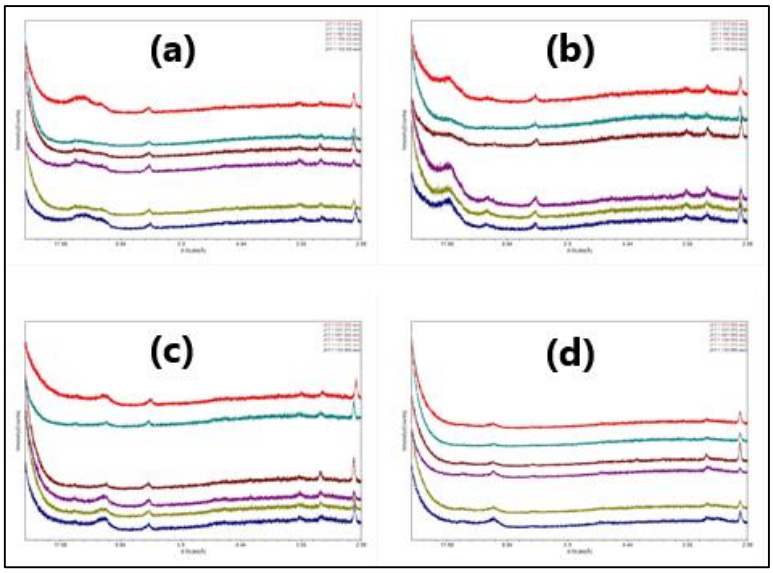

Figure B- 20. Oriented clay fraction X-ray diffractogram sets of AT-1 consisting (a) air-dried, (b) ethylene glycolized, (c) 300 °C heated, (d) 550 °C heated sample analysis results of AT-1 073 (red), AT-1 085 (light blue), AT-1 097 (brown), AT-1 109 (purple), AT-1 121 (green), and AT-1 133 (dark blue)

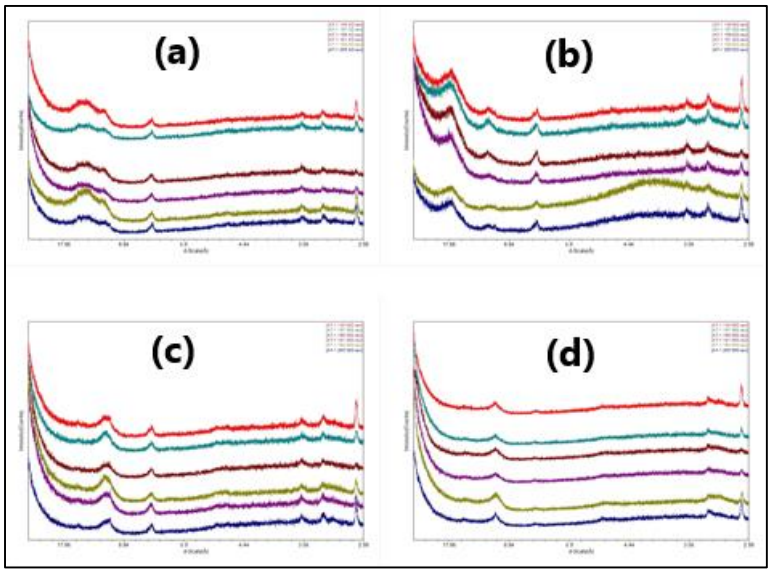

Figure B- 21. Oriented clay fraction X-ray diffractogram sets of AT-1 consisting (a) air-dried, (b) ethylene glycolized, (c) 300 °C heated, (d) 550 °C heated sample analysis results of AT-1 145 (red), AT-1 157 (light blue), AT-1 169 (brown), AT-1 181 (purple), AT-1 193 (green), and AT-1 205 (dark blue)

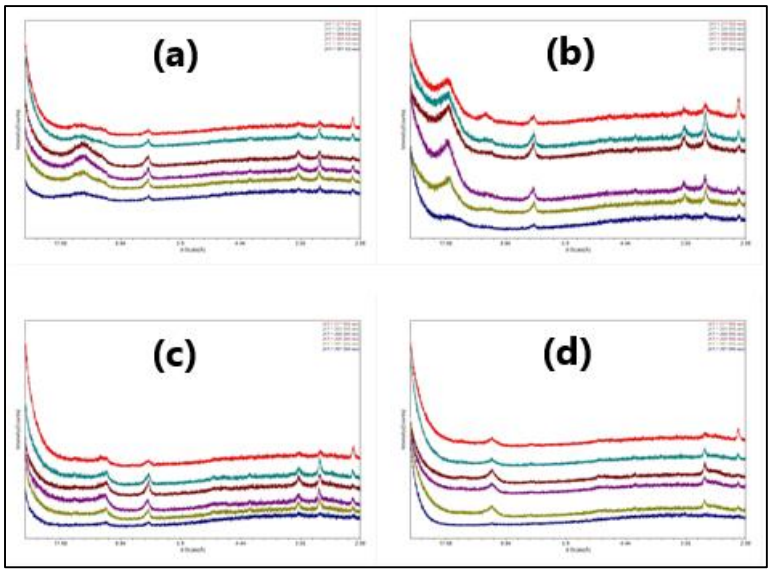

Figure B- 22. Oriented clay fraction X-ray diffractogram sets of AT-1 consisting (a) air-dried, (b) ethylene glycolized, (c) 300 °C heated, (d) 550 °C heated sample analysis results of AT-1 217 (red), AT-1 253 (light blue), AT-1 289 (brown), AT-1 325 (purple), AT-1 361 (green), and AT-1 397 (dark blue)

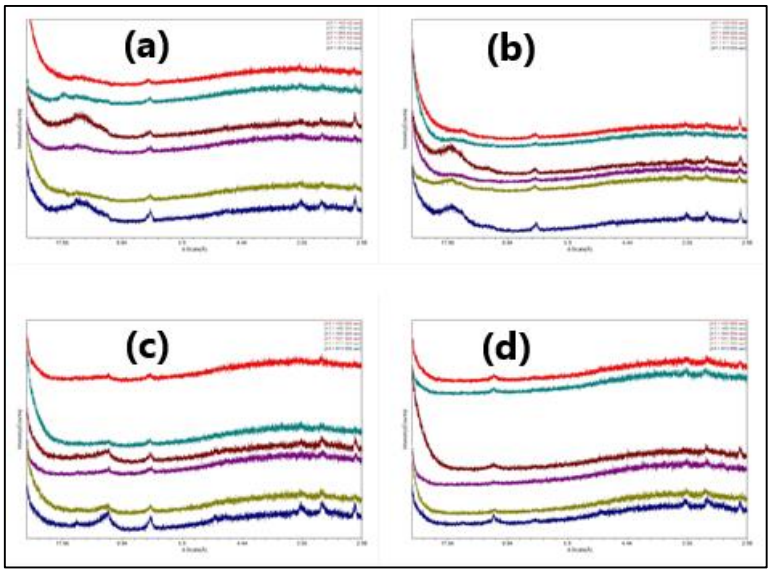

Figure B- 23. Oriented clay fraction X-ray diffractogram sets of AT-1 consisting (a) air-dried, (b) ethylene glycolized, (c) 300 °C heated, (d) 550 °C heated sample analysis results of AT-1 433 (red), AT-1 469 (light blue), AT-1 505 (brown), AT-1 541 (purple), AT-1 577 (green), and AT-1 613 (dark blue)

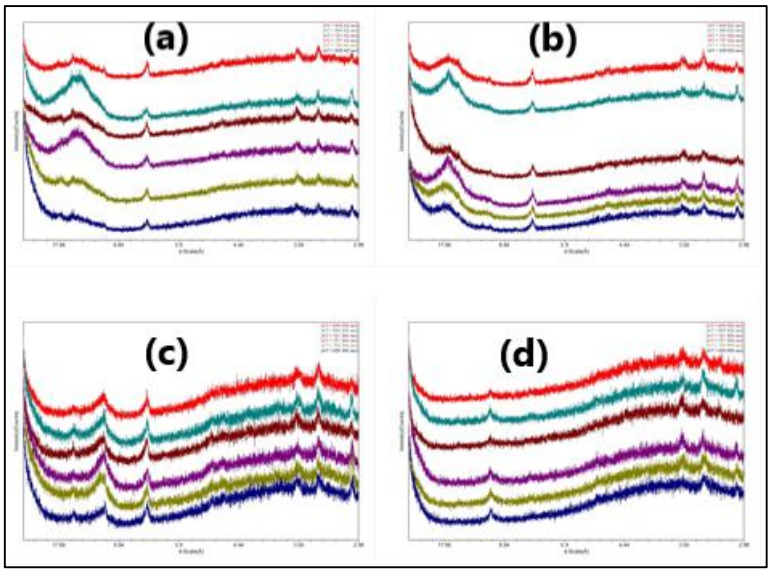

Figure B- 24. Oriented clay fraction X-ray diffractogram sets of AT-1 consisting (a) air-dried, (b) ethylene glycolized, (c) 300 °C heated, (d) 550 °C heated sample analysis results of AT-1 649 (red), AT-1 685 (light blue), AT-1 721 (brown), AT-1 757 (purple), AT-1 793 (green), and AT-1 829 (dark blue)

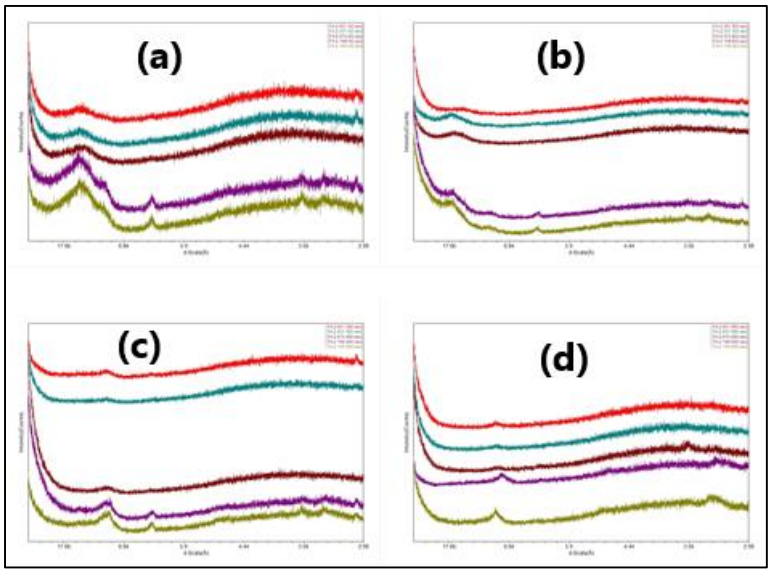

Figure B- 25. Oriented clay fraction X-ray diffractogram sets of TA-2 consisting (a) air-dried, (b) ethylene glycolized, (c) 300 °C heated, (d) 550 °C heated sample analysis results of TA-2 001 (red), TA-2 037 (blue), TA-2 073 (brown), TA-2 109 (purple), and TA-2 145 (green)

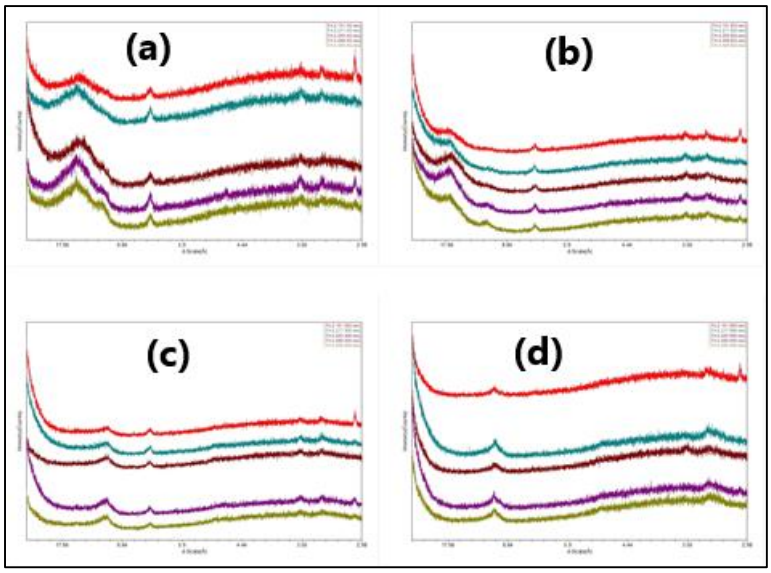

Figure B- 26. Oriented clay fraction X-ray diffractogram sets of TA-2 consisting (a) air-dried, (b) ethylene glycolized, (c) 300 °C heated, (d) 550 °C heated sample analysis results of TA-2 181 (red), TA-2 217 (blue), TA-2 253 (brown), TA-2 289 (purple), and TA-2 325 (green)

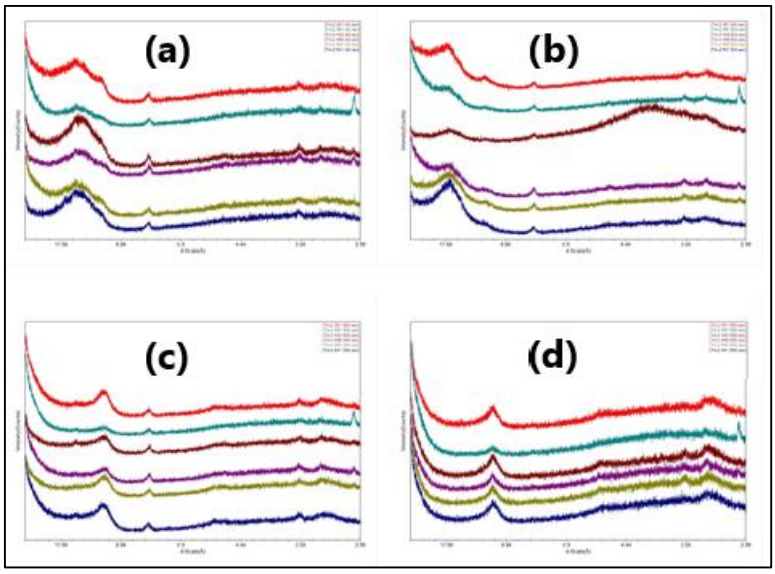

Figure B- 27. Oriented clay fraction X-ray diffractogram sets of TA-2 consisting (a) air-dried, (b) ethylene glycolized, (c) 300 °C heated, (d) 550 °C heated sample analysis results of TA-2 361 (red), TA-2 397 (light blue), TA-2 433 (brown), TA-2 469 (purple), TA-2 505 (green), and TA-2 541 (dark blue)

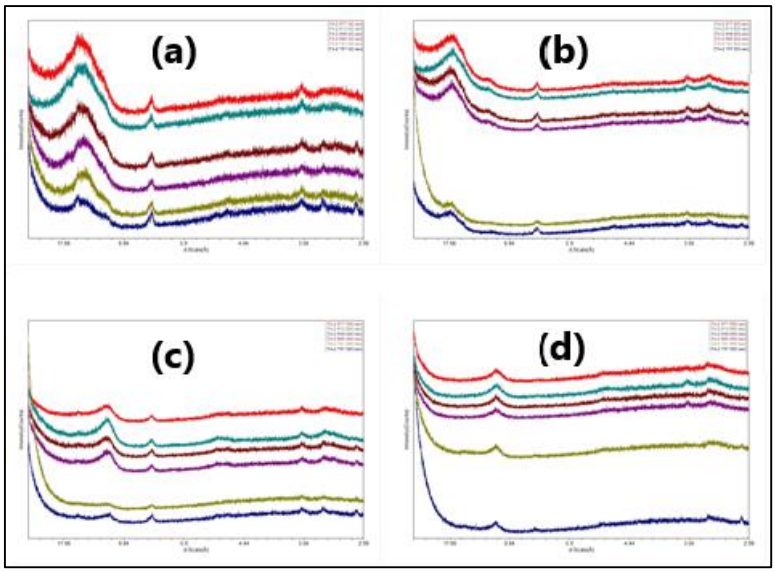

Figure B- 28. Oriented clay fraction X-ray diffractogram sets of TA-2 consisting (a) air-dried, (b) ethylene glycolized, (c) 300 °C heated, (d) 550 °C heated sample analysis results of TA-2 577 (red), TA-2 613 (light blue), TA-2 649 (brown), TA-2 685 (purple), TA-2 721 (green), and TA-2 757 (dark blue)

C. ICP-MS/OES Measurements

Table C- 1. Geochemical concentrations of 50 samples of AL-5

AL-5	Si	Ca	Al	Fe	K	Na	Mg	V
	wt%	wt%	wt%	wt%	wt%	wt%	wt%	ppm
1	13.076	17.618	3.409	2.751	0.556	0.173	2.222	73.101
2	12.689	18.495	3.163	2.583	0.498	0.166	2.138	61.917
3	16.481	12.665	4.386	3.456	0.688	0.172	2.459	86.035
4	15.221	14.558	3.933	3.332	0.595	0.258	2.890	83.649
5	22.923	4.268	3.298	2.999	0.472	0.129	1.899	100.269
6	10.408	20.487	2.207	1.949	0.353	0.156	1.583	60.934
7	14.659	16.203	3.503	3.372	0.532	0.224	1.999	85.557
8	13.265	18.440	3.082	2.798	0.485	0.239	1.777	70.545
9	13.568	18.119	3.316	3.058	0.525	0.213	1.868	79.407
10	13.907	17.028	3.520	3.251	0.566	0.201	2.100	89.135
11	14.208	16.860	3.664	3.231	0.579	0.192	2.152	85.290
12	14.049	17.165	3.486	3.159	0.530	0.189	2.023	82.567
13	16.079	14.860	3.884	3.347	0.576	0.181	1.994	89.100
14	15.944	15.050	3.954	3.197	0.589	0.189	1.953	85.982
15	13.585	18.217	3.168	2.982	0.491	0.259	2.421	79.618
16	15.438	15.801	3.047	3.232	0.417	0.287	3.189	75.565
17	15.085	16.478	3.621	3.008	0.535	0.246	2.248	89.047
18	16.135	14.505	3.888	3.215	0.574	0.206	2.064	83.093
19	17.406	12.691	4.313	3.453	0.623	0.166	2.156	99.146
20	14.061	17.281	3.399	3.008	0.526	0.294	2.384	82.614
21	15.287	16.139	3.062	3.138	0.423	0.276	3.093	79.971
22	13.205	17.853	3.129	3.115	0.478	0.245	2.408	81.737
23	13.825	17.804	3.303	2.842	0.500	0.265	2.323	80.786
24	18.307	11.573	4.579	3.501	0.662	0.147	2.011	95.676
25	18.142	13.383	4.194	3.310	0.618	0.171	1.976	93.614
26	16.545	14.042	3.896	3.621	0.585	0.178	2.139	92.826
27	18.149	10.980	4.625	3.932	0.645	0.142	1.781	107.513
28	15.671	14.452	4.101	3.119	0.636	0.154	2.029	94.079
29	15.643	14.590	4.535	4.043	0.747	0.177	2.580	122.664
30	17.483	11.436	4.871	3.302	0.696	0.123	1.989	103.212
31	15.184	14.857	3.817	3.311	0.579	0.171	1.998	81.943
32	14.718	15.367	3.881	3.135	0.573	0.118	1.850	76.290
33	12.296	17.798	3.371	3.005	0.557	0.158	2.056	74.469
34	9.874	22.164	2.372	2.355	0.380	0.123	1.527	46.130

35	8.593	25.479	1.625	1.439	0.237	0.329	1.968	44.816
36	13.423	15.881	3.970	3.564	0.650	0.146	2.083	116.691
37	22.479	3.433	5.800	4.283	0.891	0.319	2.543	152.088
38	12.285	18.621	3.430	3.054	0.585	0.190	1.972	81.641
39	11.888	19.131	3.456	3.280	0.547	0.139	1.979	85.484
40	8.803	23.053	2.620	2.112	0.453	0.186	1.720	74.472
41	6.298	26.583	1.787	1.482	0.298	0.120	1.369	60.976
42	12.679	17.889	2.170	3.123	0.341	0.398	4.167	59.843
43	9.893	21.168	2.372	2.236	0.452	0.274	2.207	61.236
44	10.066	20.526	2.643	2.589	0.490	0.204	2.263	68.559
45	11.653	18.166	3.409	2.914	0.611	0.148	2.297	82.342
46	7.655	24.674	1.948	1.761	0.373	0.189	1.905	45.716
47	13.303	15.712	4.345	3.044	0.782	0.162	1.890	112.308
48	8.810	22.965	2.423	2.138	0.426	0.214	2.045	61.308
49	8.937	22.464	2.563	2.126	0.436	0.166	1.917	68.319
50	8.926	22.680	2.331	2.140	0.410	0.224	2.002	64.196

Continued from Table C- 1

AL-5	**Cr**	**Mn**	**Co**	**Ni**	**Cu**	**Zn**	**Sr**	**Ba**
	ppm	ppm	ppm	ppm	ppm	ppm	ppm	ppm
1	202.540	740.652	22.452	253.764	29.687	59.587	787.826	201.483
2	189.452	753.036	21.339	226.622	24.205	44.953	815.002	206.406
3	206.260	674.292	23.799	278.520	35.101	63.942	476.528	191.867
4	397.788	756.247	28.803	353.095	32.551	62.527	678.751	159.574
5	203.259	246.926	25.610	421.638	59.172	57.131	314.483	139.973
6	201.992	649.258	16.966	195.821	29.128	33.751	1080.375	225.527
7	336.094	573.261	23.939	301.796	39.484	58.373	839.339	175.861
8	356.203	664.766	22.786	250.130	29.550	48.717	897.402	150.591
9	320.255	766.523	25.709	277.668	27.340	60.252	855.827	146.914
10	346.624	710.255	28.563	312.315	31.264	61.178	830.958	157.740
11	308.481	732.758	27.837	367.188	33.334	62.211	816.522	155.757
12	334.750	831.778	25.429	315.110	33.798	67.591	792.712	178.974
13	279.009	867.617	28.714	280.387	39.766	62.873	620.598	172.071
14	251.073	832.882	23.777	279.240	40.296	76.989	636.794	192.034
15	371.774	726.293	26.441	348.231	33.039	59.713	962.780	174.907
16	411.954	681.467	30.495	428.437	33.284	48.091	723.574	162.621
17	472.551	780.773	25.778	312.842	37.401	61.697	789.834	205.015
18	265.521	911.222	25.069	286.695	41.038	66.088	635.499	191.806

19	300.468	948.711	27.103	269.029	44.521	76.809	569.910	201.541
20	484.499	823.966	27.173	347.561	34.513	71.977	918.387	190.902
21	455.765	708.016	30.548	381.108	33.617	61.976	786.545	156.552
22	532.609	803.068	26.610	348.719	32.410	59.406	967.232	152.698
23	396.754	881.391	26.120	288.155	40.430	64.823	918.904	163.728
24	227.411	1023.183	27.726	275.959	45.480	76.788	485.646	182.477
25	281.273	877.677	25.157	253.640	53.788	85.436	547.063	241.599
26	253.037	920.041	30.077	274.143	39.737	68.953	591.941	193.319
27	192.125	730.099	24.561	244.402	46.766	85.981	469.234	205.568
28	282.543	710.494	26.283	297.917	47.881	69.051	599.564	176.158
29	420.997	419.774	43.731	516.713	35.934	81.741	664.809	142.157
30	265.845	582.453	25.528	253.743	38.803	95.281	442.463	207.440
31	241.643	672.498	24.618	279.591	39.063	87.715	603.053	174.849
32	213.178	651.232	22.691	245.578	32.925	52.622	604.977	156.700
33	244.894	790.436	25.461	305.950	31.496	51.102	780.886	166.491
34	160.722	832.611	17.387	197.963	25.751	47.813	1029.345	167.051
35	659.578	454.766	17.064	201.994	13.175	26.350	1417.788	130.822
36	276.806	434.000	22.189	309.605	35.779	56.771	790.566	147.556
37	575.562	251.742	33.068	446.226	51.620	107.216	300.756	159.068
38	339.529	449.811	23.951	286.114	24.742	70.548	872.201	127.205
39	219.411	526.329	22.999	270.074	17.436	60.972	772.321	138.142
40	198.653	566.512	17.904	213.151	19.861	39.310	1012.266	133.661
41	209.124	485.467	25.217	251.843	17.874	36.286	1088.494	125.886
42	597.984	568.896	44.727	597.860	16.480	43.927	983.972	124.195
43	356.958	444.750	21.917	294.328	16.747	47.295	1278.276	128.054
44	304.282	596.954	22.427	282.961	23.147	59.382	1108.780	120.032
45	290.957	512.808	25.474	356.050	27.949	71.413	872.923	127.558
46	199.005	680.241	16.389	174.234	12.041	39.096	1112.576	149.352
47	317.875	470.888	27.836	385.756	32.842	81.983	776.723	162.182
48	233.488	635.276	19.377	210.663	27.329	52.550	943.214	140.597
49	231.637	639.604	19.694	224.500	21.036	63.833	854.332	136.948
50	243.844	589.062	20.816	228.881	19.255	46.831	931.441	137.688

Continued from Table C- 1

AL-5	**P**	**S**	**Ti**	**Sc**	**Hf**	**Y**	**La**	**Ce**
	ppm	wt%	wt%	mg/kg	ppm	ppm	ppm	ppm
1	910.234	0.434	0.238	10.518	1.118	13.657	13.030	24.378
2	806.640	0.510	0.241	9.659	1.044	13.582	13.492	25.485

3	795.067	0.373	0.277	12.820	1.517	15.762	15.855	30.374
4	738.014	0.407	0.294	13.115	1.322	14.548	13.242	24.878
5	699.307	0.342	0.183	9.062	0.701	10.233	9.763	18.304
6	743.981	0.525	0.176	7.743	0.535	8.810	8.674	16.491
7	769.093	0.426	0.284	10.899	1.401	14.490	15.325	26.867
8	730.625	0.424	0.282	10.085	1.228	14.538	14.155	26.940
9	746.054	0.411	0.294	10.293	1.220	14.992	14.614	27.654
10	692.283	0.366	0.314	11.335	1.396	15.346	14.502	27.385
11	672.649	0.391	0.315	11.296	1.394	16.248	15.032	28.285
12	740.661	0.411	0.308	11.025	1.519	15.993	15.001	28.172
13	778.181	0.358	0.317	11.642	1.746	17.209	16.294	31.195
14	844.037	0.404	0.323	11.538	1.664	17.576	17.096	32.930
15	730.351	0.486	0.312	10.936	1.239	14.820	13.320	25.269
16	683.750	0.412	0.268	10.564	0.979	14.147	12.168	23.607
17	844.463	0.421	0.326	10.970	1.721	17.175	15.629	29.344
18	800.124	0.381	0.317	10.717	1.614	17.029	16.363	32.170
19	804.390	0.371	0.328	12.474	1.942	18.140	18.005	35.109
20	805.135	0.430	0.326	10.515	1.411	15.924	14.397	27.702
21	748.665	0.370	0.281	10.685	0.997	14.286	12.728	24.590
22	806.455	0.420	0.314	10.352	1.221	15.075	13.922	26.089
23	831.921	0.356	0.325	10.592	1.310	15.396	14.069	26.866
24	893.418	0.281	0.330	12.123	1.895	17.785	18.906	36.627
25	1138.335	0.284	0.335	12.173	1.975	20.310	18.821	34.607
26	998.170	0.311	0.306	11.037	4.238	17.504	16.304	31.365
27	937.118	0.117	0.330	11.625	1.883	17.553	18.820	36.983
28	951.650	0.353	0.318	12.087	1.667	18.086	17.187	31.901
29	782.201	0.357	0.348	15.306	1.759	17.539	15.320	27.604
30	978.480	0.274	0.360	12.421	2.156	20.142	21.083	38.110
31	934.403	0.389	0.301	11.093	1.428	16.427	16.359	31.445
32	832.186	0.355	0.287	10.741	1.647	16.698	16.850	32.102
33	786.606	0.408	0.250	10.002	1.299	15.049	14.303	26.923
34	844.110	0.530	0.190	7.538	0.686	10.593	11.074	21.818
35	675.836	0.596	0.182	6.109	0.266	9.766	9.838	18.702
36	730.240	0.420	0.285	11.033	1.618	15.480	14.426	26.181
37	675.767	0.168	0.476	15.461	2.445	18.348	19.854	37.825
38	734.695	0.442	0.297	10.767	1.385	15.131	14.021	25.800
39	631.863	0.503	0.254	10.012	1.231	13.258	12.504	22.670
40	573.582	0.673	0.201	8.895	0.779	10.803	10.231	18.712
41	427.173	0.783	0.153	6.054	0.362	7.885	7.800	14.325
42	560.976	0.456	0.169	7.291	0.290	10.097	9.015	17.098

43	668.328	0.950	0.265	7.435	0.907	12.882	12.310	22.435
44	678.622	0.871	0.260	8.926	0.936	14.075	13.315	24.215
45	664.431	0.664	0.267	11.003	1.137	15.083	14.456	26.630
46	776.950	0.859	0.198	6.555	0.526	10.915	11.223	20.377
47	862.138	0.531	0.313	12.457	1.863	23.403	21.709	36.431
48	800.889	0.742	0.241	8.180	1.549	13.633	13.297	23.812
49	826.317	0.581	0.235	8.069	0.843	13.673	13.517	24.593
50	766.180	0.866	0.222	7.866	0.687	12.726	12.311	22.343

Continued from Table C- 1

AL-5	Pr	Nd	Sm	Eu	Gd	Tb	Dy	Ho
	ppm	ppm	ppm	ppm	ppm	ppm	ppm	ppm
1	2.972	11.701	2.472	0.633	2.444	0.380	2.247	0.430
2	3.098	12.296	2.560	0.622	2.562	0.383	2.225	0.445
3	3.604	14.036	2.898	0.733	3.095	0.424	2.569	0.509
4	3.051	12.157	2.565	0.655	2.837	0.399	2.337	0.480
5	2.224	8.784	1.841	0.437	1.839	0.271	1.619	0.327
6	2.006	7.945	1.743	0.440	1.768	0.255	1.461	0.285
7	3.256	12.870	2.688	0.676	2.925	0.406	2.318	0.467
8	3.308	13.039	2.727	0.670	2.970	0.408	2.415	1.238
9	3.406	13.656	2.767	0.701	3.050	0.429	2.478	0.495
10	3.387	13.525	2.812	0.723	2.958	0.443	2.667	0.497
11	3.521	13.856	2.916	0.766	3.252	0.456	2.636	0.514
12	3.453	13.473	2.847	0.745	3.122	0.438	2.590	0.504
13	3.814	14.925	3.146	0.785	3.399	0.471	2.673	0.544
14	3.976	15.809	3.230	0.809	3.350	0.500	2.791	0.544
15	3.114	12.486	2.700	0.707	2.708	0.408	2.354	0.474
16	2.872	11.388	2.466	0.624	2.708	0.384	2.271	0.453
17	3.675	14.419	3.070	0.789	3.267	0.470	2.745	0.533
18	3.805	14.987	3.054	0.782	3.228	0.472	2.789	0.523
19	4.151	16.131	3.289	0.796	3.350	0.495	2.908	0.567
20	3.414	13.601	2.864	0.748	3.129	0.449	2.563	0.533
21	2.925	11.811	2.475	0.655	2.741	0.391	2.368	0.444
22	3.220	12.935	2.660	0.705	3.015	0.421	2.501	0.489
23	3.316	13.222	2.780	0.698	2.833	0.434	2.408	0.476
24	4.228	16.216	3.289	0.801	3.631	0.503	2.844	0.574
25	4.267	16.673	3.489	0.852	3.852	0.525	3.099	0.626
26	3.801	15.038	3.108	0.789	3.357	0.464	2.691	0.537

27	4.307	16.503	3.366	0.840	3.642	0.497	2.847	0.878
28	3.943	15.498	3.233	0.775	3.318	0.491	2.902	0.566
29	3.601	14.212	2.948	0.795	3.200	0.487	2.798	0.731
30	4.712	18.443	3.792	0.902	3.831	0.554	3.250	0.639
31	3.822	14.738	3.071	0.780	3.359	0.473	2.678	0.518
32	3.893	15.217	3.069	0.759	3.172	0.459	2.662	0.540
33	3.306	12.879	2.712	0.683	2.713	0.402	2.408	0.473
34	2.550	10.104	1.992	0.516	2.098	0.304	1.695	0.341
35	2.342	9.425	1.843	0.475	1.863	0.277	1.526	0.302
36	3.308	13.097	2.660	0.700	2.905	0.430	2.459	0.481
37	4.762	18.617	3.803	0.988	3.835	0.566	3.277	0.608
38	3.271	12.910	2.738	0.672	3.054	0.414	2.439	0.477
39	2.891	11.588	2.340	0.601	2.639	0.352	2.101	0.403
40	2.357	9.390	1.967	0.502	2.102	0.297	1.778	0.354
41	1.779	6.987	1.503	0.385	1.660	0.221	1.346	0.262
42	2.085	8.486	1.729	0.502	1.892	0.281	1.690	0.335
43	2.885	11.453	2.370	0.638	2.455	0.367	2.148	0.422
44	3.042	12.141	2.526	0.641	2.760	0.392	2.300	0.456
45	3.372	13.349	2.676	0.683	2.910	0.431	2.534	0.477
46	2.564	10.122	2.077	0.509	2.299	0.312	1.812	0.367
47	4.924	19.398	3.976	0.977	4.505	0.628	3.665	0.723
48	3.056	12.051	2.421	0.665	2.618	0.391	2.269	0.451
49	3.123	12.214	2.468	0.654	2.700	0.385	2.301	0.455
50	2.831	11.055	2.278	0.630	2.682	0.366	2.141	0.423

Continued from Table C- 1

AL-5	**Er**	**Tm**	**Yb**	**Lu**	**Th**	**Ga**	**As**	**Se**
	ppm	ppm	ppm	ppm	ppm	ppm	ppm	ppm
1	1.294	0.176	1.197	0.173	3.339	9.297	2.941	17.301
2	1.295	0.184	1.140	0.172	3.327	8.895	7.255	6.673
3	1.557	0.207	1.372	0.202	4.334	12.591	3.789	4.977
4	1.439	0.202	1.232	0.194	3.516	10.775	3.184	2.572
5	0.923	0.134	0.847	0.135	2.653	11.073	2.801	2.377
6	0.814	0.119	0.751	0.112	2.139	6.002	2.048	7.994
7	1.335	0.187	1.238	0.184	3.349	9.719	6.891	0.000
8	1.387	0.192	1.210	0.180	3.236	8.385	4.660	9.463
9	1.396	0.193	1.264	0.185	3.273	9.218	7.462	0.000
10	1.488	0.213	1.336	0.211	3.339	10.095	4.961	0.000

11	1.495	0.207	1.312	0.191	3.565	10.562	3.664	0.000
12	1.474	0.203	1.325	0.199	3.412	10.173	2.557	7.444
13	1.552	0.211	1.380	0.211	3.948	11.626	3.700	5.533
14	1.631	0.227	1.429	0.204	4.205	11.648	5.168	4.563
15	1.377	0.187	1.208	0.186	2.999	8.848	3.901	1.299
16	1.274	0.184	1.127	0.170	2.562	8.691	2.466	5.893
17	1.594	0.216	1.343	0.213	3.663	10.262	4.055	4.707
18	1.600	0.222	1.368	0.211	3.996	11.411	5.297	10.558
19	1.680	0.237	1.465	0.229	4.459	13.097	5.943	7.767
20	1.481	0.212	1.303	0.197	3.234	9.719	4.562	3.663
21	1.308	0.180	1.156	0.165	2.783	8.882	3.078	0.000
22	1.360	0.197	1.220	0.190	2.997	8.975	2.471	0.000
23	1.431	0.190	1.264	0.182	3.158	8.918	1.951	0.000
24	1.627	0.229	1.519	0.219	4.745	13.560	3.715	0.000
25	1.795	0.248	1.642	0.245	4.544	12.197	5.008	0.000
26	1.543	0.212	1.419	0.206	3.934	11.537	5.561	8.377
27	1.661	0.231	1.482	0.226	4.915	14.132	7.673	14.012
28	1.660	0.243	1.493	0.226	4.208	11.597	3.125	0.000
29	1.617	0.226	1.419	0.214	3.599	11.769	3.356	0.000
30	1.871	0.259	1.707	0.250	5.512	14.620	4.645	9.493
31	1.510	0.209	1.400	0.207	4.008	11.310	2.714	12.306
32	1.586	0.216	1.410	0.207	4.236	11.280	2.538	4.535
33	1.402	0.194	1.275	0.189	3.763	9.606	1.409	6.836
34	1.008	0.138	0.927	0.135	2.740	6.536	1.935	12.057
35	0.918	0.122	0.785	0.122	1.656	3.548	4.965	16.302
36	1.391	0.196	1.235	0.194	3.413	11.156	2.931	0.000
37	1.758	0.247	1.583	0.235	5.259	16.395	3.444	11.587
38	1.431	0.195	1.255	0.181	3.202	9.392	1.770	0.000
39	1.207	0.171	1.083	0.160	2.861	9.015	2.063	7.931
40	1.009	0.144	0.878	0.133	2.298	6.685	3.102	16.248
41	0.705	0.103	0.669	0.099	1.610	4.432	13.215	32.148
42	0.956	0.131	0.824	0.121	1.698	6.182	3.893	26.488
43	1.238	0.173	1.084	0.161	2.609	6.303	9.324	28.199
44	1.377	0.181	1.154	0.174	2.899	7.567	4.600	31.221
45	1.420	0.194	1.260	0.178	3.415	9.810	3.532	26.276
46	1.037	0.137	0.935	0.136	2.652	5.117	4.386	27.095
47	2.058	0.303	1.897	0.266	4.935	12.860	4.585	27.897
48	1.311	0.183	1.178	0.169	2.928	6.340	5.441	30.403
49	1.315	0.179	1.154	0.170	3.000	7.126	5.675	37.906
50	1.238	0.165	1.106	0.165	2.695	6.393	5.260	0.000

Continued from Table C- 1

AL-5	Rb	Cs	Pb	U	Zr	Nb	Mo
	ppm	ppm	ppm	ppm	ppm	ppm	ppm
1	33.831	1.909	15.413	1.379	59.018	7.816	0.559
2	30.349	1.711	8.029	1.276	57.354	8.175	0.456
3	40.747	2.465	9.584	1.374	71.814	9.754	1.187
4	35.383	1.996	8.730	1.359	66.091	8.188	0.453
5	37.816	2.159	7.513	2.065	50.325	5.879	0.619
6	23.956	1.279	5.652	1.044	40.677	5.106	0.292
7	36.497	1.730	9.305	1.234	68.468	8.626	0.812
8	30.402	1.474	6.113	1.172	62.056	8.273	0.469
9	30.405	1.533	6.381	1.287	63.213	8.660	0.339
10	31.957	1.664	6.381	1.428	68.051	9.450	0.369
11	32.694	1.770	6.735	1.515	67.918	9.663	0.517
12	30.712	1.741	6.887	1.493	71.809	9.696	0.630
13	33.879	1.905	8.180	1.531	77.753	10.602	0.848
14	34.596	1.932	8.553	1.599	77.248	11.634	0.834
15	24.838	1.393	6.187	1.652	62.879	8.783	0.561
16	22.108	1.167	30.263	1.142	53.582	7.627	0.597
17	29.681	1.674	7.667	1.671	76.973	10.152	0.796
18	32.754	1.813	8.240	1.441	75.568	10.763	1.123
19	38.254	2.194	8.899	1.552	88.565	11.718	1.278
20	28.046	1.518	6.517	1.769	73.168	9.660	11.254
21	23.292	1.262	6.591	1.276	58.770	7.933	0.567
22	26.026	1.391	6.071	1.321	68.940	8.830	0.621
23	26.573	1.417	6.373	1.381	64.913	9.033	0.488
24	40.400	2.317	9.495	1.469	87.428	12.246	0.852
25	38.686	2.169	12.893	1.603	87.071	11.433	0.818
26	33.928	1.885	8.876	1.377	147.592	10.225	0.855
27	42.271	2.378	10.502	1.323	87.272	12.195	1.180
28	38.344	2.127	8.302	1.634	77.889	10.543	0.748
29	40.783	2.181	7.849	1.804	75.313	9.989	0.646
30	48.640	2.652	10.538	1.461	100.730	13.589	0.311
31	34.984	1.999	10.960	1.261	72.865	10.387	0.268
32	36.943	2.122	11.445	1.231	77.796	10.251	0.623
33	35.594	2.126	10.148	1.368	67.805	8.336	0.288
34	24.757	1.504	9.271	0.823	46.973	6.703	0.471
35	11.591	0.568	5.970	1.115	30.138	3.829	0.318
36	40.148	2.267	23.529	1.570	76.311	9.604	0.872

37	55.983	2.839	9.711	1.316	105.518	14.661	0.804
38	32.376	1.806	7.374	1.525	69.414	9.058	0.541
39	32.142	1.856	5.359	1.392	59.801	7.996	0.422
40	25.199	1.491	7.170	2.170	50.256	6.405	0.650
41	17.013	0.968	3.163	8.413	38.463	4.438	3.336
42	15.759	0.806	8.180	2.549	35.701	4.515	0.540
43	22.627	1.204	4.949	1.989	54.543	7.323	1.247
44	26.753	1.436	5.783	1.761	61.069	8.122	1.096
45	35.487	1.998	6.460	1.713	64.263	8.636	1.265
46	20.504	1.166	35.199	1.309	46.257	6.144	0.358
47	48.627	2.754	10.234	1.899	89.620	11.761	0.964
48	23.015	1.227	5.780	1.559	77.908	7.478	0.467
49	25.841	1.481	5.844	1.526	57.170	7.939	0.181
50	23.089	1.304	5.544	1.453	50.135	6.962	0.383

Table C- 2. Geochemical concentrations of 36 samples of AT-1

AT-1	**Si**	**Ca**	**Al**	**Fe**	**K**	**Na**	**Mg**	**V**
	wt%	wt%	wt%	wt%	wt%	wt%	wt%	ppm
1	9.769	18.536	2.310	2.418	0.461	0.240	2.648	76.270
2	9.922	18.283	2.353	2.563	0.473	0.240	2.651	81.564
3	11.571	16.427	3.196	2.977	0.556	0.201	2.514	95.099
4	11.517	16.015	3.142	2.895	0.597	0.219	2.844	93.838
5	11.783	15.760	3.149	2.975	0.578	0.209	2.765	93.402
6	11.972	16.189	3.187	2.949	0.582	0.226	2.395	98.238
7	11.977	16.696	3.043	2.876	0.585	0.231	2.251	96.234
8	11.293	17.136	2.930	2.797	0.560	0.216	2.137	96.732
9	13.300	15.398	3.494	3.140	0.636	0.232	2.173	101.256
10	12.557	15.938	3.183	2.970	0.626	0.207	2.167	97.862
11	11.766	16.472	3.022	2.861	0.622	0.206	2.119	103.850
12	11.455	16.890	3.151	2.813	0.606	0.206	2.148	102.151
13	11.288	16.649	2.950	2.913	0.592	0.219	2.180	106.590
14	12.430	15.301	3.276	3.138	0.625	0.226	2.160	106.899
15	14.976	14.102	3.787	3.473	0.689	0.262	2.255	103.576
16	13.605	13.607	3.651	3.565	0.665	0.252	2.213	117.724
17	12.370	15.287	3.373	3.153	0.627	0.217	2.142	107.591
18	11.414	16.096	3.163	3.062	0.617	0.201	2.065	103.837
19	11.315	17.277	2.949	2.779	0.617	0.213	2.055	89.491
20	16.960	11.209	3.852	3.597	0.720	0.257	2.210	113.394

21	17.487	10.112	4.266	3.560	0.705	0.236	2.085	110.417
22	18.017	10.124	4.397	3.522	0.735	0.243	1.995	111.343
23	13.557	15.224	3.247	2.901	0.541	0.231	2.089	84.899
24	12.732	16.411	2.601	2.799	0.464	0.281	2.373	71.488
25	13.365	15.759	2.464	2.760	0.419	0.307	2.493	72.749
26	11.652	17.448	2.509	2.564	0.441	0.276	2.337	68.287
27	11.247	17.651	2.326	2.469	0.431	0.292	2.614	76.349
28	12.362	17.117	2.200	2.815	0.325	0.355	3.165	98.054
29	13.099	15.455	2.875	3.132	0.502	0.243	2.580	95.482
30	11.62	16.01	3.21	3.10	0.53	0.20	1.94	96.24
31	12.00	16.07	3.50	3.11	0.51	0.19	1.85	89.78
32	11.99	16.37	3.49	3.17	0.48	0.19	1.82	85.18
33	11.95	16.05	3.50	3.22	0.49	0.20	1.83	86.00
34	11.45	17.28	3.47	3.19	0.51	0.20	1.87	93.90
35	11.49	17.18	3.36	3.32	0.55	0.21	1.91	97.03
36	10.38	18.51	3.09	2.77	0.50	0.19	1.94	90.16

Continued from Table C- 2

AT-1	**Cr**	**Mn**	**Co**	**Ni**	**Cu**	**Zn**	**Sr**	**Ba**
	ppm	ppm	ppm	ppm	ppm	ppm	ppm	ppm
1	416.878	445.128	25.148	334.258	28.343	67.675	1430.694	109.346
2	344.586	464.113	23.900	347.521	30.833	104.597	1345.530	109.477
3	293.473	533.327	27.090	339.555	30.881	85.069	1093.746	120.748
4	286.731	508.564	25.214	334.273	31.276	88.997	1020.947	109.164
5	306.926	506.233	24.063	338.761	53.770	80.063	1005.072	87.515
6	321.843	672.716	29.561	358.554	33.047	68.761	1070.034	147.969
7	320.324	576.081	26.608	328.206	34.279	84.339	1103.277	112.257
8	315.343	625.308	27.119	327.794	37.741	104.546	1070.359	140.277
9	392.511	654.317	28.620	363.910	39.432	92.579	976.304	132.851
10	323.912	626.363	28.062	351.107	33.670	86.273	1010.492	147.296
11	324.257	625.786	26.621	316.375	34.900	69.889	1050.613	107.093
12	313.072	617.893	27.549	353.508	34.799	74.006	1080.526	150.558
13	341.776	641.336	27.375	320.639	32.342	89.276	1073.069	111.474
14	339.155	655.609	28.861	393.422	35.960	74.916	947.594	123.636
15	327.775	720.059	32.861	372.926	40.250	124.835	754.001	147.816
16	414.781	775.513	37.238	452.255	41.490	137.793	788.264	124.659
17	313.296	724.341	29.003	399.464	35.187	96.675	963.582	213.313
18	270.665	781.049	29.785	347.569	34.489	72.522	976.246	152.425

19	281.324	815.494	33.643	342.046	36.607	82.313	1109.798	117.495
20	341.037	727.533	32.634	370.123	53.800	89.786	668.642	217.214
21	347.805	789.894	32.758	331.683	61.544	121.268	556.333	241.458
22	276.756	732.190	31.226	315.065	56.842	124.082	538.834	189.296
23	286.913	577.957	22.987	263.018	39.312	66.710	870.391	202.909
24	399.138	600.291	25.281	328.750	26.045	78.338	990.263	122.049
25	494.684	664.418	26.637	347.309	28.325	55.602	930.596	196.529
26	454.794	554.722	24.359	331.322	25.200	70.125	1009.477	106.126
27	955.151	536.752	35.462	415.176	23.297	57.026	1061.940	153.293
28	3088.552	643.968	32.026	416.607	20.397	82.484	972.231	118.585
29	702.625	640.096	31.659	410.713	30.828	76.021	859.684	122.922
30	333.16	454.03	23.77	337.04	26.41	68.44	813.04	152.79
31	312.93	440.90	25.73	338.58	29.97	69.61	775.26	163.20
32	350.14	417.87	22.36	344.20	27.56	83.35	717.21	173.70
33	326.24	441.65	23.13	311.90	25.93	91.42	724.27	170.47
34	312.74	504.97	22.53	315.28	28.61	83.16	761.36	177.33
35	312.21	524.60	21.85	321.06	27.73	84.03	854.21	181.25
36	270.09	509.66	28.89	296.20	29.07	86.29	907.09	147.23

Continued from Table C- 2

AT-1	**P**	**S**	**Ti**	**Sc**	**Hf**	**Y**	**La**	**Ce**
	ppm	wt%	wt%	mg/kg	ppm	ppm	ppm	ppm
1	471.381	0.362	0.233	8.615	0.409	13.839	14.126	25.123
2	519.401	0.398	0.237	10.504	0.393	14.245	14.169	25.922
3	518.864	0.330	0.272	11.288	0.847	17.107	18.061	32.433
4	491.022	0.320	0.264	11.208	0.781	16.841	17.556	31.719
5	527.814	0.000	0.283	11.985	0.804	17.100	18.106	32.295
6	601.052	0.331	0.279	11.081	0.776	17.499	18.335	33.318
7	602.791	0.000	0.280	10.807	0.847	17.738	18.719	33.298
8	602.275	0.000	0.281	10.915	0.761	17.117	18.079	32.932
9	667.231	0.308	0.288	11.138	1.045	18.401	19.455	35.260
10	624.243	0.338	0.255	11.477	0.795	16.314	17.153	31.487
11	609.052	0.326	0.256	11.295	0.702	16.353	16.805	30.271
12	575.047	0.388	0.241	11.963	0.739	16.610	16.847	31.141
13	591.728	0.000	0.246	11.396	0.717	16.006	16.393	29.895
14	610.776	0.277	0.263	12.116	0.860	17.244	18.340	32.947
15	689.632	0.276	0.307	13.236	1.085	17.167	20.510	37.884
16	687.968	0.000	0.300	12.767	1.285	18.392	20.241	36.400

17	732.205	0.387	0.264	12.248	0.874	17.183	18.163	32.191
18	754.035	0.333	0.263	11.615	0.849	16.944	18.244	32.491
19	729.460	0.337	0.261	11.169	0.750	16.273	17.038	30.013
20	983.351	0.238	0.336	13.036	1.170	19.193	22.739	42.324
21	850.526	0.255	0.329	12.935	1.404	19.568	23.058	44.544
22	881.422	0.192	0.334	13.067	1.409	19.748	23.868	46.698
23	710.427	0.281	0.288	11.033	0.743	15.882	16.327	30.673
24	689.709	0.326	0.283	11.729	0.539	14.201	14.661	27.268
25	714.634	0.300	0.293	9.823	0.452	14.121	14.750	27.597
26	686.712	0.364	0.262	9.512	0.324	13.650	14.673	26.411
27	675.806	0.416	0.288	10.566	0.399	12.841	14.484	26.034
28	663.448	0.432	0.377	11.661	0.296	12.032	12.829	23.503
29	681.672	0.295	0.318	12.127	0.565	14.849	16.007	29.392
30	709.74	0.30	0.30	12.07	0.79	16.44	19.07	33.88
31	715.27	0.35	0.30	12.37	0.92	17.03	20.58	36.37
32	684.47	0.38	0.32	11.64	0.95	16.60	19.54	34.83
33	706.60	0.31	0.33	11.76	1.04	19.15	19.72	35.17
34	694.30	0.34	0.31	12.86	1.08	17.04	18.74	33.75
35	729.68	0.32	0.31	12.41	1.02	16.95	19.36	34.86
36	765.83	0.40	0.30	11.89	0.68	17.22	18.19	31.79

Continued from Table C- 2

AT-1	**Pr**	**Nd**	**Sm**	**Eu**	**Gd**	**Tb**	**Dy**	**Ho**
	ppm	ppm	ppm	ppm	ppm	ppm	ppm	ppm
1	3.246	13.545	3.017	0.670	2.860	0.413	2.516	0.500
2	3.320	12.982	2.695	0.714	4.522	0.429	2.458	0.494
3	4.006	16.400	3.284	0.864	5.490	0.507	2.991	0.914
4	3.956	16.114	3.620	0.821	5.264	0.508	2.913	0.598
5	4.166	16.870	3.551	0.818	5.454	0.505	3.025	0.620
6	4.266	16.760	3.444	0.863	5.606	0.508	2.974	0.608
7	4.269	16.773	3.633	0.859	3.764	0.530	3.042	0.625
8	4.209	17.120	3.737	0.844	5.482	0.512	3.009	0.617
9	4.534	18.028	3.589	0.912	5.889	0.548	3.212	0.642
10	3.826	16.008	3.201	0.792	5.260	0.503	2.889	0.570
11	3.859	15.394	3.392	0.757	3.443	0.488	2.841	0.565
12	3.871	14.985	3.104	0.816	5.206	0.467	2.822	0.561
13	3.765	14.903	3.088	0.793	3.387	0.471	2.765	0.544
14	4.128	16.665	3.356	0.853	5.501	0.521	3.083	0.610

15	4.674	18.292	3.629	0.950	6.163	0.548	3.206	0.649
16	4.593	18.502	3.677	0.946	3.840	0.573	3.266	0.664
17	4.134	16.413	3.334	0.835	5.394	0.498	3.016	0.608
18	4.154	16.636	3.684	0.828	5.546	0.502	2.950	0.595
19	3.933	15.433	3.474	0.778	5.210	0.485	2.883	0.581
20	5.063	19.914	4.029	1.040	6.578	0.614	3.524	0.780
21	5.234	20.037	4.691	1.025	4.350	0.583	3.550	0.691
22	5.335	20.996	4.645	1.026	6.899	0.615	3.570	0.687
23	3.722	14.879	3.057	0.770	2.977	0.451	2.556	0.506
24	3.381	13.428	2.760	0.721	4.412	0.413	2.430	0.487
25	3.441	13.604	2.763	0.754	3.106	0.420	2.464	0.501
26	3.321	13.529	2.764	0.704	2.990	0.418	2.445	0.487
27	3.244	12.925	2.974	0.681	4.286	0.409	2.427	0.485
28	2.876	11.671	2.399	0.624	2.547	0.368	2.183	0.441
29	3.717	14.875	2.967	0.730	0.458	0.458	2.745	0.541
30	4.34	17.45	3.84	0.86	3.56	0.53	3.05	0.59
31	4.57	18.10	3.67	0.90	6.06	0.54	3.15	0.64
32	4.47	17.45	3.92	0.87	5.67	0.52	3.00	0.60
33	4.44	17.16	3.56	0.88	5.85	0.53	3.09	0.62
34	4.33	17.37	3.89	0.88	5.67	0.52	3.01	0.61
35	4.40	17.60	4.04	0.89	5.81	0.53	3.10	0.61
36	4.04	16.10	3.65	0.82	5.44	0.48	2.78	0.56

Continued from Table C- 2

AT-1	**Er**	**Tm**	**Yb**	**Lu**	**Th**	**Ga**	**As**	**Se**
	ppm	ppm	ppm	ppm	ppm	ppm	ppm	ppm
1	1.454	0.206	1.248	0.188	2.998	11.136	5.614	27.503
2	1.455	0.202	1.221	0.194	3.014	11.664	6.287	22.078
3	1.750	0.244	1.549	0.226	4.115	15.258	6.052	14.143
4	1.742	0.240	1.525	0.230	4.087	10.453	7.243	18.499
5	1.774	0.235	1.563	0.227	4.126	12.970	5.617	27.059
6	1.773	0.243	1.563	0.222	4.160	10.434	6.624	30.652
7	1.762	0.247	1.590	0.246	4.213	14.134	6.692	17.015
8	1.742	0.243	1.547	0.233	4.130	15.245	7.607	26.794
9	1.839	0.259	1.677	0.248	4.504	11.179	7.008	28.642
10	1.694	0.238	1.435	0.226	3.924	16.753	5.669	0.000
11	1.679	0.233	1.482	0.221	3.864	10.211	7.215	0.000
12	1.681	0.227	1.447	0.219	3.816	16.440	7.061	36.708

13	1.623	0.226	1.481	0.222	3.796	9.778	8.916	33.779
14	1.746	0.242	1.618	0.233	4.197	15.988	8.507	0.000
15	1.914	0.264	1.671	0.259	4.568	16.733	7.387	24.846
16	1.951	0.277	1.799	0.254	4.724	12.478	9.163	0.000
17	1.720	0.250	1.552	0.238	4.080	11.003	6.092	0.000
18	1.739	0.240	1.573	0.229	4.051	10.640	6.796	19.652
19	1.630	0.242	1.489	0.227	3.763	14.104	4.565	16.832
20	1.978	0.277	1.857	0.274	5.293	21.103	6.031	13.458
21	2.050	0.282	1.819	0.281	5.616	24.208	6.365	30.629
22	2.055	0.282	1.901	0.281	5.830	15.528	3.011	32.443
23	1.469	0.210	1.352	0.198	3.545	9.710	2.303	0.089
24	1.408	0.200	1.265	0.179	3.022	12.702	2.293	0.000
25	1.449	0.199	1.288	0.191	2.918	14.883	3.427	0.000
26	1.423	0.204	1.296	0.186	2.912	17.949	2.181	6.936
27	1.349	0.193	1.278	0.190	2.887	12.607	5.334	0.000
28	1.329	0.184	1.200	0.177	2.361	6.670	4.025	12.738
29	1.587	0.226	1.443	0.215	3.393	13.723	3.926	0.000
30	1.74	0.25	1.65	0.24	4.30	10.14	2.08	12.46
31	1.85	0.25	1.67	0.25	4.75	10.89	2.34	0.00
32	1.77	0.24	1.62	0.24	4.46	16.99	1.79	0.00
33	1.79	0.26	1.60	0.24	4.50	17.55	2.36	0.00
34	1.78	0.25	1.62	0.24	4.33	10.30	2.05	0.00
35	1.81	0.26	1.60	0.25	4.41	18.33	3.81	0.00
36	1.65	0.24	1.50	0.21	3.93	15.93	4.28	0.00

Continued from Table C- 2

AT-1	**Rb**	**Cs**	**Pb**	**U**	**Zr**	**Nb**	**Mo**
	ppm	ppm	ppm	ppm	ppm	ppm	ppm
1	24.813	1.508	9.169	2.041	51.901	7.240	1.663
2	25.458	1.544	7.446	2.054	50.292	6.592	2.566
3	35.715	2.215	8.691	2.020	65.643	8.382	2.263
4	36.729	2.222	9.496	2.096	65.100	8.412	5.261
5	35.461	2.173	9.777	2.038	65.707	8.460	1.702
6	36.452	2.099	8.889	2.084	64.212	8.719	2.256
7	35.907	2.058	8.636	2.090	65.603	8.801	2.120
8	35.274	2.035	9.035	2.043	63.834	8.866	2.847
9	40.646	2.280	8.485	1.990	74.210	9.535	1.588
10	38.583	2.285	7.054	1.919	66.158	8.315	1.017

11	36.799	2.232	7.141	2.020	64.180	7.933	1.307
12	36.885	2.201	6.941	2.038	64.669	7.846	1.391
13	35.593	2.131	6.524	2.130	64.316	7.960	1.598
14	37.656	2.311	8.253	2.031	67.765	8.594	1.806
15	36.906	2.545	8.982	1.877	70.004	9.449	1.745
16	38.828	2.492	8.694	1.993	73.473	9.249	2.381
17	36.958	2.343	8.051	2.098	65.401	8.445	3.458
18	37.276	2.333	7.155	2.081	66.003	8.712	2.371
19	33.954	2.114	6.705	2.115	58.796	7.663	1.755
20	42.438	2.467	9.798	1.715	80.103	11.163	0.994
21	43.051	2.602	11.193	1.653	87.176	11.234	1.328
22	45.054	2.734	11.485	2.381	92.042	12.237	2.142
23	30.430	1.768	7.849	1.427	65.915	8.856	0.557
24	24.670	1.447	6.953	1.358	55.709	7.548	1.635
25	21.604	1.270	6.124	1.320	54.469	7.218	0.488
26	23.203	1.508	5.941	1.398	48.569	6.411	0.351
27	21.561	1.352	5.570	6.506	50.635	6.572	1.496
28	15.911	0.947	6.591	1.361	50.076	6.399	0.671
29	29.235	1.799	7.677	1.642	56.692	7.722	0.454
30	34.01	2.24	7.52	1.91	65.13	8.51	0.62
31	38.78	2.32	8.20	1.83	68.98	9.13	0.46
32	37.69	2.23	7.87	1.71	65.20	8.87	2.02
33	38.14	2.23	7.73	1.63	71.67	9.03	1.41
34	34.94	2.13	8.85	1.75	72.35	8.68	0.42
35	35.46	2.20	7.54	1.72	69.09	8.76	0.34
36	30.91	2.05	7.29	2.37	60.53	7.88	0.59

Table C- 3. Geochemical concentrations of 41 samples of KR-1

KR-1	**Si**	**Ca**	**Al**	**Fe**	**K**	**Na**	**Mg**	**V**
	wt%	wt%	wt%	wt%	wt%	wt%	wt%	ppm
37	19,423	9,236	3,980	3,747	0,511	0,282	2,685	91,842
38	18,760	10,865	3,708	3,529	0,473	0,287	2,763	87,377
39	18,868	10,613	4,265	3,613	0,544	0,263	2,365	98,028
40	18,559	11,673	3,915	3,441	0,515	0,296	2,298	94,051
41	18,727	10,443	4,299	3,669	0,568	0,270	2,233	91,357
42	19,623	9,483	4,410	3,839	0,602	0,332	2,333	97,595
43	19,243	9,372	4,542	3,840	0,628	0,331	2,339	95,784
44	19,534	9,194	4,661	3,944	0,619	0,330	2,412	98,036
45	19,721	9,091	4,549	3,915	0,606	0,321	2,513	98,524

46	18,943	9,681	4,145	3,702	0,568	0,331	2,629	96,258
47	19,109	1,053	0,537	0,403	0,060	0,028	0,325	90,198
48	19,274	8,746	4,669	3,888	0,627	0,318	2,638	90,944
49	19,424	8,870	4,449	3,826	0,616	0,310	2,708	88,754
50	18,896	9,584	4,323	3,813	0,620	0,314	2,717	89,338
51	20,474	7,858	4,797	3,955	0,654	0,309	2,578	92,578
52	19,332	8,855	4,992	3,864	0,680	0,288	2,511	89,358
53	20,506	6,764	4,869	4,432	0,664	0,330	3,087	99,212
54	20,718	7,400	4,654	3,931	0,653	0,323	2,923	88,513
55	20,128	8,189	4,662	3,884	0,654	0,318	2,670	88,012
56	20,192	7,035	4,665	3,914	0,682	0,322	2,978	86,000
57	18,817	10,083	3,545	3,691	0,533	0,396	3,681	90,285
58	17,859	10,145	3,993	3,781	0,614	0,327	3,456	81,749
59	18,201	9,648	4,284	3,789	0,633	0,307	3,306	84,375
60	17,615	9,776	4,192	3,799	0,648	0,359	3,101	84,715
61	19,812	7,607	4,549	4,103	0,772	0,312	3,112	76,449
62	18,888	8,056	4,035	3,904	0,813	0,328	3,917	76,516
63	18,293	8,431	3,678	3,834	0,643	0,316	4,398	77,327
64	15,429	12,362	2,665	3,451	0,384	0,359	5,217	76,762
65	15,691	12,067	3,071	3,491	0,460	0,392	4,890	77,178
66	18,454	9,542	3,333	4,166	0,525	0,385	5,058	85,687
67	17,519	10,354	3,250	3,973	0,481	0,383	4,719	85,172
68	18,952	9,388	2,776	4,093	0,424	0,380	5,247	96,353
69	18,900	9,485	3,842	4,393	0,616	0,448	4,249	90,127
70	20,232	6,131	4,667	6,124	0,771	0,393	3,763	105,960
71	19,204	9,429	3,795	4,440	0,613	0,483	4,228	94,312
72	19,578	8,266	4,480	4,902	0,709	0,425	3,958	93,763
73	21,362	6,334	5,708	4,954	0,837	0,404	3,059	112,778
74	19,794	7,116	5,169	5,229	0,796	0,346	2,835	111,299
75	23,282	2,541	6,748	5,340	0,965	0,400	2,988	153,177
76	21,293	5,055	6,021	5,197	0,863	0,376	2,696	110,672
77	21,694	5,905	6,157	5,558	0,878	0,360	2,703	110,465

Continued from Table C- 3

KR -1	**Cr**	**Mn**	**Co**	**Ni**	**Cu**	**Zn**	**Sr**	**Ba**
	ppm	ppm	ppm	ppm	ppm	ppm	ppm	ppm
37	291,457	1100,121	30,761	314,066	53,661	75,946	285,761	197,943

38	365,444	942,975	29,617	299,358	43,320	81,049	314,344	142,297
39	292,423	943,283	28,142	261,694	83,619	94,358	327,781	180,093
40	254,895	1096,725	27,735	265,097	43,488	63,176	361,599	231,497
41	237,837	1081,545	28,851	266,371	45,886	85,790	319,397	182,412
42	248,865	985,101	31,323	286,850	48,389	139,231	325,330	195,040
43	269,091	1096,027	31,999	269,860	51,453	94,391	337,017	210,076
44	247,592	1153,459	30,783	284,500	53,940	93,002	332,553	187,676
45	240,405	1076,740	29,773	273,034	52,941	93,389	351,301	197,180
46	238,889	1119,512	31,394	304,579	48,103	73,661	361,035	197,111
47	208,218	1033,812	27,858	246,482	48,782	92,195	364,885	242,847
48	183,909	1088,173	29,877	263,840	48,646	73,039	367,543	182,253
49	205,085	1112,236	29,483	253,142	48,408	70,623	365,591	194,655
50	223,986	696,599	25,548	269,286	45,348	93,995	405,681	156,596
51	194,876	967,892	28,302	253,502	48,429	90,392	352,406	188,282
52	186,177	754,629	20,157	208,350	44,693	76,196	379,153	179,041
53	281,612	1179,730	38,905	378,136	52,471	74,545	305,575	173,624
54	211,793	1141,419	30,435	299,372	45,451	72,469	331,517	165,838
55	212,335	934,851	30,023	295,642	51,098	78,212	353,336	165,422
56	205,987	1010,037	28,081	288,276	48,556	73,870	320,808	156,202
57	375,252	957,581	30,532	372,692	43,018	83,339	376,821	148,207
58	229,640	1011,285	30,352	335,982	44,872	106,880	420,522	164,852
59	212,713	844,200	29,479	335,078	41,856	84,139	404,741	137,276
60	257,539	880,493	30,699	303,271	44,146	87,547	382,279	140,529

61	273,496	614,309	27,271	323,561	39,848	77,857	352,086	161,129
62	379,796	879,448	30,320	392,770	39,640	96,517	394,102	141,854
63	421,675	1012,975	32,775	415,958	44,694	78,932	447,356	125,463
64	910,536	1088,527	36,193	485,586	23,789	49,212	448,433	117,674
65	626,052	1121,253	34,343	478,908	26,190	55,600	459,944	162,420
66	576,371	707,998	44,813	685,635	29,827	62,035	359,757	166,480
67	751,452	633,988	36,731	587,748	27,641	56,954	394,970	115,855
68	1477,801	596,192	40,371	623,811	33,989	74,417	314,601	122,961
69	611,196	583,346	40,096	614,922	33,362	81,423	337,834	142,187
70	471,137	553,519	53,046	667,471	37,839	90,924	246,009	163,992
71	647,953	540,954	43,490	648,833	33,361	77,762	335,981	117,500
72	604,068	534,901	42,603	616,357	35,018	84,309	308,435	153,735
73	470,042	542,894	48,331	573,869	48,573	97,168	278,204	219,279
74	397,735	655,889	45,256	514,288	40,789	84,003	268,965	205,203
75	404,007	344,018	49,483	591,950	57,739	103,696	175,016	216,465
76	312,903	540,072	38,230	424,020	37,546	90,711	241,386	194,539
77	304,003	653,951	33,461	397,530	41,783	98,499	267,042	207,161

Continued from Table C- 3

KR-1	P	S	Ti	Sc	Hf	Y	La	Ce
	ppm	wt%	wt%	mg/kg	ppm	ppm	ppm	ppm
37	603,425	0,286	0,319	11,973	1,640	17,556	17,283	34,427
38	562,028	0,289	0,294	11,474	1,577	16,237	15,544	30,530
39	605,506	0,271	0,314	11,605	1,821	17,933	17,924	35,499
40	616,867	0,316	0,316	11,242	1,703	17,996	17,551	35,493

41	566,040	0,296	0,314	16,020	1,902	17,511	18,185	36,900
42	597,105	0,026	0,353	12,194	1,976	19,460	19,677	40,213
43	578,450	0,286	0,361	12,191	2,307	20,308	20,601	42,057
44	643,197	0,252	0,364	12,434	2,160	20,762	20,097	40,031
45	626,336	0,026	0,345	11,942	2,014	19,437	19,756	39,441
46	592,270	0,260	0,323	11,461	1,862	18,483	18,104	36,697
47	614,552	0,111	0,039	1,015	2,214	18,979	18,944	37,927
48	600,472	0,281	0,339	12,239	2,210	19,352	18,911	38,606
49	570,890	0,245	0,335	12,417	2,168	19,483	18,446	37,474
50	665,834	0,270	0,332	12,094	2,013	19,796	18,505	35,933
51	559,759	0,239	0,340	16,135	2,297	19,196	19,058	38,630
52	639,658	0,271	0,325	12,756	2,032	19,586	19,000	35,062
53	569,125	0,261	0,332	13,178	2,029	18,606	18,560	38,200
54	608,014	0,204	0,330	12,060	2,138	19,410	18,249	37,683
55	683,904	0,235	0,325	16,766	1,950	19,742	18,267	36,059
56	694,921	0,216	0,317	12,430	1,931	17,370	17,817	36,646
57	701,143	0,264	0,295	11,708	1,412	15,594	13,484	26,939
58	712,584	0,300	0,299	11,677	1,618	17,254	15,828	31,909
59	681,633	0,257	0,290	11,764	1,622	16,741	15,783	32,023
60	722,853	0,284	0,322	11,777	1,728	17,040	15,916	31,578
61	914,757	0,244	0,317	16,953	1,893	17,506	16,850	32,135
62	1524,408	0,281	0,312	11,269	1,676	16,435	15,819	31,187
63	997,988	0,265	0,293	11,043	1,536	15,208	14,866	29,587
64	550,222	0,348	0,293	9,259	1,363	12,309	11,448	22,841
65	560,828	0,378	0,324	13,918	1,458	14,001	13,588	27,138
66	629,442	0,274	0,318	15,497	1,403	14,898	14,871	29,412
67	585,559	0,000	0,318	10,364	1,572	15,384	14,990	30,187
68	597,499	0,283	0,328	10,115	1,316	13,715	13,471	26,139
69	704,022	0,223	0,379	11,222	1,819	18,101	18,181	36,527
70	698,775	0,114	0,367	13,281	1,993	18,002	20,220	40,451
71	747,939	0,194	0,396	11,246	1,784	17,943	17,943	36,085
72	697,197	0,137	0,388	12,473	2,105	18,826	19,202	38,264
73	756,731	0,145	0,414	14,613	2,471	22,112	23,011	45,531
74	728,472	0,134	0,367	13,391	2,151	20,242	21,735	43,162
75	648,766	0,129	0,421	17,275	2,636	23,990	25,660	49,471
76	812,158	0,093	0,403	19,744	2,360	20,233	22,995	45,161
77	749,917	0,179	0,408	14,840	2,408	21,208	22,931	44,398

Continued from Table C- 3

KR-1	Pr	Nd	Sm	Eu	Gd	Tb	Dy	Ho
	ppm	ppm	ppm	ppm	ppm	ppm	ppm	ppm
37	4,017	15,275	3,260	0,828	5,279	0,488	2,844	0,566
38	3,563	14,009	3,283	0,719	4,988	0,448	2,645	0,515
39	4,177	15,844	3,860	0,803	3,595	0,495	2,830	0,567
40	4,131	15,697	3,304	0,824	3,547	0,486	2,924	0,571
41	4,171	15,567	3,261	0,821	3,590	0,497	2,881	0,565
42	4,635	17,403	4,100	0,873	3,913	0,535	3,118	0,596
43	4,765	17,916	4,341	0,913	3,739	0,555	3,370	0,636
44	4,668	17,675	4,248	0,925	6,439	0,561	3,305	0,619
45	4,554	17,072	4,045	0,886	6,063	0,529	3,159	0,606
46	4,327	16,251	3,305	0,825	3,690	0,498	2,975	0,568
47	4,426	16,979	4,056	0,871	3,740	0,514	2,841	0,576
48	4,532	16,866	3,409	0,835	3,476	0,507	3,001	0,568
49	4,286	16,900	3,286	0,819	5,496	0,504	2,866	0,558
50	4,269	16,510	3,788	0,839	3,432	0,506	2,827	0,594
51	4,407	17,111	3,353	0,825	3,694	0,501	2,962	0,565
52	4,166	16,073	3,215	0,793	5,425	0,476	2,826	0,554
53	4,316	16,365	3,287	0,803	3,387	0,498	2,859	0,764
54	4,246	15,853	3,776	0,827	5,547	0,498	2,825	0,566
55	4,212	15,828	3,363	0,811	3,600	0,479	2,857	0,576
56	4,103	15,300	3,604	0,768	3,376	0,462	2,736	0,513
57	3,150	12,395	2,524	0,648	2,808	0,399	2,369	0,451
58	3,708	14,158	2,806	0,716	3,244	0,443	2,594	0,502
59	3,694	13,786	2,778	0,692	2,879	0,427	2,444	0,829
60	3,718	14,392	3,336	0,747	2,959	0,439	2,560	0,506
61	3,799	14,461	3,078	0,736	5,033	0,447	2,718	0,490
62	3,644	14,131	3,225	0,697	4,877	0,415	2,450	0,491
63	3,474	13,012	3,065	0,656	4,546	0,391	2,229	0,443
64	2,778	11,008	2,162	0,561	2,321	0,332	1,904	0,377
65	3,232	12,183	2,931	0,649	2,846	0,386	2,167	0,490
66	3,550	13,248	2,729	0,713	4,699	0,420	2,392	0,473
67	3,558	13,478	3,176	0,699	2,883	0,415	2,583	0,471
68	3,196	12,259	2,598	0,637	2,703	0,384	2,173	0,435
69	4,366	16,641	3,765	0,834	3,448	0,501	2,887	0,566
70	4,712	17,720	3,929	0,883	3,901	0,508	2,976	0,588
71	4,300	17,238	3,390	0,859	3,518	0,504	2,937	0,543
72	4,416	17,070	3,392	0,872	3,866	0,521	2,986	0,584

73	5,292	19,526	3,908	0,972	4,009	0,588	3,667	0,685
74	5,014	19,349	4,239	0,908	6,382	0,548	3,209	0,626
75	5,767	21,155	4,148	1,035	7,355	0,632	3,756	0,735
76	5,307	19,558	4,407	0,936	4,309	0,577	3,340	0,658
77	5,171	19,157	3,899	0,947	4,181	0,570	3,409	0,656

Continued from Table C- 3

KR-1	Er	Tm	Yb	Lu	Th	Ga	As	Se
	ppm	ppm	ppm	ppm	ppm	ppm	ppm	ppm
37	1,624	0,222	1,502	0,220	4,143	11,431	0,852	0,000
38	1,564	0,214	1,399	0,210	3,669	14,680	1,256	0,000
39	1,677	0,241	1,552	0,231	4,465	11,925	2,169	0,000
40	1,651	0,226	1,498	0,221	4,337	18,125	1,576	0,000
41	1,673	0,228	1,520	0,218	4,555	12,096	2,353	0,000
42	1,781	0,246	1,539	0,242	4,985	18,865	1,851	0,000
43	1,866	0,250	1,764	0,262	5,326	19,886	1,936	0,000
44	1,889	0,262	1,720	0,249	5,181	13,599	2,004	0,000
45	1,789	0,246	1,656	0,237	4,869	13,137	1,981	0,000
46	1,708	0,234	1,544	0,219	4,547	18,242	2,557	0,000
47	1,717	0,233	1,526	0,221	4,236	18,741	2,043	0,000
48	1,730	0,232	1,553	0,217	4,352	18,443	2,176	0,000
49	1,645	0,233	1,493	0,227	4,439	19,083	1,983	0,000
50	1,704	0,235	1,534	0,232	4,338	12,136	2,052	0,000
51	1,671	0,233	1,545	0,224	4,680	13,278	2,740	0,000
52	1,658	0,229	1,547	0,223	4,495	18,951	2,425	0,000
53	1,630	0,221	1,508	0,215	4,601	13,906	3,365	0,000
54	1,670	0,224	1,498	0,228	4,614	13,543	2,835	0,000
55	1,680	0,236	1,569	0,231	4,525	12,561	1,898	0,000
56	1,514	0,211	1,446	0,211	4,418	13,352	1,662	0,000
57	1,340	0,188	1,205	0,188	3,113	24,208	1,771	0,000
58	1,497	0,204	1,370	0,195	3,780	15,525	1,052	0,000
59	1,458	0,205	1,338	0,200	3,807	14,754	1,089	0,000
60	1,511	0,206	1,328	0,202	3,785	10,995	1,044	0,000
61	1,528	0,221	1,405	0,206	4,230	11,855	0,000	0,000
62	1,463	0,193	1,338	0,192	3,864	10,941	0,302	0,000
63	1,330	0,185	1,234	0,179	3,715	10,382	0,822	0,000
64	1,107	0,154	1,046	0,155	2,669	6,610	1,749	0,000
65	1,272	0,175	1,140	0,168	3,200	7,741	1,505	0,000

66	1,340	0,187	1,246	0,187	3,699	9,253	3,495	0,000
67	1,430	0,200	1,298	0,189	3,533	11,554	5,394	0,000
68	1,272	0,176	1,166	0,165	3,175	7,988	4,957	0,000
69	1,678	0,226	1,509	0,224	4,606	10,727	4,467	11,470
70	1,731	0,231	1,571	0,229	5,437	16,555	6,320	0,000
71	1,638	0,230	1,510	0,212	4,512	13,062	5,008	0,000
72	1,717	0,239	1,620	0,233	4,994	14,921	4,243	0,000
73	2,005	0,279	1,882	0,278	6,054	15,103	4,244	14,403
74	1,880	0,253	1,681	0,254	5,634	18,901	3,776	10,276
75	2,150	0,299	2,025	0,299	6,590	17,349	4,325	0,395
76	1,917	0,262	1,757	0,265	6,330	15,638	5,820	10,576
77	1,948	0,269	1,805	0,261	6,383	16,008	4,238	0,000

Continued from Table C- 3

KR-1	**Rb**	**Cs**	**Pb**	**U**	**Zr**	**Nb**	**Mo**
	ppm	ppm	ppm	ppm	ppm	ppm	ppm
37	34,662	1,745	40,443	1,333	79,762	9,738	0,887
38	28,715	1,533	10,194	1,272	73,738	8,629	0,694
39	33,752	1,877	10,811	1,431	87,361	10,310	1,022
40	29,452	1,634	9,958	1,390	84,498	10,207	1,122
41	32,705	1,909	9,565	1,417	87,798	10,405	1,117
42	35,252	1,974	10,907	1,454	93,289	11,646	1,097
43	36,928	2,082	10,382	1,565	106,387	12,076	1,299
44	37,159	2,109	10,175	1,577	99,736	12,108	1,491
45	36,892	2,078	11,513	1,471	93,123	11,655	1,368
46	33,169	1,895	9,138	1,386	83,891	10,412	1,509
47	36,482	2,004	9,054	1,254	90,905	11,654	1,783
48	38,155	2,032	9,216	1,266	92,525	11,912	2,308
49	37,466	1,982	10,291	1,253	91,281	11,653	2,688
50	38,155	1,960	9,080	1,362	93,759	11,434	1,680
51	40,666	2,134	9,387	1,309	102,005	12,267	2,283
52	43,044	2,243	9,051	1,345	90,860	11,875	2,159
53	40,808	2,090	9,282	1,254	94,180	11,628	2,936
54	41,345	1,980	9,156	1,231	96,892	11,818	2,724
55	40,387	2,031	10,329	1,316	91,916	11,677	2,035
56	41,550	2,053	9,129	1,197	92,871	11,238	1,453
57	28,561	1,317	8,485	1,077	69,909	8,422	1,465
58	34,498	1,686	9,853	1,250	78,847	9,575	1,026

59	35,012	1,738	9,228	1,261	75,416	9,362	0,725
60	33,909	1,650	7,640	1,246	79,290	9,920	0,881
61	40,291	1,937	9,295	1,335	83,684	9,982	0,661
62	37,453	1,724	8,457	1,429	80,634	9,373	0,473
63	33,346	1,591	9,579	1,372	70,743	8,462	0,489
64	18,151	0,930	6,024	1,189	59,514	6,706	0,694
65	22,016	1,115	6,965	1,213	69,431	8,060	0,483
66	26,928	1,356	8,877	1,244	71,088	8,534	0,632
67	24,517	1,257	7,333	1,247	76,269	7,958	0,000
68	21,637	1,039	8,277	1,102	69,236	7,586	0,000
69	31,976	1,578	8,656	1,330	84,985	10,386	0,000
70	42,533	2,200	11,687	1,384	90,430	11,727	0,000
71	30,713	1,455	8,313	1,333	86,474	10,316	0,000
72	37,542	1,860	9,769	1,386	94,989	10,984	0,000
73	48,867	2,520	11,684	1,502	113,644	13,282	0,000
74	46,683	2,371	10,999	1,378	100,946	12,343	0,000
75	59,216	3,111	12,799	1,569	115,206	14,082	0,000
76	56,043	2,778	13,809	1,501	111,261	13,714	0,000
77	53,322	2,674	11,533	1,533	109,524	13,016	0,166

Table C- 4. Geochemical concentrations of 22 samples of KR-1

TA-2	**Si**	**Ca**	**Al**	**Fe**	**K**	**Na**	**Mg**	**V**
	wt%	wt%	wt%	wt%	wt%	wt%	wt%	ppm
78	9,334	20,428	2,404	2,520	0,471	0,232	2,595	82,072
79	9,847	17,330	1,770	2,434	0,343	0,358	3,697	77,029
80	10,578	16,371	1,744	2,725	0,307	0,378	4,203	92,237
81	11,407	15,257	2,713	2,669	0,630	0,240	2,737	93,495
82	10,424	17,092	2,532	2,363	0,507	0,200	2,230	85,019
83	11,636	15,823	2,648	2,471	0,463	0,237	1,978	79,576
84	12,230	15,515	2,679	2,517	0,473	0,243	1,962	90,412
85	12,150	15,814	2,491	2,448	0,429	0,255	2,150	92,819
86	11,087	15,442	3,120	3,017	0,620	0,201	1,974	124,648
87	10,168	17,103	2,576	2,426	0,540	0,197	1,866	89,593
88	11,106	16,193	2,630	2,665	0,573	0,275	2,044	105,918
89	11,585	15,432	3,078	3,089	0,560	0,300	2,112	124,995
90	11,522	14,483	3,301	3,189	0,610	0,318	2,175	126,745
91	11,341	14,645	3,297	3,209	0,644	0,328	2,270	129,619
92	11,085	14,565	3,182	3,140	0,622	0,331	2,427	136,043
93	13,750	11,559	3,835	3,820	0,669	0,352	2,682	142,041

94	13,694	11,138	3,709	3,705	0,668	0,336	2,678	131,999
95	13,704	11,813	3,762	3,890	0,714	0,327	2,669	146,022
96	13,533	11,786	3,973	3,920	0,701	0,359	2,871	140,023
97	14,194	10,296	3,960	4,234	0,770	0,290	2,607	146,080
98	14,557	9,513	3,935	4,209	0,783	0,273	2,656	184,486
99	12,874	12,130	3,472	3,418	0,657	0,274	2,197	113,740

Continued from Table C- 4

TA-2	Cr	Mn	Co	Ni	Cu	Zn	Sr	Ba
	ppm	ppm	ppm	ppm	ppm	ppm	ppm	ppm
78	333,019	470,961	23,348	300,261	24,902	54,273	1557,489	103,729
79	1272,588	503,635	29,849	471,566	22,943	80,550	1748,198	107,304
80	1549,797	552,931	35,577	599,990	21,849	75,576	1358,282	97,753
81	406,911	396,281	24,671	353,230	31,163	76,974	1267,696	121,805
82	350,573	436,567	23,129	296,008	26,138	56,321	1032,820	124,543
83	416,586	636,481	28,536	298,693	30,763	62,540	810,924	139,655
84	463,051	694,439	30,708	306,878	29,268	94,298	797,388	157,724
85	681,352	582,080	24,525	316,812	28,980	59,120	818,014	136,817
86	407,939	598,218	23,888	366,441	29,557	63,756	898,549	146,175
87	315,777	521,111	23,443	274,867	29,946	84,750	1113,397	153,777
88	414,052	649,424	31,006	369,210	29,575	86,077	1039,654	150,986
89	445,238	594,957	31,165	440,217	35,071	85,073	946,523	127,777
90	424,337	513,560	30,689	446,967	33,947	70,856	863,914	100,334
91	394,395	570,634	30,641	405,177	35,234	115,653	897,188	120,492
92	400,474	633,463	30,091	453,211	38,604	85,647	971,622	118,417
93	466,048	738,234	36,211	554,733	44,174	87,294	876,476	233,161
94	444,174	694,650	39,409	546,419	38,585	121,935	747,239	107,151
95	492,459	651,455	36,588	557,322	36,836	80,899	865,544	174,123
96	500,461	588,433	37,796	577,872	38,702	99,457	788,366	161,855
97	705,330	1060,924	45,448	904,812	52,579	393,385	654,076	140,494
98	523,054	605,035	42,799	642,988	42,517	95,359	674,134	180,224
99	437,285	713,831	33,708	423,414	39,401	96,352	808,565	179,816

Continued from Table C- 4

TA-2	P	S	Ti	Sc	Hf	Y	La	Ce
	ppm	wt%	wt%	mg/kg	ppm	ppm	ppm	ppm
78	697,786	0,493	0,213	7,950	0,381	16,094	13,942	24,554
79	716,626	0,000	0,206	11,480	0,086	11,062	10,891	19,524
80	691,313	0,275	0,245	9,677	0,000	10,307	10,350	18,756
81	1052,218	0,325	0,240	13,378	0,512	5,000	16,612	29,488
82	882,498	0,292	0,222	11,562	0,456	13,396	16,173	29,713
83	1037,330	0,324	0,248	12,273	0,582	14,629	19,342	36,770
84	1074,404	0,261	0,261	13,490	0,685	15,621	20,351	39,007
85	1039,260	0,310	0,246	12,287	0,597	14,344	18,550	35,289
86	868,476	0,000	0,294	13,742	1,036	17,264	21,976	39,555
87	976,875	0,378	0,233	12,542	0,393	13,528	17,363	31,111
88	933,519	0,307	0,244	13,601	0,484	14,375	18,073	32,669
89	808,654	0,312	0,271	14,868	0,765	16,202	20,543	36,758
90	781,363	0,344	0,272	15,428	0,783	17,573	21,095	37,329
91	779,363	0,383	0,270	15,547	0,903	17,664	21,907	38,851
92	765,929	0,332	0,258	14,694	0,740	16,933	20,812	36,812
93	793,216	0,336	0,312	16,607	1,157	18,940	23,589	41,530
94	793,751	0,314	0,317	15,371	1,056	20,221	22,906	40,407
95	825,572	0,323	0,320	16,491	1,113	18,795	22,791	40,405
96	886,201	0,361	0,323	15,697	1,063	17,896	21,831	38,866
97	923,690	0,259	0,318	16,809	0,998	18,878	22,103	39,635
98	954,430	0,283	0,315	15,817	1,093	18,908	22,781	40,459
99	1125,990	0,252	0,305	15,138	1,063	18,524	22,901	41,125

Continued from Table C- 4

TA-2	Pr	Nd	Sm	Eu	Gd	Tb	Dy	Ho
	ppm	ppm	ppm	ppm	ppm	ppm	ppm	ppm
78	3,171	12,829	2,600	0,668	4,281	0,411	2,378	0,485
79	2,543	10,110	2,423	0,591	2,257	0,337	2,008	0,403
80	2,410	10,074	2,401	0,578	3,454	0,328	1,907	0,378
81	3,772	15,155	3,081	0,782	5,109	0,484	2,803	0,600
82	3,673	14,668	2,856	0,744	3,086	0,436	2,611	0,524
83	4,337	16,754	3,345	0,845	3,716	0,508	2,929	0,590
84	4,629	18,023	3,981	0,887	6,121	0,537	3,059	0,616
85	4,123	16,632	3,686	0,835	3,343	0,505	2,960	0,578

86	4,922	19,626	4,257	0,980	6,502	0,590	3,486	0,694
87	3,904	15,360	3,094	0,775	3,457	0,471	2,711	0,558
88	4,067	16,091	3,209	0,816	3,363	0,498	2,988	0,570
89	4,637	18,148	3,549	0,911	4,112	0,545	3,309	0,660
90	4,708	18,376	3,657	0,921	6,252	0,577	3,428	0,681
91	4,868	19,116	4,114	0,947	6,558	0,598	3,604	0,792
92	4,650	18,348	3,731	0,898	6,134	0,578	3,374	0,677
93	5,295	20,739	4,163	1,072	7,063	0,630	3,838	0,741
94	5,107	20,342	4,112	1,013	6,835	0,601	3,593	0,711
95	5,087	20,181	4,522	1,037	4,604	0,635	3,755	0,734
96	4,901	19,312	3,787	0,997	4,438	0,604	3,584	0,708
97	4,953	19,412	4,313	1,024	6,593	0,607	3,564	0,702
98	5,150	20,245	4,593	1,050	4,545	0,627	3,653	0,726
99	5,204	20,423	4,005	1,043	4,479	0,625	3,522	0,733

Continued from Table C- 4

TA-2	Er	Tm	Yb	Lu	Th	Ga	As	Se
	ppm	ppm	ppm	ppm	ppm	ppm	ppm	ppm
78	1,369	0,203	1,284	0,188	2,756	11,090	6,626	0,000
79	1,204	0,167	1,100	0,162	1,992	10,090	8,867	0,000
80	1,134	0,156	1,024	0,147	1,781	9,895	10,811	25,581
81	1,680	0,230	1,504	0,225	3,520	12,701	2,023	0,000
82	1,499	0,205	1,367	0,201	3,534	8,110	2,703	19,947
83	1,733	0,243	1,581	0,235	4,400	14,471	3,370	0,000
84	1,831	0,255	1,689	0,242	4,749	14,916	5,799	0,000
85	1,647	0,249	1,525	0,226	4,180	13,854	6,033	39,998
86	2,022	0,287	1,830	0,274	4,994	10,894	9,057	31,004
87	1,618	0,222	1,428	0,215	3,872	8,315	4,276	38,054
88	1,662	0,230	1,528	0,224	3,971	15,404	4,828	38,215
89	1,880	0,267	1,716	0,257	4,580	10,992	9,419	48,487
90	1,928	0,276	1,810	0,277	4,737	11,897	8,546	0,000
91	2,079	0,290	1,910	0,274	4,972	16,151	9,387	47,646
92	1,961	0,274	1,764	0,262	4,769	11,338	9,389	48,963
93	2,146	0,302	2,003	0,296	5,597	14,370	8,152	46,187
94	2,078	0,290	1,876	0,283	5,361	13,943	8,160	41,242
95	2,194	0,303	1,987	0,287	5,275	20,350	11,113	40,354
96	2,067	0,283	1,845	0,281	5,069	18,967	10,788	39,715
97	2,107	0,296	1,875	0,287	5,268	18,787	10,671	42,943

98	2,189	0,311	2,066	0,310	5,493	21,914	9,541	65,759
99	2,126	0,292	1,911	0,285	5,296	13,381	4,595	48,224

Continued from Table C- 4

TA-2	Rb	Cs	Pb	U	Zr	Nb	Mo
	ppm	ppm	ppm	ppm	ppm	ppm	ppm
78	24,720	1,560	7,116	2,375	47,043	5,990	2,542
79	15,195	0,902	6,798	1,910	37,913	4,424	3,043
80	13,021	0,735	7,022	1,813	32,521	4,679	2,779
81	34,454	2,028	7,393	2,263	55,742	6,974	0,959
82	30,936	1,906	7,782	2,006	51,243	6,918	0,442
83	31,543	2,088	10,202	1,734	57,641	7,296	1,056
84	32,304	2,170	10,794	1,807	61,213	8,434	1,101
85	28,085	1,883	10,155	1,781	58,983	6,935	1,447
86	36,243	2,372	9,107	2,218	71,327	8,778	2,204
87	33,834	2,013	7,362	2,036	49,891	6,574	0,651
88	32,487	2,091	7,624	2,548	53,863	7,071	1,274
89	35,973	2,479	8,324	2,226	63,277	8,157	1,410
90	38,822	2,674	8,097	2,276	66,797	8,298	1,312
91	39,270	2,749	9,173	2,485	68,483	8,459	3,861
92	37,688	2,639	8,471	2,672	63,374	8,158	2,933
93	46,349	3,086	9,537	2,263	78,587	9,683	1,413
94	44,453	2,989	9,115	2,234	72,506	9,527	1,177
95	44,187	2,969	8,996	2,318	78,247	9,581	1,568
96	42,141	2,772	8,769	2,375	74,746	9,392	1,844
97	43,635	2,977	11,985	2,426	76,105	9,869	33,264
98	45,677	3,097	9,665	2,322	76,709	9,991	1,415
99	45,363	2,766	11,820	2,095	74,849	9,938	0,870